POLITECNICO
MILANO 1863

DEPARTMENT OF ELECTRONICS, INFORMATION AND BIOENGINEERING
DOCTORAL PROGRAMME IN BIOENGINEERING

Development of tissue culture systems for biomechanical conditioning of small-caliber arterial vessels

Doctoral Dissertation of:
Simona Seminati

Supervisor:
Prof. Monica Soncini
Prof. Gianfranco Beniamino Fiore
Tutor:
Prof. Maria Gabriella Signorini
The Chair of the Doctoral Program
Prof. Andrea Aliverti

2019- XXXII Cycle

Contents

List of abbreviations

A

APCs = adventitial progenitor cells

ANGPT1 = angiopoietin-1

C

CAECs = human coronary artery endothelial cells

CAD = computer-aided design

CCM = cell conditioned medium

CD31 = cluster of differentiation 31

c-DNA = complementary DNA

CPD = citrate-phosphate-dextrose

CVD = cardiovascular disease

D

DMEM = Dulbecco's modified eagle medium

E

EC = endothelial cell

ECM = extracellular matrix

EGM - 2 = Endothelial Growth Medium 2

EMT = epithelial-to-mesenchymal transition

EVCS = *ex vivo* vascular culture systems

F

FB = fibroblast

FBS = fetal bovine serum

FCS = fetal calf serum

G

GL= gelatin

GPTMS = γ-glycidoxypropyltrimethoxy silane

H

HBSS = Hank's balanced salt solution

H&E= haematoxylin and eosin

HIF = hypoxia-inducible factor

I

IMA = internal mammary artery

L

LDL = low density lipoproteins

N

NHP = non human primate

NO = nitric oxide

O

OCT = optimal cutting temperature compound

P

PA12 = Polyamide 12

PBS = phosphate buffer solution

PC = polycarbonate

PCL = polycaprolactone

PDMS = polydimethylsiloxane

PenStrep = Penicillin- Streptomycin

PFA = paraformaldehyde

PMMA = poly(methyl methacrylate)

PP = polypropylene

POM = polyoxymethylene

pO_2= oxygen partial pressure

PPFC= parallel plate flow chamber

PS = polysulfone

Q

q-PCR = quantitative polymerase chain reaction

R

RCA = right coronary artery

S

SMC = smooth muscle cell

SM22 = Smooth muscle protein 22-α

SEM = Scanning Electron Microscopy

α-SMA = α-Smooth-Muscle Actin

T

TPBG = trophoblast glycoprotein

TF = tissue factor

TNF-α = tumor necrosis factor-α

V

VCAM-1 = vascular-cell adhesion molecule-1

VEGF = vascular endothelium growth factor

vWF = von Willebrand factor

Abstract

Cardiovascular diseases (CVDs) are the leading cause of death in the world. Within the scenario of CVDs, atherosclerosis plays a key role, as it is responsible for myocardial infarction, stroke, and vascular diseases.

Atherosclerosis is a complex multi-factorial inflammatory disease of the arteries. It is characterized by the accumulation of cholesterol containing low-density lipoproteins in the intima with subsequent activation of the endothelium. Then, the recruitment of monocytes is promoted by chemokines and leukocytes adhesion molecules. Monocytes differentiate into macrophages and upregulate pattern recognition receptors, leading to foam-cell formation. The plaque starts to grow up due to pro-inflammatory cytokines. Increase in the inflammatory activation may induce plaque rupture and thrombus formation, leading to acute manifestation of the disease with ischaemia and infarction.

Traditionally, two approaches have been extensively used to study the mechanisms involved in atherosclerosis and to evaluate the effectiveness of therapies or devices: *in vitro* and *in vivo* models.
In vitro methods are well-established, easy to perform and quantify, relatively not expensive and allow to study isolated and controlled stimuli. Moreover, they are suitable to investigate cell-cell interaction and cell migration when co-cultures with different cell types or cytokines are performed, but they lack of biological realism and often the behaviour of cultured cells can be very different from somatic cells *in vivo*. *In vivo* models, instead, provide a complex environment and the possibility to induce more realistic pathological conditions. They are still unavoidable for testing hypothesis addressed by *in vitro* models and pharmacological treatments. Nevertheless, the scientific community insists on the reduce, replacement and refinement (3 Rs) in the use of animals for experiments. Besides strong ethical implications, animal models have also economical and technical drawbacks. The supply, the maintenance, the facilities for animals are in fact very expensive, and, technically, animal studies may fail to represent human diseases.

Ex vivo models can bridge the gap between *in vitro* and *in vivo* models, because they permit to isolate and investigate specific stimuli, but without loosing the complexity of the tissue. In addition, with *ex vivo* models the bias of the use of animal tissue can be overcame. These approaches do not claim to substitute

in vitro and *in vivo* models. But, instead, they yearn for supporting traditional approaches.

Therefore, the goal of this doctoral thesis was to design and develop innovative *ex vivo* models aiming at investigating different aspects related to the atherosclerotic process.

An innovative model for studying the cellular and molecular mechanisms involved in the spreading of thrombosis is presented in Chapter 3. The culture system consisted in a parallel-plate optically accessible chamber for culturing human arterial slices exposed to a controlled blood flow. Computational studies were used to assess that shear rate produced on the arterial slice within the chamber is of 500 s^{-1}. Moreover, the system proved to be compliant with standard laboratory procedure and microscopy techniques, in particular with confocal microscopy. It could be therefore used for culturing arterial slices with atherosclerotic plaques to assess the nature of vascular components involved in thrombus formation. The project was carried out in collaboration with the Cardiovascular Research Area of IRCSS Ospedale San Raffaele.

Chapter 4 is focused on the design, development and characterization of an *ex vivo* culture system aimed at translating in *ex vivo* models procedures that have been employed to study thrombosis *in vivo*. In particular, we focused on the ferric-chloride induced thrombosis, that, as far as we know, has been studied only with animal models. The bioreactor was designed and developed to culture whole vessels with different diameters and lengths under fluid-dynamic controlled conditions. A first preliminary prototype is presented in the thesis. This bioreactor proved to be suitable for culturing human vessels, but the manipulation of the samples could be harmful for the vessel itself. Therefore, starting from the strengths of the bioreactor, a second advanced prototype was developed. An innovative way to mount the vessels within the system was designed and tested with porcine coronaries. The *ex vivo* platform was realized exploiting additive manufacturing techniques. The hydraulic characterization of the system proved that it is capable of inducing a controlled fluid dynamic status on the vessel. Preliminary experiments with porcine coronaries were performed to assess the viability of the tissue cultured within the system. Results proved that the structure of the vessel was generally preserved and viability guaranteed. In perspective, the system could be used to induce vessel damage and to study the cellular pathways involved. This platform, in fact, could provide a reproducible and well controlled model of vessel damage and it is suitable for investigating the effects of pharmacological treatments. The preliminary validation of the system was performed in collaboration with the Cardiovascular Research Area of IRCSS Ospedale San Raffaele.

In the chapter 5 a tissue-engineered model for studying atherosclerosis was investigated. In fact, tissue-engineered inspired models have been used for their possibility to maintain the complexity of *in vivo* structures, but controlling cellular composition. As a proof of concept, we cultivated adventitial progenitor cells on tubular

electrospun scaffolds under fluid-dynamic conditions to assess angiogenic effects of hypoxia. Angiogenesis, in fact, is an important trigger for the vulnerability of the atherosclerotic plaque and it could be addressed as a therapeutic target. The model proved to be suitable for this kind of consideration, but, before exploiting its potentiality, technical problems must be solved. In fact, one main drawback of tissue-engineered models is related to the necessity to adapt traditional analysis protocols to these innovative approaches. The study was entirely performed at the School of Translational Health Science of the University of Bristol, during a six-months period sponsored by the Erasmus Plus Traineeship.

In the present Ph.D. thesis technical novelties were achieved. The platforms presented could be therefore used for establishing biological novelties. Technological advancements comprised: i) the development of a parallel-plate chamber addressed to human tissue instead of single cell populations, (ii) the development of an innovative culture system for translating *ex vivo* ferric-chloride induced thrombosis model, and (iii) the study of angiogenic effects of hypoxia on adventitial progenitor cells cultured in structure mimicking physiological conditions.

"La scelta di un giovane dipende dalla sua inclinazione,
ma anche dalla fortuna di incontrare un grande maestro"

Rita Levi Montalcini

Chapter 1

Introduction

1.1 The clinical problem: cardiovascular diseases and atherosclerosis

Cardiovascular diseases (CVDs) are a class of pathology that involve the heart and the blood vessels. They include hypertension, coronary artery disease that can lead to heart attack, cerebrovascular disease with possible consequent stroke, peripheral vascular disease, heart failure, rheumatic heart disease, congenital heart disease and cardiomyopathy. According to the World Health Organization, the CVDs are the leading cause of death in the world [1], such as they currently provoke more death each year than cancer and chronic lung disease combined [2].

The economic impact of CVDs have significantly increased over the last two decades and it is projected to increase in the next years [2, 3]. The overall cost of CVDs in the European Union in 2017 has been estimated at € 210 billion a year, with indirect costs related to the loss of productivity that are even comparable to direct costs [4].

For all these reasons, CVDs and their complications are a running sore in the healthcare of developed countries. Therefore, it is still worth it to deeply examine the causes of the pathology and to study the processes involved in its progression, with the final aim of proposing innovative and increasingly effective therapies.

Considering the main causes of CVDs, the atherosclerosis is responsible for a large proportion of them, including myocardial infarction, cerebrovascular diseases and pathology of the aorta and of the arteries, like hypertension and peripheral vascular disease [5, 6].

Atherosclerosis is a complex multi-factorial phenomenon, characterized by a chronic inflammatory process of the arterial wall that arises in specific areas of disturbed laminar flow [7, 8].

The arterial wall in mammals consists of three histological layers.
The *tunica intima* is the internal part and it is composed by a monolayer of endothelial cells (EC) and a thin layer of subendothelial connective tissue. The endothelial lining plays as an interface with the blood and as a transducer of both chemical and mechanical stimuli.
The internal elastic lamina separates the *intima* from the intermediate layer, the *tunica media*. The *media* is composed by smooth muscle cells (SMCs) and extracellular matrix (ECM), that mainly comprises elastin, collagen and proteoglycans. The *media* stands the biomechanical stimuli and supports the blood vessel.
Finally, the outer layer is the *tunica adventitia*, separated from the *tunica media* by the external elastic lamina. Fibroblasts (FB) and a loose connective tissue constitute the *adventitia*, where it is possible to find the *vasa vasorum*, small vessels that supply oxygen and nutrients to the vascular wall [9, 10]. Perivascular fat surround most blood vessels, releasing important vasoactive factors and playing other relevant physiological roles [11, 12] (Figure 1.1).

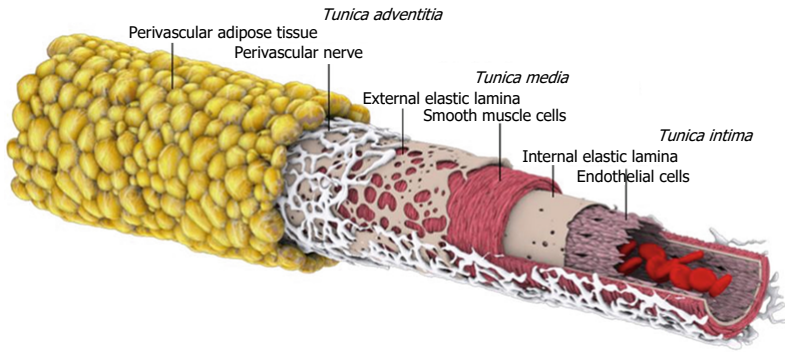

Figure 1.1: Structure of arteries. The picture show a 3D model of the layers composing the vascular wall. The model was constructed adjusting data from laser scanning confocal microscopy. The three histological layers (*tunica intima*, *media* and *adventitia*) are surrounded by the perivascular adipose tissue. Each layer is characterized by different cellular components: the *intima* is mainly composed by endothelial cells, the *media* by smooth muscle cells and the *adventitia,* deeply connected with the adipose tissue, by fibroblasts. Adapted from [13].

The first event that occurs in the arterial wall (Figure 1.2) during the atherosclerotic process is the endothelial dysfunction. This is related to structural alterations with the exposure of proteoglycans and the loss of continuity of the luminal elastin layer.
Low-density lipoproteins (LDL) can then penetrate and accumulate in the subendothelial area, triggering the inflammatory response [8]. Reactive species and enzymes secreted by inflammatory cells provoke the oxidation of LDL and lipids and the consequent release of phospholipids that activate endothelial cells, especially in sites with disturbed fluid-dynamics, as mentioned above.
ECs activation results in an increased expression of adhesion molecules, like the vascular-cell adhesion molecule 1 (VCAM-1), and inflammatory genes [14]. Therefore, activated endothelial cells, that normally would resist the adhesion of leukocytes, cause rolling blood cells to adhere to the vascular surface.
Chemokines released in the *intima* stimulate the migration of the attached blood cells into the subendothelial layer. Monocytes are then targeted by chemokines and other growth factors and differentiate into macrophages. Macrophages in turn are ligated by several endogenous and microbial molecules through pattern-recognition receptors (especially toll-like receptors). As a consequence, inflammatory cytokines, chemokines and other molecules are released in the intima with a resulting inflammation and tissue damage[15, 16, 17].

The inclusion of lipids within the macrophages generate the foam cells, but at this stage isolated foam cells or small pool of foam cells are not considered yet atherosclerosis and the process is still reversible [18].

As the accumulation of foam cells increase, fatty streaks appear and give rise to the atherosclerotic lesion [20](Figure 1.3). The progression of the lesion involves the migration of SMCs from the *media* to the *intima*, the proliferation of intimal

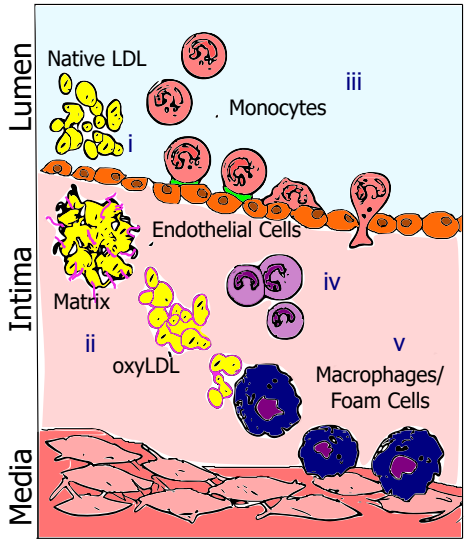

Figure 1.2: The first steps in the atherosclerotic process. The dysfunction of the endothelium allow the infiltration of low-density lipoproteins (LDL) in the intima and the activation of the inflammatory response (i). Inflammatory molecules induce the oxidation of LDL and lipids and the activation of endothelial cells (ii), which make circulating monocytes to adhere to the vascular surface (iii). Chemokines in the intima induce the migration of monocytes and the differentiation into macrophages (iv), that include lipids forming the so called foam cells (v). Adapted from Tymchuk et al. [19].

and of media-derived SMCs and the synthesis of ECM macromolecules (*e.g.,* collagen, elastin and proteoglycans). In advancing lesions, macrophages and SMCs of the plaque can be subjected to apoptosis and the resulting accumulation of extracellular lipid from apoptotic bodies often denote the necrotic core in the centre of the plaque [21].

Atherosclerotic lesions alone may obstruct blood flow into the vessels and their clinical manifestation is a stable *angina pectoris*, but this is rarely fatal [22].

Advanced lesions are indicated with the term atheromas or fibroatheromas; these lesions present a fibrous cap constituted mainly by SMCs. The advanced lesions are characterized by the presence of vascularization [20, 23].

The ultimate complication of the atherosclerosis is the thrombosis, which often follow a physical disruption of the atherosclerotic plaque [21]. The rupture of the plaque, in fact, is more frequent than the plaque erosion, and it is the major cause of acute coronary syndrome. Plaques subjected to rupture present characteristic features as a thin fibrous cap made mainly by type I collagen and a small necrotic core.
After the rupture, the necrotic core components are exposed to the circulating blood and trigger the activation of the coagulation cascade. This process induces the formation of a thrombus inside the lumen and the consequent interruption of the blood flow in the vessel with fatal clinical outcomes [24, 25, 26].

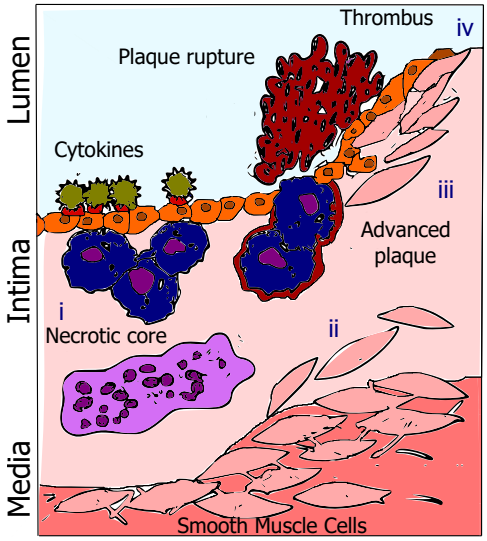

Figure 1.3: Progression of the atherosclerotic plaque and thrombosis. As foam cells increase, they stimulate the release of cytokines and eventually undergo apoptosis, contributing to the formation of a necrotic core (i). This process is accompanied by the migration of smooth muscle cells from the media to the intima and the formation of a fibrotic cap (ii). The lesion continues to grow and become unstable (iii). The vulnerable plaque can be subjected to rupture, which results in the formation of a thrombus (iv). Adapted from Tymchuk et al. [19].

1.2 Rationale of the doctoral project

My doctoral project deals with the design and the development of innovative methods and culturing platforms for studying some mechanisms involved in the progression of the atherosclerosis.

In particular, the aim is to analyse different aspects related to the atherosclerotic process and to propose for each aspect an *ex vivo* approach that suits laboratory practice.

Starting from specific needs coming from the analysis of the state of the art, we designed solutions that are alternative to *in vitro* assays and animals models. These *ex vivo* models could not be considered, of course, as a replacement of the traditional strategies used in laboratory, but they can represent a reliable and powerful aid for analysing the pathology with a different multi-disciplinary approach. In fact, they allow to study complex structures, to isolate and control the stimuli addressed to the tissue and to perform experiments with human tissue. For all these reasons, they can in some ways fill the gap between *in vitro* and *in vivo* models [27, 28].

Moreover, the availability of new *ex vivo* models offers not only the possibility to investigate the pathological cues involved in a disease but also to facilitate the pre-clinical screening of potential pharmacological treatments and medical devices [29, 30].

In this doctoral project, we mainly focused on the development of culture platforms to study three specific aspects related to atherosclerosis: the cellular composition of thrombi, the players involved in the mechanism of thrombosis and the angiogenic profile of some cellular components of the vascular wall.

The approach of the work has a strong multi-disciplinary nature, the models were developed in collaboration with a team of biologists and clinicians.

This project was prominently experimental, supported by computer aided design and numerical modelling. The designing and prototyping of the *ex vivo* culture systems were performed at the Laboratory of Experimental Micro- and Biofluid-dynamics (μBS Lab) of the Dipartimento di Elettronica, Informazione e Bioingegneria of the Politecnico di Milano (Milano, Italy). A preliminary biological validation campaign with human samples was performed at the Cardiovascular Research Area of IRCCS Ospedale San Raffaele of Milano (Milano, Italy). One part of the project was carried out at the School of Translational Health Science of the University of Bristol (Bristol, UK) supported by the Erasmus Plus Traineeship.

1.3 Outline of the thesis

The dissertation consists of four main chapters that describe the various steps that brought to the realization of the different platforms designed in this doctoral project. After a chapter dealing with the state of the art, each chapter hinges on a single platform/model and highlights the characteristic aspects of the engineering solutions applied to address specific requirements.

The Chapter 2 presents a short *excursus* on the current strategies used to study the pathophysiology of atherosclerosis, showing limitations and potentialities of each strategy.

In Chapter 3 an innovative platform for studying the cellular composition of the thrombus by culturing slices of arteries is presented. The project was carried out in collaboration with the Cardiovascular Research Area of IRCSS Ospedale San Raffaele.

Chapter 4 is focused on the design, development and characterization of an *ex vivo* culture system to condition a whole vessels with the final aim of translating *ex vivo* the mechanisms used to study thrombosis in animal models. A preliminary validation of the system was performed in collaboration with the Cardiovascular Research Area of IRCSS Ospedale San Raffaele.

In Chapter 5 it is presented the model of a synthetic vascular graft to assess the angiogenic profile induced by hypoxia on adventitial progenitor cells. Angiogenesis, in fact, is an important trigger for the vulnerability of the atherosclerotic plaque and it could be addressed as a therapeutic target. The project was carried out at the School of Translational Health Science of the University of Bristol and

supported by the Erasmus Plus Traineeship.

In Chapter 6, a general discussion of the PhD dissertation and conclusive remarks are presented.

Bibliography

[1] World Health Organization. World health statistics overview 2019: monitoring health for the SDGs, sustainable development goals. In *World health statistics overview 2019*, Geneva, 2019. World Health Organization.

[2] E. J. Benjamin, P. Muntner, A. Alonso, et al. Heart Disease and Stroke Statistics 2019 Update: A Report From the American Heart Association. *Circulation*, 139(10):e56–e528, 2019.

[3] L. E. Rohde, E. G. Bertoldi, L. Goldraich, and C. A. Polanczyk. Cost-effectiveness of heart failure therapies. *Nature Reviews Cardiology*, 10(6):338–354, 2013.

[4] K. Kotseva, L. Gerlier, E. Sidelnikov, et al. Patient and caregiver productivity loss and indirect costs associated with cardiovascular events in Europe. *European Journal of Preventive Cardiology*, 26(I):1150–1157, 2019.

[5] J. Frostegard. Immunity, atherosclerosis and cardiovascular disease. *BMC Medicine*, 11:117–130, 2013.

[6] W. Herrington, B. Lacey, P. Sherliker, J. Armitage, and S. Lewington. Epidemiology of Atherosclerosis and the Potential to Reduce the Global Burden of Atherothrombotic Disease. *Circulation Research*, 118(4):535–546, 2016.

[7] V. Mehta and E. Tzima. A turbulent path to plaque formation Sharks shift their. *Nature*, 540:531–532, 2016.

[8] C. Weber and H. Noels. Atherosclerosis: Current pathogenesis and therapeutic options. *Nature Medicine*, 17(11):1410–1422, 2011.

[9] C. Camaré, M. Pucelle, A. Nègre-Salvayre, and R. Salvayre. Angiogenesis in the atherosclerotic plaque. *Redox Biology*, 12(2017):18–34, 2017.

[10] D. Wang, Z. Wang, L. Zhang, and Y. Wang. Roles of Cells from the Arterial Vessel Wall in Atherosclerosis. *Mediators of Inflammation*, 2017(2017):1–9, 2017.

[11] W. Wang and P. Seale. Control of brown and beige fat development. *Nature Reviews Molecular Cell Biology*, 17(11):691–702, 2016.

[12] C. K. Cheng, H. A. Bakar, M. Gollasch, and Y. Huang. Perivascular Adipose Tissue: the Sixth Man of the Cardiovascular System. *Cardiovascular Drugs and Therapy*, 32(5):481–502, 2018.

[13] C. J. Daly. *Examining Vascular Structure and Function Using Confocal Microscopy and 3D Imaging Techniques*, pages 97–106. Springer International Publishing, Cham, 2019.

[14] G. K. Hansson. Inflammation, Atherosclerosis, and Coronary Artery Disease. *The New England Journal of Medicine*, 325(16):1685–1695, 2005.

[15] P. Libby. Inflammation in atherosclerosis. *Nature*, 420(6917):868–874, 2002.

[16] I. Tabas, G. García-Cardeña, and G. K. Owens. Recent insights into the cellular biology of atherosclerosis. *Journal of Cell Biology*, 209(1):13–22, 2015.

[17] M. C. Flynn, G. Pernes, M. K. S. Lee, P. R. Nagareddy, and A. J. Murphy. Monocytes, Macrophages, and Metabolic Disease in Atherosclerosis. *Frontiers in Pharmacology*, 10:666, 2019.

[18] W. Insull Jr. The Pathology of Atherosclerosis: Plaque Development and Plaque Responses to Medical Treatment. *The American Journal of Medicine*, 122(1):S3–S14, jan 2009.

[19] C. N. Tymchuk, J. Hartiala, P. I. Patel, M. Mehrabian, and H. Allayee. Nonconventional genetic risk factors for cardiovascular disease. *Current Atherosclerosis Reports*, 8(3):184–192, 2006.

[20] A. P. Burke, A. Farb, F. D. Kolodgie, J. Narula, and R. Virmani. Atherosclerotic plaque morphology and coronary thrombi. *Journal of Nuclear Cardiology*, 9(1):95–103, 2002.

[21] P. Libby, P. M. Ridker, and G. K. Hansson. Progress and challenges in translating the biology of atherosclerosis. *Nature*, 473(7347):317–325, 2011.

[22] J. F. Bentzon, F. Otsuka, R. Virmani, and E. Falk. Mechanisms of plaque formation and rupture. *Circulation Research*, 114(12):1852–1866, 2014.

[23] F. Otsuka, S. Yasuda, T. Noguchi, and H. Ishibashi-Ueda. Pathology of coronary atherosclerosis and thrombosis. *Cardiovascular diagnosis and therapy*, 6(4):396–408, 2016.

[24] P. K. Shah. Mechanisms of plaque vulnerability and rupture. *Journal of the American College of Cardiology*, 41(4 Supplement):S15 LP – S22, feb 2003.

[25] K. Sakakura, M. Nakano, F. Otsuka, et al. Pathophysiology of atherosclerosis plaque progression. *Heart Lung and Circulation*, 22(6):399–411, 2013.

[26] T. Quillard, G. Franck, T. Mawson, E. Folco, and P. Libby. Mechanisms of erosion of atherosclerotic plaques. *Current opinion in lipidology*, 28(5):434–441, 2017.

[27] L. Hung, H. Obernolte, K. Sewald, and T. Eiwegger. Human ex vivo and in vitro disease models to study food allergy. *Asia Pacific allergy*, 9(1):e4–e4, 2019.

[28] A. F. Moleiro, G. Conceição, A. F. Leite-Moreira, and A. Rocha-Sousa. A Critical Analysis of the Available In Vitro and Ex Vivo Methods to Study Retinal Angiogenesis. *Journal of ophthalmology*, 2017:3034953, 2017.

[29] A. F. van de Merbel, G. van der Horst, M. H. van der Mark, et al. An ex vivo Tissue Culture Model for the Assessment of Individualized Drug Responses in Prostate and Bladder Cancer. *Frontiers in Oncology*, 8(October):1–8, 2018.

[30] H. Cui, S. Miao, T. Esworthy, et al. 3D bioprinting for cardiovascular regeneration and pharmacology. *Advanced Drug Delivery Reviews*, 132:252–269, 2018.

Chapter 2

Tools and procedures to study the pathophysiology of atherosclerosis

2.1 Current strategies for studying atherosclerosis

Atherosclerosis is a complex disease, characterized by a chronic interplay of inflammatory conditions [1], involving both biochemical and cellular events [2]. Epidemiological studies in the last 50 years identified a wide range of risk factors that could be divided between genetic and environmental factors, with complex interactions among each other [3, 4]. Although the outcome of this deteriorating process can be easily monitored via angiography, the causes and the links among each event are still controversial[5].

Different conventional and innovative approaches are available for investigating pathogenesis and mechanisms of atherosclerosis. It is possible to identify three main classes of possible approaches: *in vitro*, *in vivo* and *ex vivo* models.

Traditional *in vitro* models of atherosclerosis mainly consist of endothelial cultures exposed to presumed risk factors, such as inflammatory factors or oxidized LDL [6]. Lalonde et al., for example, induced endothelial dysfunction in cultured ECs with tumor necrosis factor-α (TNF-α) to study the genes involved in the regulation of vascular homeostasis by ECs [7]. Vicen et al., instead, cultured ECs with 7-ketocholesterol to evaluate the effects of cholesterol on the regulation of a glycoprotein (*i.e.*, the endoglin) which is strongly involved in endothelial dysfunction and inflammation [8].

In vitro models for studying atherosclerosis often involve co-cultures of human ECs with SMCs or human leukocytes, to mimic an atherogenic environment. *In vitro* co-culture models used to study atherosclerotic events can be divided in three main groups: (i) indirect cultures with cell-conditioned media or transwell, (ii) direct cell contact co-cultures, and (iii) gel scaffold co-cultures [2, 9]. As examples of indirect co-cultures, Wang et al. used the conditioned media collected from bone-marrow derived mesenchymal stem cells to induce in vascular SMCs calcification, which is a common finding in human atherosclerotic lesions [10]. Noonan et al., instead, used a transwell system to replicate an atherosclerotic culture with a triple-cell co-culture with ECs, SMCs and macrophages [11]. Direct co-cultures were exploited, for example, by Hung et al. and by Gao et al. who made co-cultures of neutrophils and exosomes secreted from ECs treated with oxidized LDL to assess the involvement of some specific exosomes into the atherosclerotic process[12, 13]. Lavender and colleagues made a direct co-culture of ECs on SMCs mimcking the physical and physiological proximity of these populations to investigate ECs alterations induced by SMCs [14]. Finally, gel scaffold co-cultures can be found in the work of Dorweiler et al. that designed an *in vitro* model for studying the plaque development in atherosclerosis using a modified fibrin gel as a scaffold for the co-culture of ECs and SMCs [15].

Since the relationship between blood flow and atherosclerotic process has been well established for over 40 years, advanced *in vitro* models of atherosclerosis are based on the use of platforms that allow to perform blood flow or medium

flow controlled experiments on cultured ECs [16]. The first approach used to induce a shear stress on cultured ECs exploited the geometry of the cone-and-plate viscometer (Figure 2.1.a). Examples of cone-and-plate chambers to study atherogenic stimuli on endothelial cells can be found in Franzoni et al. [17] and Slegtenhorst et al. [18]. Another strategy is represented by parallel-plate flow chamber (PPFC) setups (Figure 2.1.b). These systems are versatile and permit to induce controlled variation of surface composition, geometry, cell types and fluid-dynamic conditions. Early events of the atherosclerotic process can be studied, for example, reproducing a disturbed flow with a specific geometry, as Balaguru et al. did in their work [19] or exploiting a pump with oscillatory flow rate as presented in the work of Wang et al.[20]. PPFCs have been used not only to assess changes induced in ECs by different shear stress conditions, but also to model the adhesion of leukocyte to endothelium under flow conditions [16]. An example is shown in the work of Erbeldinger et al. who developed a PPFC to investigate the changes induced by an inflammatory signal (*i.e.,* radiations) on the interactions between leukocytes and endothelium [21]. Several modifications to PPFCs design have been carried out from many groups to explore different topics but also many commercial flow systems are available for scientists without an engineering background [16].

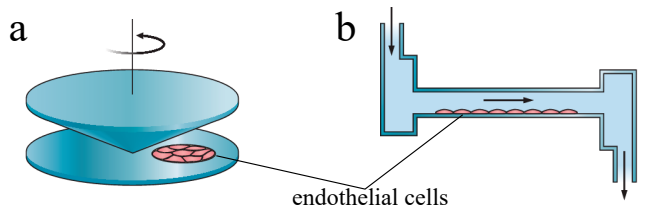

Figure 2.1: Schematic representation of traditional *in vitro* systems. (a) The cone-and-plate geometry adopts the viscometer strategy to stimulate with shear stress the endothelial cells, while (b) in the parallel-plate flow chambers a calibrated height of the chamber or a particular design permits to stimulate with a specific shear stress a monolayer of cells. Adapted from Chiu and Chien [22].

The more recent version of flow chambers is represented by microfluidic devices [16, 6]. Microfluidics exploits micro-engineering techniques, like photolithography, to produce chambers with nanometer dimensions in polydimethylsiloxane (PDMS). PDMS is an optically-clear, inert, non-toxic, gas permeable and cost-effective polymer. The devices are usually realized by curing PDMS over master molds and then bonding the chamber onto a microscope coverslip by plasma or vacuum [23]. Cells can be cultured in the devices and then exposed to blood or culture medium with different fluid-dynamic patterns.
Microfluidic chambers, compared to traditional parallel-plate devices, offer lower volumetric flow rates and the possibility to create precise channel geometries that mimic physiological or pathological conditions. In addition, one major advantage of microfluidic chambers is the possibility to have a spatial control of the microenvironment properties. For example, Westein et al. reproduced in a microfluidic platform the complex geometry and the fluid-dynamic of an atherosclerotic plaque.

In the device, they evaluated shear-dependent thrombus formation by culturing ECs into stenotic microchannels and exposing them to blood flow[24].

In vitro models are useful not only as methods to investigate the mechanisms involved in the atherosclerotic process, but also as support in the development of new pharmaceutical products. To fulfil this aim, it is necessary to have models that are simple but that, at the same time, retain the likeness to the structure of interest [5]. In this scope, microfluidic platforms have demonstrated to be suitable for investigating the effects of pharmacological agents on human ECs, as shown in the work of Zhang et al., who developed a system with an engineered micro-vessel network for testing drug efficacy and toxicity[25].

The second traditional method to study atherosclerosis is represented by animal models. For each specific atherosclerotic study it is essential to choose the appropriate animal model. The American Heart Association, with this regard, drew up a list of recommendations on the choice of the proper animal model for each kind of study [26]. A perfect animal model should be a replica of human anatomy and pathology to have the possibility to transfer the results obtained directly to human. Although this perfect copy of human physiology and pathology does not exist, animals can be manipulated to induce particular conditions[16, 27]. Other important requirements for animals used for *in vivo* models are low cost, easy supply and well-defined genetic characteristics. In addition, the animals should develop lesions spontaneously after consuming a diet comparable to human diet, even though this requirement is often failed, due to lesion topography not similar to humans [28]. In many cases, flow-dependant atherosclerosis is studied not only in areas with naturally disturbed flow, but also inducing modification of the flow through interventions [16].

Over the last years, mice have been the most used species to study atherosclerosis because of their rapid reproduction and ability to monitor the progression of the disease. However, their lipid profile is quite different from the human one, so genetic manipulation is required [29]. The two mice models most used to study the atherosclerotic process are apoliprotein E deficient ($Apoe^{-/-}$) mouse and LDL receptor-deficient mouse ($Ldlr^{-/-}$)[30]. Examples could be found in the works of, respectively, Vromman et al., who studied the role of a targeting interleukin in atherogenesis in $Apoe^{-/-}$mice [31], and of Kiss et al., who investigated the role of the haematopoietic complement factor H, a protector of tissue damage, in atherosclerosis using $Ldlr^{-/-}$mice [32].

Compared to mice, larger animals are, in contrast, more expensive and the development of atherosclerotic lesions requires more time, but they fit the specific requirements of some studies. A few studies have been carried out in species as rats, hamster, pigeons and chickens [16], but the most used larger animals are rabbits, pigs and nonhuman primates (NHPs) [29].

Rabbits are very sensitive to a cholesterol diet and they made a great contribution to translational research in the field of human lipoprotein metabolism and ath-

erosclerosis, even though it is necessary to refine the rabbit genome information [33]. A recent example is the study performed by Nie et al. to investigate in a rabbit model the correlation between hypoxia and plaque instability in advance atheromas [34].

Pigs, due to their dimensions, are models of human-like atherosclerosis, provide large RNA amount for the analyses and offer the possibility to perform percutaneous interventions [16]. The most important limitations of pig models are related to the costs for supplying and maintaining the animals and the long time needed to induce atherosclerosis. In addition, the atherosclerotic lesions can arise at unpredictable sites[35]. One example of a porcine model is shown in the work of Badin and colleagues; they used a swine model to examine the effects of diabetes and of different concentrations of intracellular free calcium on the severity of coronary atherosclerosis[36].

Atherosclerosis and lipoprotein metabolism has also been studied in nonhuman primates (NHPs) [29]. NHPs develop atherosclerosis and cardiovascular diseases spontaneously and age-related co-morbidities are accelerated proportionally faster than in humans. In addition, their size permits to conduct biopsy samples at different time points and to use advanced imaging techniques. The use of NHPs has been limited by the costs and the difficulties of genetic studies [37]. Tadin-Strapps and colleagues carried out *in vivo* experiments with lean rhesus macaque monkeys to evaluate the role played by a specific lipoprotein in atherosclerosis progression [38].

A third possible approach is represented by *ex vivo* systems, that will be discussed in detail in the following paragraphs.

2.2 The importance of developing *ex vivo* system

In the previous paragraph, a short focus on the *in vitro* and the *in vivo* models used to model the atherosclerotic process was presented.

In vitro methods have been critical in finding out molecular and cellular mechanisms involved in the onset and progression of atherosclerotic lesions. These studies have traditionally been used in biology laboratories, so they are well-established, easy to perform and quantify, relatively not expensive and allow the study of isolated and controlled stimuli. Moreover, they are suitable for investigating cell-cell interaction and cell migration when co-cultures with different cell types or cytokines are performed. On the other hand, they lack of biological realism and often the behaviour of cultured cells can be very different from somatic cells *in vivo* [16].

In vivo models, instead, provide a complex environment and the possibility to induce more realistic pathological conditions, as long as the correct animal model has been chosen. They are still unavoidable to test hypothesis addressed by *in*

vitro models and to test the safety and the efficacy of drugs and medical devices. However, the scientific community insists on the reduce, replacement and refinement (3 Rs) in the use of animals for experiments [39, 40]. Besides strong ethical implications, animal models have also economical and technical drawbacks. The supply, the maintenance, the facilities for animals are in fact very expensive, and, technically, animal studies may fail to represent human diseases, due to relevant differences with the mammalian immune systems [41].

Considering all these aspects, *ex vivo* models represent a good combination of the best of *in vivo* and *in vitro* systems (Figure 2.2). In fact, although retaining the advantage of controlling experimental conditions, *ex vivo* studies can be performed keeping the cells in their native tissue, which permits to create more realistic experimental environments. In *ex vivo* experiments it is possible to reproduce both *in vivo*-like mechanical and chemical stimuli [16] as pulsatile flow, cyclic stretch, pressure [42], and, respectively, gradients of oxygen [43]. Moreover, *ex vivo* systems offer the possibility to perform experiments with human tissue, avoiding then the translational problems observed in animal models [44, 45]. Although *in vivo* models are still unavoidable in the pre-clinical evaluation of therapeutic strategies, medical devices and pharmacological treatments, *ex vivo* systems can play as a preliminary screening of the potential solutions, reducing the product development cycle by implementing different prototype modifications in *ex vivo* studies [46].

For all these reasons, the use of *ex vivo* systems can bridge the gap between *in vitro* and animal models and can help in designing a complete and thorough study.

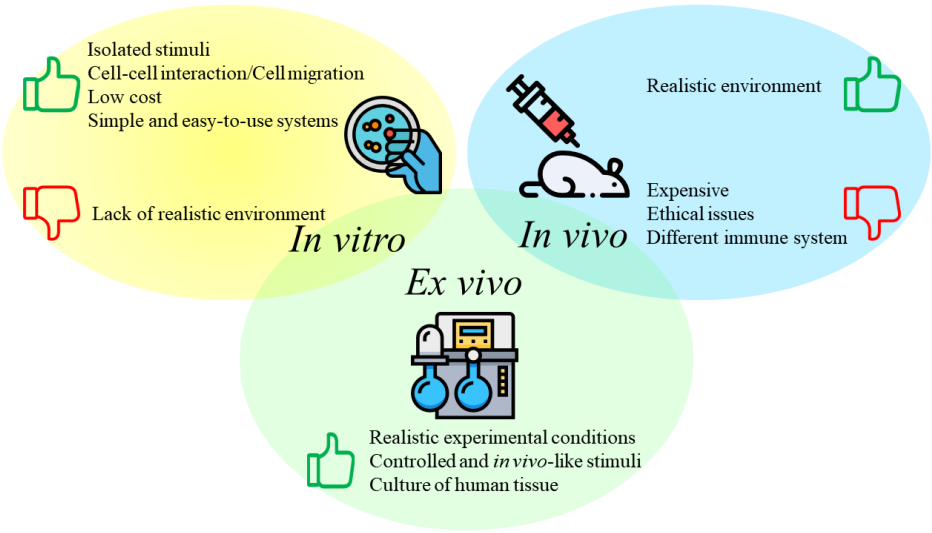

Figure 2.2: The importance of developing *ex vivo* models. *Ex vivo* models bridge the gap between *in vitro* and *in vivo* studies. In fact, they allow to perform experiments with controlled stimuli in a more realistic scenario than *in vitro* models but, at the same time, permit to use human tissue and to reduce the costs and the ethical issues related to animal tests.

2.2.1 *Ex vivo* systems for the study of the atherosclerotic process

It has been since the early 1990s that *ex vivo* models have been used to replicate successfully physiological and pathological *in vivo* conditions. These models, in general, are constituted by explanted arteries or vein segments cannulated within a culture chamber. The vessel sample is preserved in culture medium enriched with nutrients and connected to a perfusion circuit. Therefore, the hydraulic system can provide the control of intra-luminal pressure, flow pulsatility and flow rate. As an alternative, specific designs are developed to induce biochemical stimulation to the tissue (*e.g.,* gradients of oxygen or inflammatory molecules). In addition, working in a sterile environment and keeping the system in a controlled atmosphere (*i.e.,* a cell culture incubator), potentially long-term organ culture studies can be performed[16].

Beyond the traditional *ex vivo* systems, engineered tissue have gained importance as disease models. In fact, the rapid expansion of cardiovascular tissue engineering offered the possibility to develop biomaterials and engineered tissue, which have been widely studied in the regeneration field, but which can also be suitable to model diseases, assess pharmacological treatments, and to evaluate devices before pre-clinical work [47].

In the following paragraphs we focused on some recent examples of vessel perfusion systems and tissue engineering-derived models for the study of vascular diseases.

2.2.1.1 *Ex vivo* whole vessel culture systems

Whole tissue cultures have been extensively employed in *ex vivo* models because the use of native tissues permit to keep in consideration complex aspects as the multiple cellular composition and the interactions between cells and ECM, which is difficult to obtain in simple two-dimensional cell cultures. Over the last decades, organ cultures have been performed using bioreactors, which can be defined as complex systems that permit to culture cells or tissues in a well-defined biological environment [48].
In the field of cardiovascular diseases, many aspects of the atherosclerotic process have been addressed by *ex vivo* vessels culture systems (EVCS) using both animal and human tissue.

Since the correlation between the onset of atherosclerosis and areas with a disturbed fluid dynamics has been widely accepted [22, 49, 50, 51], many EVCS have been developed to elucidate the effects of this biomechanical stimulus. One example is the work of Lu and Kassab. This study describes an *ex vivo* model to investigate the relations between reverse flow and the reduction of athero-protective factors as nitric oxide (NO) in explanted porcine carotid and femoral arteries. In the culture system, these segments were cannulated and stretched in an organ bath with Krebs solution at 36−37°C and subjected to a controlled flow rate in

both directions[52].

Ex vivo models can provide interesting insights even on the effects induced on the wall of elastic arteries by the vascular mechanical environment. Leloup and colleagues, for example, investigated the alteration of the contractile properties of aortic segments with a bioreactor[42] designed to stimulate mouse aortic segments with different controlled cyclic stresses. In the system, aortic segments were mounted between to parallel wire hooks in an organ bath and force and displacement of the upper hook were controlled and measured through a transducer[53].

Besides biomechanical stimuli, also biochemical stimuli play a key part in the progression of atherosclerotic lesions[54, 55, 56]. Among these, inflammatory cues have been broadly studied using EVCS not only to understand their role in atherosclerosis, but even as therapeutic target. In the work of Alexander et al., an endothelium-mimicking nanomatrix with potentially anti-inflammation properties was tested on rat mesenteric arterioles cultured in a custom made chamber (Figure 2.3.a). In the chamber, the isolated arterioles were cannulated with glass micropipettes, secured with monofilament suture, pressurized and cultured with the nanomatrix. To assess the anti-inflammatory properties, it was evaluated the release of NO induced by the nanomatrix (Figure 2.3.b)[57].

The complex interactions between cellular populations and the immune system is another crucial aspect related to the development of the atherosclerotic plaque. Nevertheless, many aspects of this phenomenon remain unrevealed, due to technical limitations. *In vitro* systems, in fact, cannot faithfully reproduce all the intercellular interactions within human atherosclerotic plaques, animal arterial wall composition is different from human and the *in vivo* access to human atherosclerotic plaques is limited. Lebedeva and colleagues proposed therefore a new *ex vivo* model of human atherosclerotic plaques. Their model was based on a technique of histoculture that permits to maintain mammalian tissue for weeks at the air-liquid interface [58, 59]. Their approach proved to be useful to investigate the function of immune cells in the context of complex cell–cell interactions within the tissue in atherogenesis[60].

The remodelling of the vascular wall after injury is a critical point in the formation of atherosclerotic plaques. Kural et al. developed an *ex vivo* model for investigating the response to intraluminal arterial injuries with a bioreactor that enables the control of intramural pressure and shear stress. The system allows to isolate different factors and to explore the complex interactions between ECs and SMCs in the arterial remodeling. After a validation with animal tissue (*i.e.,* rat aorta), human tissue (*i.e.,* human umbilical artery) was cultured into the bioreactor, overcoming the issues related to the differences between animal and human tissue. The bioreactor consisted of a glass medium reservoir where the vessels were placed after being cannulated with glass pipettes and secured with silk sutures (Figure 2.3.c). The re-circulation of the medium was obtained by a hydraulic circuit connected to a peristaltic pump. Parameters like flow rate, intramural pressure and wall shear

stress were adjusted by varying pump speed, tubing resistance and media viscosity [61].

Finally, *ex vivo* bioreactors with excised tissue offer the possibility to evaluate the performances of biomedical devices. These devices interact with the surrounding tissue, inducing in some cases modification that can lead to atherosclerosis in the vessel[62, 63]. Viability of the tissue, vascular response, drug release, pharmacokinetics and tissue penetration are the parameters considered for evaluating the devices [64, 65]; Mundargi et al. designed a simple *ex vivo* bioreactor with biosensors to monitor real time the viability and the response of the tissue. The system was validated with porcine carotid arteries mounted in a sterile glass chamber filled with medium and connected to a reservoir and to the peristaltic pump (Figure 2.3.d). Initial experiments indicated that shear stress and oxygen levels in the bioreactor are vital parameters in deciding the tissue viability. The system proved to be capable of monitoring vascular responses in the setup and, therefore, that can be used for screening biopharmaceutical drugs and biomedical devices [46].

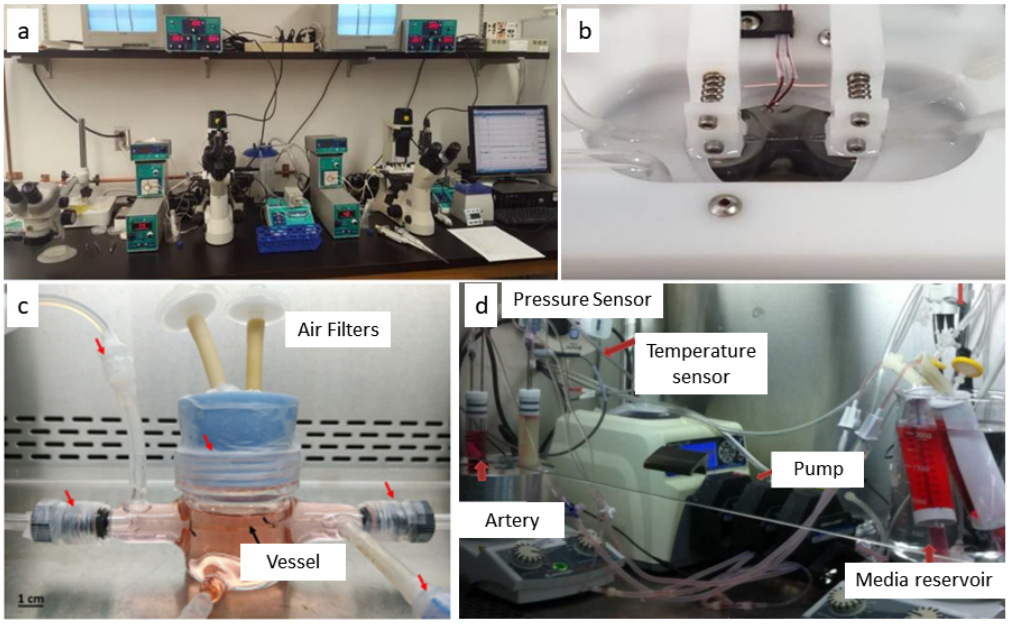

Figure 2.3: Examples of *ex vivo* models exploiting whole vessel culture. (a) Experimental setup and (b) culture chamber of the *ex vivo* model developed by Alexander et al. to study anti-inflammation properties of a nanomatrix on rat mesenteric arterioles. Adapted from Alexander et al. [57]. (c) In the model proposed by Kural the vessel, animal or human, is placed within a simple bioreactor controlling arterial shear stress and intramural pressure. Adapted from Kural et al. [61]. (d) The sensor-enabled *ex vivo* bioreactor designed by Mundargi et al. consists of a chamber containing the selected artery placed in an aluminium block with control of the temperature. The circulation of the medium from the reservoir to the vessel is obtained with a peristaltic pump. Adapted from Mundargi et al.[46].

2.2.1.2 Tissue-engineered vascular models

The expansion of tissue engineering has provided in the last decades an increasingly larger number of three-dimensional models, including spheroids, hydrogels, ECM-derived matrices, scaffolds, and decellularised tissues and organs [66]. Biomaterials act as support for the culture of multiple types of cells, eventually in combination with genes, growth factors and ECM components [47]. One of the major advantage derived by the use of tissue-engineered vascular models is the possibility to finely tune the mechanical and architectural properties of biomaterials, varying their stiffness, their porosity and pore size [67, 68, 69]. Moreover, biomaterials offer the possibility to incorporate surface-binding ligands and antibodies to encourage specific cell adhesion[70, 71]. The three-dimensional constructs can be exposed to biochemical stimuli [72], and dynamic forces can be applied to investigate responses observed *in vivo*[73, 74, 75]. In addition, the perfused bioengineered vascular construct can be realized using both animal or human cells, and these cells could be obtained from healthy subjects or patients [75]. Innovative biofabrication techniques, advanced cell manipulation, and the use of bioreactors to apply physiological conditions are used to mimic the biological structures[47] (Figure 2.4).

In the field of cardiovascular diseases, for example, Martorell et al. investigated the relationship between flow disruption and local expression of atherogenic markers. The model was realized seeding ECs and SMCs on PDMS scaffolds presenting patient-specific vessel bifurcation geometries (*i.e.,* coronary and carotid bifurcations) [76].

Rouleau et al., instead, developed a model to keep in consideration also the complex interactions between arterial wall cells and immune system in atherosclerotic lesions. In their study, in fact, they presented a stenosis model consisting of a fibronectin-coated silicone tube seeded with human aortic ECs. The cells were exposed to varying shear stress and it was studied the correlation between haemodynamic forces and adhesion of leukocytes to ECs, either stimulated or not stimulated with TNF-α[77, 78].

To study initial events occurring in atherosclerosis, Robert et al. used human vascular cells to develop a three-dimensional artery model mimicking the structures and the functional characteristics of arteries. The vascular construct consisted of biodegradable tubular scaffolds made of non-woven polyglycol-acid meshes seeded with human umbilical vein endothelial cells and human umbilical cord derived myofibroblasts. During the exposure to dynamic conditions within a bioreactor, fluorescent labelled LDL and labelled monocytes were injected to mimic early events occurring in the atherosclerosis progression.
Then, the system was used to investigate the effects induced by the TNF-α on the monocytes migration, and the anti-atherosclerotic potential of high density lipoproteins in the arterial wall.

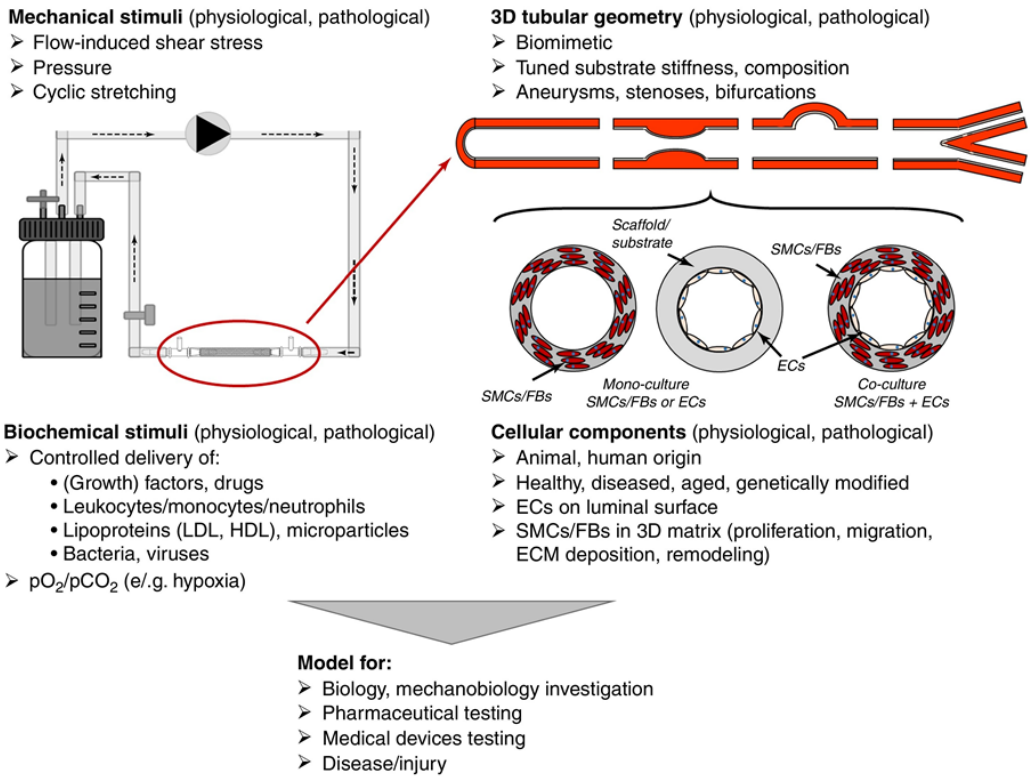

Figure 2.4: Schematic representation of the characteristics of tissue-engineered vessels. Tissue-engineered vessels combined with bioreactors can be exposed both to biomechanical and biochemical stimuli. Different characteristics can be obtained by changing the geometry of the scaffolds and the cell components. Models can be used to investigate physiology of biological tissue but also for the pre-clinical test of drugs and medical devices or for modelling diseases. From Wolf et al. [75]

The model proposed by Robert and colleagues showed a good combination of a native-like multilayer three-dimensional architecture of the vascular wall with native-analogous pulsatile flow profiles and proved to be a reliable atherosclerosis disease model [79].

A tissue-engineered model was proposed by Mallone et al. to replicate and study, instead, the mechanisms involved in atherosclerotic plaques progression and regression. The work describes a complex human model of late atherosclerotic lesion consisting of a core of monocytes, macrophages and dendritic cells embedded in a matrix of collagen and lipids,surrounded by a thin layer of myofibroblasts. The model was exploited to investigate the role of LDL in plaque remodeling and cell viability[80].

Finally, tissue engineering-derived vascular grafts will potentially become a valid alternative to animal models for pre-clinical assessment of medical device and pharmacological treatments [75].
Cardinal and colleagues, used a tissue-engineered blood vessel as a testing envir-

onment for stents. Their aim was to evaluate the sensitivity of this model towards different kinds of stents. As a proof of concept, they modified a stent through adsorption of ECM proteins and evaluated with the model the different cellular regeneration induced by bare metal stents and modified stents. The results proved the capability of this model to distinguish effects induced by different medical devices [81].
Fernandez et al., instead, proposed a platform with a tissue-engineered vessel to evaluate drug-induced vasodilation under arterial-like flow conditions. They developed a collagen-based engineered blood vessel and assessed the role played by ECs in modulating vasodilation through the release of NO. In addition they used the model to study the acute inflammatory response induced by TNF-α and the potential therapeutic effect of the exposure to lovastatin, a statin, prior to exposure to TNF-α[82].

Although great advances have been made in the field of vascular tissue engineering, important efforts are still required towards an increased physiological relevance, necessary for disease modelling and device and drug testing [47]. Nevertheless, the rapid progression of bioengineering and biotechnology suggest that tissue engineering-derived models are likely to be successfully used in the near future for disease modelling and medicine screening [83, 84].

2.3 Conclusions

Cardiovascular diseases and atherosclerosis have been one of the biggest issue that the healthcare of the developed countries has been facing for the last decades.

The complicated network of risk factors, pathological cues, and cell interactions has been widely studied, but the complexity of the phenomenon still needs to be unveiled.

As largely debated in this chapter, the approaches involved in the study of the atherosclerosis are mainly three: *in vitro*, *in vivo* and *ex vivo* models.

In vitro models are the golden standard for the preliminary investigation of mechanisms involved in the atherosclerotic process, thanks to their ease and the possibility to isolate specific stimuli. On the other hand, they lack of the complexity required for studying a problem as complicated as atherosclerosis.

In vivo models, instead, allow to replicate the physiological or pathological environment and they are still unavoidable for the pre-clinical assessment of drugs and medical devices, but they have many drawbacks. Firstly, there are problems in translating the results to human due to differences in the immune system of mammalian species, secondly they are very expensive, and, finally, the ethical implication involved in these studies pushed the scientific community towards a reduce, replacement and refinement of animal models.

Ex vivo models, as shown, allow to replicate more realistic conditions than *in vitro* studies, maintaining the complexity of the native tissue, and they could be a valid aid for screening potential therapeutic solutions, reducing the product development cycle by implementing different prototype modifications in *ex vivo* models.
Ex vivo models using bioreactors to stimulate whole tissue/organs have been well established, whereas the use of tissue-engineered vascular model is very promising but still needs efforts to reach more realistic architecture and composition of the construct.

In conclusion, *ex vivo* models offer an important multi-disciplinary approach towards the investigation of physiological and pathological aspects of the cardiovascular system; the cooperation among bioengineers, biologists, biotechnologist and doctors can lead to more and more exhaustive and realistic *ex vivo* models. This can certainly bring to an increasingly complete comprehension of the phenomena involved in atherosclerosis and to innovative and decisive clinical treatments.

Bibliography

[1] M. Harangi, P. Szodoray, and G. Paragh. Atherosclerosis: A complex interplay of inflammatory processes. *Future Lipidology*, 4(2):167–187, 2009.

[2] K. Islam, S. B. H. Timraz, R. Nasser, et al. Co-culture Methods Used to Model Atherosclerosis In Vitro Using Endothelial, Smooth Muscle and Monocyte Cells. *SM Journal of Biomedical Engineering*, 2(1):1008, 2016.

[3] A. J. Lusis. Atherosclerosis. *Nature*, 407(6801):233–241, 2000.

[4] I. Soltero-Pérez. Toward a new definition of atherosclerosis including hypertension: A proposal. *Journal of Human Hypertension*, 16((Suppl 1)):S23–S25, 2002.

[5] E. R. Zakiev, N. G. Nikiforov, and A. N. Orekhov. Cell-Based Models for Development of Antiatherosclerotic Therapies. *BioMed Research International*, 2017:1–8, 2017.

[6] K. H. Benam, S. Dauth, B. Hassell, et al. Engineered In Vitro Disease Models. *Annual Review of Pathology: Mechanisms of Disease*, 10(1):195–262, 2015.

[7] S. Lalonde, V.-A. Codina-Fauteux, S. M. de Bellefon, et al. Integrative analysis of vascular endothelial cell genomic features identifies AIDA as a coronary artery disease candidate gene. *Genome Biology*, 20(1):133, 2019.

[8] M. Vicen, B. Vitverova, R. Havelek, et al. Regulation and role of endoglin in cholesterol-induced endothelial and vascular dysfunction in vivo and in vitro. *FASEB journal : official publication of the Federation of American Societies for Experimental Biology*, 33(5):6099–6114, 2019.

[9] M. C. Zuniga, S. L. White, and W. Zhou. Design and utilization of macrophage and vascular smooth muscle cell co-culture systems in atherosclerotic cardiovascular disease investigation. *Vascular Medicine (United Kingdom)*, 19(5):394–406, 2014.

[10] S. Wang, S. Hu, J. Wang, et al. Conditioned medium from bone marrow-derived mesenchymal stem cells inhibits vascular calcification through blockade of the BMP2 Smad1 5 8 signaling pathway. *Stem Cell Research & Therapy*, 9(1):160, 2018.

[11] A. J. Noonan, G. Grassia, N. MacRitchie, et al. A novel triple-cell two-dimensional model to study immune vascular interplay in atherosclerosis. *Frontiers in Immunology*, 10:849, 2019.

[12] C. Huang, J. Han, Y. Wu, et al. Exosomal MALAT1 derived from oxidized low-density lipoprotein-treated endothelial cells promotes M2 macrophage polarization. *Molecular Medicine Reports*, 18(1):509–515, 2018.

[13] H. Gao, W. XiaoLi, L. Chaolan, et al. Exosomal MALAT1 derived from ox-LDL-treated endothelial cells induce neutrophil extracellular traps to aggravate atherosclerosis, 2019.

[14] M. D. Lavender, Z. Pang, C. S. Wallace, L. E. Niklason, and G. A. Truskey. A system for the direct co-culture of endothelium on smooth muscle cells. *Biomaterials*, 26(22):4642–4653, 2005.

[15] B. Dorweiler, M. Torzewski, M. Dahm, et al. A novel in vitro model for the study of plaque development in atherosclerosis. *Thrombosis and Haemostasis*, 95(01):182–189, 2006.

[16] A. Rezvan, C.-W. Ni, N. Alberts-Grill, and H. Jo. Animal, In Vitro , and Ex Vivo Models of Flow-Dependent Atherosclerosis: Role of Oxidative Stress. *Antioxidants & Redox Signaling*, 15(5):1433–1448, 2011.

[17] M. Franzoni, I. Cattaneo, B. Ene-Iordache, et al. Design of a cone-and-plate device for controlled realistic shear stress stimulation on endothelial cell monolayers. *Cytotechnology*, 68(5):1885–1896, 2016.

[18] B. R. Slegtenhorst, O. R. Fajardo Ramirez, Y. Zhang, et al. A Mechano-Activated Cell Reporter System as a Proxy for Flow-Dependent Endothelial Atheroprotection. *SLAS DISCOVERY: Advancing Life Sciences R&D*, 23(8):869–876, 2018.

[19] U. M. Balaguru, L. Sundaresan, J. Manivannan, et al. Disturbed flow mediated modulation of shear forces on endothelial plane: A proposed model for studying endothelium around atherosclerotic plaques. *Scientific Reports*, 6(May):1–15, 2016.

[20] Z. Wang, F. Wang, X. Kong, et al. Oscillatory Shear Stress Induces Oxidative Stress via TLR4 Activation in Endothelial Cells. *Mediators of Inflammation*, 2019:1–13, 2019.

[21] N. Erbeldinger, F. Rapp, S. Ktitareva, et al. Measuring Leukocyte Adhesion to (Primary) Endothelial Cells after Photon and Charged Particle Exposure with a Dedicated Laminar Flow Chamber. *Frontiers in Immunology*, 8:627, 2017.

[22] J.-J. Chiu and S. Chien. Effects of Disturbed Flow on Vascular Endothelium: Pathophysiological Basis and Clinical Perspectives. *Physiological Reviews*, 91(1):327–387, 2011.

[23] J. Zilberman-Rudenko, J. L. Sylman, K. S. Garland, et al. Utility of microfluidic devices to study the platelet endothelium interface. *Platelets*, 28(5):449–456, 2017.

[24] E. Westein, A. D. van der Meer, M. J. E. Kuijpers, et al. Atherosclerotic geometries exacerbate pathological thrombus formation poststenosis in a von Willebrand factor-dependent manner. *Proceedings of the National Academy of Sciences of the United States of America*, 110(4):1357–1362, 2013.

[25] B. Zhang, C. Peticone, S. K. Murthy, and M. Radisic. A standalone perfusion platform for drug testing and target validation in micro-vessel networks. *Biomicrofluidics*, 7(4):44125, 2013.

[26] D. Alan, T. A. R., D. M. J.A.P., et al. Recommendation on Design, Execution, and Reporting of Animal Atherosclerosis Studies: A Scientific Statement From the American Heart Association. *Circulation Research*, 121(6):e53–e79, sep 2017.

[27] F. R. Kapourchali, G. Surendiran, L. Chen, et al. Animal models of atherosclerosis. *World journal of clinical cases*, 2(5):126–132, may 2014.

[28] B. Emini Veseli, P. Perrotta, G. R. A. De Meyer, et al. Animal models of atherosclerosis. *European Journal of Pharmacology*, 816(2017):3–13, 2017.

[29] G. S. Getz and C. A. Reardon. Animal Models of Atherosclerosis. *Arterioscler Thromb Vasc Biol*, 32(5):1104–1115, 2012.

[30] C. Wu, A. Daugherty, and H. S. Lu. Updates on Approaches for Studying Atherosclerosis. *Arteriosclerosis, thrombosis, and vascular biology*, 39(4):e108–e117, 2019.

[31] A. Vromman, V. Ruvkun, E. Shvartz, et al. Mechanistic Insights to the Differential Effects of Interleukin-1 Isoforms on Experimental Atherosclerosis. *Atherosclerosis Supplements*, 32:105, 2018.

[32] M. Kiss, N. Papac-Milicevic, D. Tsiantoulas, et al. Hematopoietic complement factor h deficiency reduces atherosclerosis in LDR deficient mice. *Atherosclerosis*, 263:e58–e59, 2017.

[33] J. Fan, S. Kitajima, T. Watanabe, et al. Rabbit models for the study of human atherosclerosis: from pathophysiological mechanisms to translational medicine. *Pharmacology & therapeutics*, 146:104–119, 2015.

[34] X. Nie, R. Laforest, A. Elvington, et al. PET/MRI of Hypoxic Atherosclerosis Using 64Cu-ATSM in a Rabbit Model. *Journal of Nuclear Medicine*, 57(12):2006–2011, 2016.

[35] J. F. Granada, G. L. Kaluza, R. L. Wilensky, et al. Porcine models of coronary atherosclerosis and vulnerable plaque for imaging and interventional research. *EuroIntervention*, 5(1):140–148, 2009.

[36] J. K. Badin, A. Kole, B. Stivers, et al. Alloxan-induced diabetes exacerbates coronary atherosclerosis and calcification in Ossabaw miniature swine with metabolic syndrome. *Journal of Translational Medicine*, 16(1):58, 2018.

[37] L. A. Cox, M. Olivier, K. Spradling-Reeves, et al. Nonhuman Primates and Translational Research Cardiovascular Disease. *ILAR Journal*, 58(2):235–250, 2017.

[38] M. Tadin-Strapps, M. Robinson, L. Le Voci, et al. Development of Lipoprotein(a) siRNAs for Mechanism of Action Studies in Non-Human Primate Models of Atherosclerosis. *Journal of Cardiovascular Translational Research*, 8(1):44–53, 2015.

[39] W. M. S. Russel and R. L. Burch. *The principles of humane experimental technique*. London, Methuen, 1959.

[40] J. Tannenbaum and B. T. Bennett. Russell and Burch's 3Rs then and now: the need for clarity in definition and purpose. *Journal of the American Association for Laboratory Animal Science : JAALAS*, 54(2):120–132, 2015.

[41] L. Hung, H. Obernolte, K. Sewald, and T. Eiwegger. Human ex vivo and in vitro disease models to study food allergy. *Asia Pacific allergy*, 9(1):e4–e4, 2019.

[42] A. J. A. Leloup, C. E. Van Hove, A. Kurdi, et al. A novel set-up for the ex vivo analysis of mechanical properties of mouse aortic segments stretched at physiological pressure and frequency. *The Journal of physiology*, 594(21):6105–6115, 2016.

[43] M. Piola, F. Prandi, G. B. Fiore, et al. Human Saphenous Vein Response to Trans-wall Oxygen Gradients in a Novel Ex Vivo Conditioning Platform. *Annals of Biomedical Engineering*, 44(5):1449–1461, 2016.

[44] C. R. Becker, K. Nikolaou, M. Muders, et al. Ex vivo coronary atherosclerotic plaque characterization with multi-detector-row CT. *European Radiology*, 13(9):2094–2098, 2003.

[45] D. Larsson, J. Roy, T. C. Gasser, et al. An ex-vivo setup for characterization of atherosclerotic plaque using shear wave elastography and micro-computed tomography. In *IEEE International Ultrasonics Symposium, IUS*, 2016.

[46] R. Mundargi, D. Venkataraman, S. Kumar, et al. Novel Sensor-Enabled Ex Vivo Bioreactor : A New Approach towards Physiological Parameters and Porcine Artery Viability. *BioMed Research International*, 2015:8, 2015.

[47] A. J. Ryan, C. M. Brougham, C. D. Garciarena, S. W. Kerrigan, and F. J. O'Brien. Towards 3D in vitro models for the study of cardiovascular tissues and disease. *Drug Discovery Today*, 21(9):1437–1445, 2016.

[48] M. Peroglio, D. Gaspar, D. I. Zeugolis, and M. Alini. Relevance of bioreactors and whole tissue cultures for the translation of new therapies to humans. *Journal of Orthopaedic Research*, 36(1):10–21, 2018.

[49] I. Tabas, G. García-Cardeña, and G. K. Owens. Recent insights into the cellular biology of atherosclerosis. *Journal of Cell Biology*, 209(1):13–22, 2015.

[50] D. A. Chistiakov, A. N. Orekhov, and Y. V. Bobryshev. Effects of shear stress on endothelial cells: go with the flow. *Acta Physiologica*, 219(2):382–408, 2017.

[51] I. C. Harding, R. Mitra, S. A. Mensah, I. M. Herman, and E. E. Ebong. Pro-atherosclerotic disturbed flow disrupts caveolin-1 expression, localization, and function via glycocalyx degradation. *Journal of Translational Medicine*, 16(1):1–20, 2018.

[52] X. Lu and G. S. Kassab. Nitric oxide is significantly reduced in ex vivo porcine arteries during reverse flow because of increased superoxide production. *The Journal of physiology*, 561(Pt 2):575–582, 2004.

[53] A. Leloup, S. De Moudt, C. Van Hove, and P. Fransen. Cyclic Stretch Alters Vascular Reactivity of Mouse Aortic Segments. *Frontiers in physiology*, 8:858, 2017.

[54] E. P. C. van der Vorst, Y. Döring, and C. Weber. Chemokines and their receptors in Atherosclerosis. *Journal of molecular medicine (Berlin, Germany)*, 93(9):963–971, 2015.

[55] A. Aarup, T. X. Pedersen, N. Junker, et al. Hypoxia-inducible factor-1α expression in macrophages promotes development of atherosclerosis. *Arteriosclerosis, Thrombosis, and Vascular Biology*, 36(9):1782–1790, 2016.

[56] J. W. Moss and D. P. Ramji. Cytokines: roles in atherosclerosis disease progression and potential therapeutic targets. *Future medicinal chemistry*, 8(11):1317–1330, 2016.

[57] G. C. Alexander, J. B. Vines, P. Hwang, et al. Novel Multifunctional Nanomatrix Reduces Inflammation in Dynamic Conditions in Vitro and Dilates Arteries ex Vivo. *ACS applied materials & interfaces*, 8(8):5178–5187, 2016.

[58] R. M. Hoffman. Three-dimensional histoculture: origins and applications in cancer research., 1991.

[59] L. N. Li, L. B. Margolis, and R. M. Hoffman. Skin toxicity determined in vitro by three-dimensional, native-state histoculture. *Proceedings of the National Academy of Sciences*, 88(5):1908–1912, 2006.

[60] A. Lebedeva, D. Vorobyeva, M. Vagida, et al. Ex vivo culture of human atherosclerotic plaques: A model to study immune cells in atherogenesis. *Atherosclerosis*, 267:90–98, 2017.

[61] M. H. Kural, G. Dai, L. E. Niklason, and L. Gui. An Ex Vivo Vessel Injury Model to Study Remodeling. *Cell Transplantation*, 27(9):1375–1389, 2018.

[62] D. Gastaldi, S. Morlacchi, R. Nichetti, et al. Modelling of the provisional side-branch stenting approach for the treatment of atherosclerotic coronary

bifurcations: Effects of stent positioning. *Biomechanics and Modeling in Mechanobiology*, 9(5):551–561, 2010.

[63] K. Yahagi, F. D. Kolodgie, F. Otsuka, et al. Pathophysiology of native coronary, vein graft, and in-stent atherosclerosis. *Nature Reviews Cardiology*, 13(2):79, 2015.

[64] M. A. Punchard, C. Stenson-Cox, E. D. O'Cearbhaill, et al. Endothelial cell response to biomechanical forces under simulated vascular loading conditions. *Journal of Biomechanics*, 40(14):3146–3154, 2007.

[65] M. A. Punchard, E. D. O'Cearbhaill, J. N. Mackle, et al. Evaluation of Human Endothelial Cells Post Stent Deployment in a Cardiovascular Simulator In Vitro. *Annals of Biomedical Engineering*, 37(7):1322–1330, 2009.

[66] S. A. Langhans. Three-Dimensional in Vitro Cell Culture Models in Drug Discovery and Drug Repositioning. *Frontiers in Pharmacology*, 9:1–6, 2018.

[67] G. Chen, C. Dong, L. Yang, and Y. Lv. 3D Scaffolds with Different Stiffness but the Same Microstructure for Bone Tissue Engineering. *ACS Applied Materials and Interfaces*, 7(29):15790–15802, 2015.

[68] E. Entekhabi, M. Haghbin Nazarpak, F. Moztarzadeh, and A. Sadeghi. Design and manufacture of neural tissue engineering scaffolds using hyaluronic acid and polycaprolactone nanofibers with controlled porosity. *Materials Science and Engineering: C*, 69(2016):380–387, 2016.

[69] A. Di Luca, B. Ostrowska, I. Lorenzo-Moldero, et al. Gradients in pore size enhance the osteogenic differentiation of human mesenchymal stromal cells in three-dimensional scaffolds. *Scientific Reports*, 6(February):1–13, 2016.

[70] E. B. Peters, N. Christoforou, K. W. Leong, G. A. Truskey, and J. L. West. Poly(Ethylene Glycol) Hydrogel Scaffolds Containing Cell-Adhesive and Protease-Sensitive Peptides Support Microvessel Formation by Endothelial Progenitor Cells. *Cellular and Molecular Bioengineering*, 9(1):38–54, 2016.

[71] A. S. Cheung, D. K. Y. Zhang, S. T. Koshy, and D. J. Mooney. Scaffolds that mimic antigen-presenting cells enable ex vivo expansion of primary T cells. *Nature Biotechnology*, 36(2):160, 2018.

[72] E. Quinlan, S. Partap, M. M. Azevedo, et al. Hypoxia-mimicking bioactive glass/collagen glycosaminoglycan composite scaffolds to enhance angiogenesis and bone repair. *Biomaterials*, 52(2015):358–366, 2015.

[73] D. Seliktar, R. A. Black, R. P. Vito, and R. M. Nerem. Dynamic Mechanical Conditioning of Collagen-Gel Blood Vessel Constructs Induces Remodeling In Vitro. *Annals of Biomedical Engineering*, 28(4):351–362, 2000.

[74] A. M. Throm Quinlan, L. N. Sierad, A. K. Capulli, L. E. Firstenberg, and K. L. Billiar. Combining Dynamic Stretch and Tunable Stiffness to Probe Cell Mechanobiology In Vitro. *PLOS ONE*, 6(8):e23272, 2011.

[75] F. Wolf, F. Vogt, T. Schmitz-rode, S. Jockenhoevel, and P. Mela. Bioengineered vascular constructs as living models for in vitro cardiovascular research. *Drug Discovery Today*, 21(9):1446–1455, 2016.

[76] J. Martorell, P. Santoma, K. Kolandaivelu, et al. Extent of flow recirculation governs expression of atherosclerotic and thrombotic biomarkers in arterial bifurcations. *Cardiovascular Research*, 103(1):37–46, 2014.

[77] L. Rouleau, I. B. Copland, J.-C. Tardif, R. Mongrain, and R. L. Leask. Neutrophil Adhesion on Endothelial Cells in a Novel Asymmetric Stenosis Model: Effect of Wall Shear Stress Gradients. *Annals of Biomedical Engineering*, 38(9):2791–2804, 2010.

[78] L. Rouleau, M. Farcas, J.-C. Tardif, R. Mongrain, and R. L. Leask. Endothelial Cell Morphologic Response to Asymmetric Stenosis Hemodynamics: Effects of Spatial Wall Shear Stress Gradients. *Journal of Biomechanical Engineering*, 132(8):81010–81013, 2010.

[79] J. Robert, B. Weber, L. Frese, et al. A Three-Dimensional Engineered Artery Model for In Vitro Atherosclerosis Research. *PLOS ONE*, 8(11):e79821, 2013.

[80] A. Mallone, C. Stenger, A. V. Eckardstein, S. P. Hoerstrup, and B. Weber. Biomaterials Biofabricating atherosclerotic plaques : In vitro engineering of a three- dimensional human fi broatheroma model. *Biomaterials*, 150(2018):49–59, 2018.

[81] K. O. H. Cardinal, D. Ph, S. K. Williams, and D. Ph. Assessment of the Intimal Response to a Protein-Modified Stent in a Tissue-Engineered Blood Vessel Mimic. 15(12):3869–3876, 2009.

[82] C. E. Fernandez, R. W. Yen, S. M. Perez, et al. Human Vascular Microphysiological System for in vitro Drug Screening. *Nature Scientific Report*, 6(February):1–14, 2016.

[83] A. Khademhosseini and R. Langer. A decade of progress in tissue engineering. *Nature Protocols*, 11(10):6–9, 2016.

[84] B. Weber and S. P. Hoerstrup. Human Bioengineered Artery Models for In Vitro Atherosclerosis Research: Fact or Fiction? *Alternatives to Laboratory Animals*, 42(3):P28–P32, 2014.

Chapter 3

Design of a parallel-plate flow chamber for the investigation of cellular components involved in thrombus formation

3.1 Introduction

The formation of thrombi represents the acute manifestation of atherosclerosis [1, 2]. The development of clots is typically triggered by the rupture or, less frequently, by the erosion of an atherosclerotic plaque [3, 4]. At that site, the content of plaque and the subendothelial collagen fibres are exposed to the blood flow within the lumen of the vessel. Platelets are then activated and rapidly recruited, increasing the dimension of the clot, which is stabilized by fibrin. In fact, the exposure of tissue factor (TF), an integral membrane-protein located in the subendothelial area, initiates the coagulation cascade with generation of thrombin, that in turn activates platelets and converts fibrinogen in fibrin [5, 1, 6].

Although it is generally accepted that the trigger of coagulation and thrombus formation is the exposure of TF [7], the mechanisms of thrombus propagation and the identities of the molecular species involved in this process still need to be investigated [8]. To fulfil this aim, thrombi formation has been induced in animal models with different methods, such as photochemical injury, mechanical or electrical trauma, ferric chloride or vessel ligation [9], but the choice of the proper model and the control of experimental conditions demonstrated to be difficult [10, 11]. By contrast, *in vitro* models provide a precise definition of the biomechanical environment. Therefore, *in vitro* models have been developed to mimic events that are hallmarks of late stages of the disease. From the pioneering work of Frangos et colleagues [12], the formation of thrombi have been induced in parallel-plate flow chambers by coating the chamber surface with pro-thrombotic agents, as collagen, and plaque and thrombus material, such as von Willebrand factor and fibrinogen, and then plating endothelial cells in the chamber [8, 13, 14, 15]. These models led to the identification of some mechanisms involved in late-stage atherosclerosis[16]. Nevertheless, *in vitro* models do not maintain the structural integrity of human arteries, which would provide critical information on thrombus formation [17].

In this work, we developed a new optically-accessible *ex vivo* parallel-plate flow chamber aimed at exposing to a controlled blood flow human tissue with or without atherosclerosis.

A novel disposable device was, in fact, designed to culture sections of arteries under a target shear rate of 500 s^{-1}which corresponds to a physiological shear rate value for arteries [18, 19].

The final scope of the work is to investigate the nature of vascular molecular components interacting with blood, in order to understand mechanism of thrombosis and then propose and assess the effectiveness of potential therapeutic strategies.

The study was performed in collaboration with the Cardiovascular Research Area of IRCSS Ospedale San Raffaele.

3.2 Requirements for the design of the chamber

The PPFCs are thought to expose human tissue to blood flow with a well-controlled shear rate and, as a consequence, shear stress. The geometrical characteristics of the chamber are then derived from the fluid-dynamic parameters.

One major constraint when dealing with blood is the unintended coagulation. Therefore, the materials must be compatible with blood. In addition, it is necessary to reach a good compromise with the time of stimulation, which has to be enough to stimulate the tissue but at the same time restricted to avoid unspecific coagulation, due to blood exposure to air [20]. Finally, another drawback is related to the withdrawal of blood; in fact, the volume of blood that could be withdrawn from a donor for a single experiment is limited, and this limitation must be kept in consideration when designing the chamber.

The PPFCs developed in this work are disposable, so the costs and the manufacturing techniques must be suitable for mass-production.

To meet the needs of biologists and to fulfil the requirement of good laboratory practice, chambers must guarantee an easy assembling and be compatible with standard laboratory procedures, to avoid damages to the samples due to manipulations.

A further necessary characteristic is related to the transparency of the devices; in fact, they are designed to be optically accessible for visual check during the experiment and to allow microscope imaging. Moreover, the overall dimensions of the chambers must be small to fit microscope space.

Finally, one need is related to the possibility to perform the analysis (*i.e.,* immunofluorescence staining) on the samples after the stimulation. Two possible strategies are kept in consideration: (i) designing a chamber that could be opened after the stimulation for collecting the sample, and (ii) designing a device suitable for performing the staining directly within the chamber.

3.3 Materials and methods

3.3.1 Design of the parallel-plate flow chamber

The PPFC was designed for stimulating sections of arteries with a controlled shear rate and shear stress.
The relationship between fluid-dynamic parameters, such as shear rate ($\dot{\gamma}$) and wall shear stress (τ_w) , and geometrical characteristics of the PPFC, such as flow rate (Q), chamber width (w) and chamber height (h) were derived from the Navier-Stokes and the continuity equation under the hypothesis of Newtonian incompressible fluid and laminar flow [21, 22].

The profile of the flow within the chamber must be evaluated by means of the Reynolds number (Re), which is calculated using the Eq. 3.1:

$$Re = \frac{\rho Q D_h}{\mu w h} \tag{3.1}$$

where ρ and μ are, respectively, the density and the viscosity of the fluid and $D_h$is the hydraulic diameter
Under the hypothesis of Newtonian incompressible fluid and laminar flow and referring to the coordinate system shown in Figure3.1.a, the Navier-Stokes equation can be simplified to Eq. 3.2 :

$$\frac{d^2v}{dy^2} = \frac{1}{\mu}\frac{dP}{dx} \tag{3.2}$$

where (dP/dx) is the pressure gradient along the plate, v is the fluid velocity, and y is a height position with respect to the bottom plate.
Integrating twice and after applying the no slip condition, the following equation (Eq. 3.3) was obtained:

$$v_x = \frac{1}{2\mu}\left(\frac{dP}{dx}\right)\left[\left(\frac{h}{2}\right)^2 - y^2\right] \tag{3.3}$$

The relationship among shear stress (τ), shear rate and geometrical parameters of the chamber was derived from the continuity equation (Eq. 3.4) :

$$Q = \iint_A v_x dA = w\int_0^h \frac{1}{2\mu}\frac{dP}{dx}(h^2 - y^2)dy \tag{3.4}$$

combined with the expression of τ (Eq. 3.5):

$$\tau = \mu\dot{\gamma} = \mu\frac{dv}{dy} \tag{3.5}$$

It was finally obtained the expression of the wall shear stress, expressed in Eq. 3.6:

$$\tau_w = \mu\dot{\gamma} = \frac{6\mu Q}{wh^2} \tag{3.6}$$

Shear rate and shear stress profiles in laminar flow are shown in Figure 3.1.b.

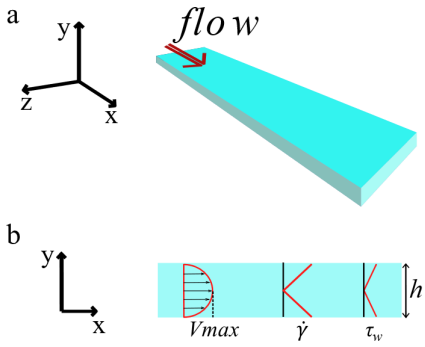

Figure 3.1: Determination of fluid-dynamic and geometrical parameters in a parallel-plate flow chamber. (a) The Navier-Stokes equation for parallel-plate flow chamber is solved with the coordinate system shown in the figure. (b) The shear rate ($\dot{\gamma}$) and the wall shear stress (τ_w) are related to the slope of the velocity (v) within the parallel-plate flow chamber. The flow velocity in a laminar developed flow has a typical parabolic profile.

The value of blood flow rate during the experiments was calculated considering a volume of blood of 10 ml and a time of stimulation of 6 minutes for each experiment.
Given a precise value of height of the chamber and applying the Eq. 3.6 the width of the chamber was derived.
Once obtained the geometrical characteristics, the Reynolds number can be calculated to verify the hypothesis of laminar flow within the chamber (Eq. 3.1).
The minimum length of the PPFC and the position of the tissue sample along the x-axis were established applying the formula in Eq. 3.7 to have a fully developed flow profile [23]:

$$x = 0.06 \cdot Re \cdot D_h \tag{3.7}$$

The shape of the chamber was designed to limit abrupt changes of section.

Two different versions were designed: (i) a version with a lid that can be removed, and (ii) a closed version (Figure 3.2).

3.3.2 Manufacturing of the parallel-plate chamber

The disposable PPFCs were manufactured by laser cutting (VersaLaser VSL 2.30, SK Laser, Germany). Each device is composed by a transparent poly(methyl methacrylate) (PMMA, Plasting S.r.l., Italy) support, a double-sided sticky tape (High Performance Adhesive Transfer Tape with Adhesive 200 MP 92015, 3M Italia srl, Italy) and a 24 x 50 mm^2coverslip. The flow chamber is obtained laser cutting with the desired geometry the tape, which is stuck to the support and also provides the tightly sealing of the coverslip to the PMMA support. In the support two channels are cut and barbed polysulfone connectors (PS, Nordson

Corporation, OH, US) glued to the support act as inlet and outlet for the blood flow. In the version with the lid, the lid is stuck to chamber using again the double-sided sticky tape. (Figure 3.2).

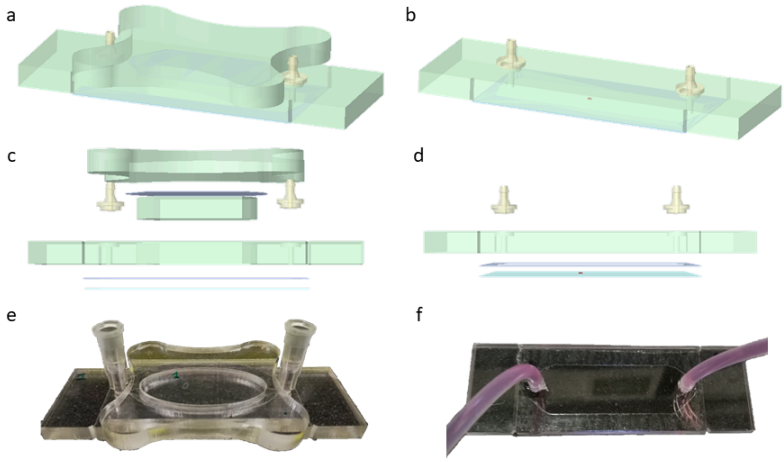

Figure 3.2: Three dimensional drawings and pictures of the two versions of the parallel-plate flow chamber. (a) and (b) show the computer-aided design (CAD) models of, respectively, the version of the parallel-plate flow chamber (PPFC) that can be opened, and the closed version. In the former version the lid and the support are assembled through double-sided tape, the design of the latter version is evidently much simpler. In (c) and (d) is shown the exploded view of, respectively, the PPFC that can be opened, and the closed one. Starting from the bottom, it is possible to identify the coverslip, the tape where the flow chamber is obtained, the support and connectors. (e) and (d) are pictures of the two different versions of the PPFC.

3.3.3 Characterization of the parallel-plate flow chamber

The values of shear rate within the parallel-plate fluid chamber were assessed through fluid-dynamic computational studies. In addition, the resistivity of the chamber was evaluated by an hydraulic characterization of the system . Finally, experiments were performed to evaluate the functionality and the thrombogenicity of the chamber.

3.3.3.1 Study of the fluid dynamic pattern with numerical studies

Fluid-dynamic studies were performed using the software Comsol Multiphysics 4.3 b (Comsol Inc., CA, US). It was simulated only a part of the fluid volume of the chamber (Figure 3.3.a), to guarantee the possibility to create a fine mesh along the y axis (Figure 3.3.b), but limiting the computational cost. It was chosen water as material of the fluid domain, but the value of viscosity was set equal to 0.003 Pa.s, to mimic rheological blood characteristics. It was imposed an inlet velocity of fluid equal to 0.013 m/s and a relative pressure at the outlet equal to zero. Symmetry along x-axis and no slip condition in the lateral walls were finally set.

3.3.3.2 Hydraulic characterization of the system

The PPFCs were characterized in terms of hydraulic resistance with the setup shown in Figure 3.3.c. Briefly, a PPFC was connected downstream to a withdrawal syringe pump (AL-100, World Precision Instrument, FL, US) and upstream to a reservoir open in atmosphere. The hydraulic circuit was realized with platinum cured silicone tubing (Saint Gobain, France). A pressure transducer (Pendotec Press, NJ, US) connected to a custom made acquisition system (LabView software, National Instruments Corp., TX, USA) was placed downstream of the chamber. The pressure was measured at different flow rate values (1.00, 1.66, 3.32, 5.00, 10.00 ml/min). The hydraulic resistance of the system was calculated applying Eq. 3.8:

$$\triangle P = R_h \cdot Q \tag{3.8}$$

where $\triangle P$ is the pressure loss along the system and R_h the hydraulic resistance of the system.
For each flow rate, three tests were conducted and in total n=8 chambers were characterized.

3.3.3.3 Functional evaluation of the parallel-plate flow chamber

The functional evaluation of the two versions of the device was performed in experiments with human blood. Experiments without biological samples were firstly performed to assess the ease-of-use of the chamber , the fluid-dynamics and the thrombogenicity of the devices. Experiments using arterial sections were then conducted to verify the possibility to stain blood and tissue components involved in thrombus formation.
Before each experiment, blood was collected in citrate-phosphate-dextrose (CPD) anticoagulant solution [24] and re-calcified immediately before flow experiment. Platelets were labelled with Mepacrine and fibrin by anti-fibrin(ogen)- AlexaFluor 555 antibody.
The setup of the experiments is the same used for the hydraulic characterization and it is shown in Figure 3.3.c and in Figure 3.3.d .
For the experiments without biological sample, briefly, a fibronectin–coated coverslip was stuck to the PPFC. The device was then connected with platinum cured silicone tubing (Saint Gobain, France) to a withdrawal syringe pump (AL-100, World Precision Instrument, FL, US). The chamber was washed with Dulbecco's Modified Eagle Medium (DMEM, EuroClone, Italy), then submitted to blood flow with a flow rate of 1.66 ml/min for 6 minutes. During the experiments, the fluid-dynamics within the chamber was monitored using a handheld digital mi-

croscope (Dino-lite digital microscope, AnMo Electronics Corporation, Taiwan). After the stimulation, a washing with DMEM was performed. Microscopy assessed the formation of unspecific thrombi.

In the experiments with biological samples, a fibronectin-coated coverslip with frozen unfixed section (10 μm thick) of internal mammary artery (IMA) was stuck to PPFC. After the second washing with DMEM, samples underwent fixation in 1% paraformaldehyde. Immunofluorescence were performed on IMA sections into the chamber. As a proof of concept, nuclei were labelled with DAPI and laminin was labelled as component of extracellular matrix. Stainings were analysed by confocal microscopy.

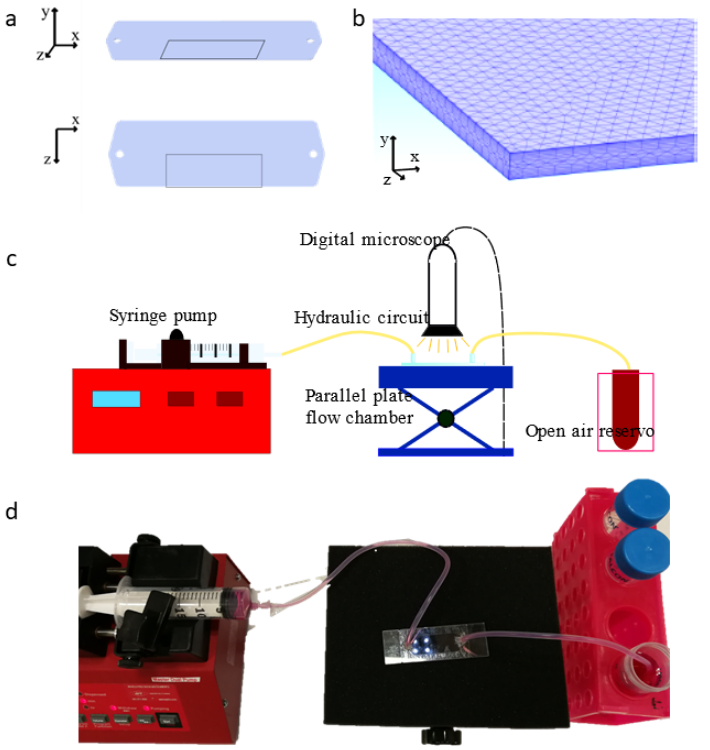

Figure 3.3: Characterization of the parallel-plate flow chamber. (a) Computational studies were performed with the software Comsol Multiphysics on a confined volume of the chamber, corresponding to the black rectangle. (b) Considering a smaller volume it was possible to create a fine mesh also in the y-direction, which is much smaller in comparison to x- and z-directions, without an excessive computational cost (c) Schematic representation of the setup used for the characterization and for the functional experiments. The parallel-plate flow chamber is connected upstream to an open air reservoir and downstream to a withdrawal syringe pump through silicone tubing. A digital microscope was used to monitor the fluid-dynamics within the chamber. For the hydraulic characterization, a pressure transducer was placed in derivation between the syringe pump and the parallel-plate flow chamber to measure the pressure loss over the chamber. (d) Picture of the setup during functional experiments.

3.4 Results

3.4.1 Evaluation of the shear rate obtained within the chamber

The control of the geometrical parameters of the chamber guaranteed a well-defined fluid-dynamic stimulation of the arterial samples. The precise height of the chamber was provided by a double-sided sticky tape with a thickness of 150 ± 6 μm. Combining values of blood volume suitable for performing experiments with human blood and stimulation time, it was set a flow rate of 1.66 ml/min. Therefore, applying the Eq. 3.6 it was found that a width of 14.77 mm was necessary to obtain in the chamber a shear rate of 500 s^{-1}. This value, considering a blood viscosity of about 0.003 Pa•s [25]corresponds to a shear stress of 15 dynes/cm^2. A Reynolds number equal to 3.7 proved that the flow profile within the chamber is laminar. Using the Eq. 3.7 it was calculated that a length of 0.07 mm is necessary for the blood flow to be completely developed after flowing into the chamber.

The computational studies confirmed that within the chamber there is a uniform shear rate of about 500 s^{-1} (Figure 3.4a, b, c, d).

3.4.2 Hydraulic characterization of the chamber

The hydraulic characterization of the chambers allowed to evaluate the pressure losses induced by the PPFC. Data concerning the characterization are shown in Figure 3.4.e. Pressure losses increased linearly, as expected, with increasing flow rate. Keeping in consideration the target flow rate of 1.66 ml/min, the value of pressure measured was equal to -1.92 ± 0.16 mmHg corresponding to a hydraulic resistance of the system of 69.40 mmHg•s/ml. The values of pressure measured at the same flow rate in different chambers are consistent with one another.

3.4.3 Assessment of the functionality of the chamber

Functional experiments confirmed that the PPFC is easy-to-use and compatible with laboratory procedures.

In the experiments with human blood, the double-sided sticky tape proved to guarantee a good sealing of the coverslip to the PMMA support.

The visual inspection of the flow profile within the chambers showed that in the version that can be opened, the presence of the lid induces an alteration of the fluid-dynamic profile (Figure 3.4.f). Moreover, unspecific thrombi were found in the chamber. On the other hand, in the closed version it was seen a fluid-dynamics consistent with theory and no unspecific thrombi where found within the chamber.

Experiments with human IMA sections proved that PPFC are suitable for performing staining within the chamber. The system proved to be compatible with

confocal microscopy. Cellular and ECM components were successfully labelled (Figure 3.5). The presence of unspecific thrombi in the PPFC provided with the lid were noticed even in experiments with human samples, .

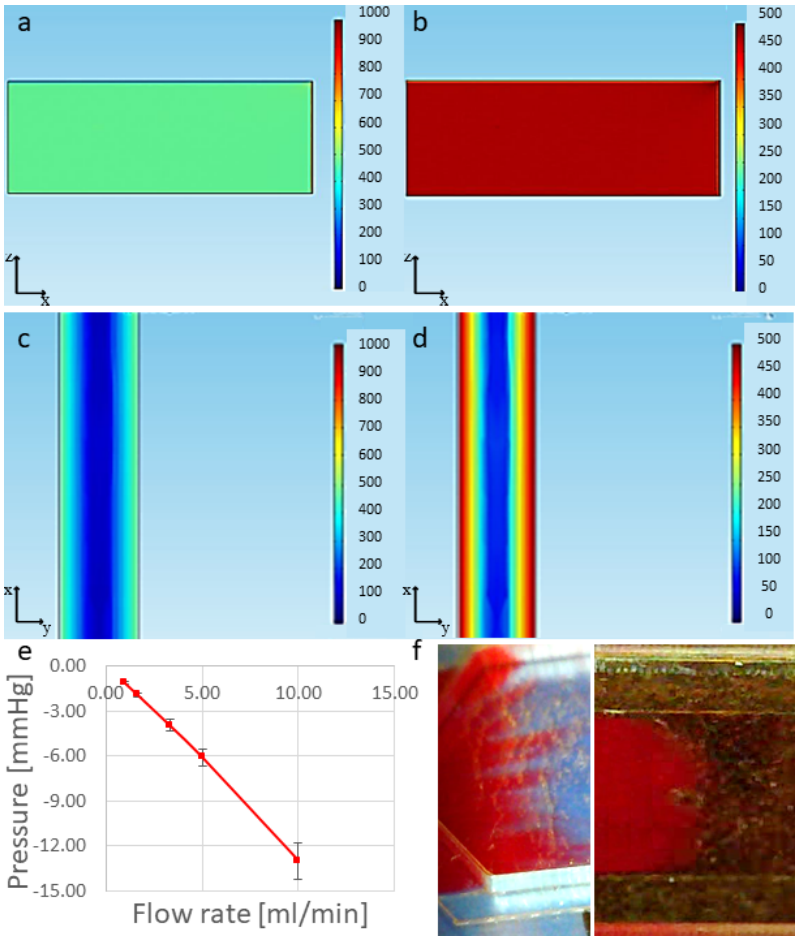

Figure 3.4: Results of the characterization and of the functional evaluation of the parallel-plate flow chamber. (a) According to the results of the numerical study, the shear rate in the plane XZ, evaluated on the floor of the chamber, is equal to 500 s^{-1}. (b) A different scale is shown for a better evaluation. (c) The results calculated in the YX plane confirmed that the target value of shear rate is reached in the chamber and, (d) a different scale is shown for a better evaluation. (e) The results of the hydraulic characterization show a linear relationship between flow rate and pressure, as expected. (f) Functional experiments proved that in chambers provided with lids, the fluid-dynamics is disturbed, as can be seen in the left picture where it is visible a blood flow with a "flame-like" profile. By contrary, chambers without lid are characterized by a parabolic fluid-dynamic profile, as can be seen to the right. This can be responsible for the presence of unspecific thrombi within the chambers with lid.

3.5 Discussion

In this work, an optically-accessible chamber for stimulating sections of human arteries was designed and manufactured. The design of the chamber was thought

to guarantee a specific fluid-dynamic stimulus on the sample. This precise biomechanical condition derived from the combination of fluid-dynamic parameters, geometrical characteristics of the chamber and rheological properties of blood. The choice of some parameters was imposed by physical needs. In fact, the value of flow rate was obtained considering that 6 minutes of conditioning were enough to induce the formation of a thrombus without provoking the detachment of the sample [15] and a volume of human blood of 10 ml allowed to perform at least three tests in the same experiment without being harmful for the donor. The precise height of the chamber was assured by the use of a commercial double-sided sticky tape. This solution contributed also to obtain an easy assembling of the PPFC and, at the same time, a good sealing. It was therefore possible to avoid more complex solutions as screws and gaskets [26, 27, 28], less suitable to biological laboratories. In addition, the resulting value of width and length of the chamber permitted to use commercial coverslips with standards dimensions, reducing the costs of manufacturing and using well-established laboratory equipment.

The possibility of manufacturing the PPFCs by laser cutting was a great advantage, because it is a quick, not expensive and precise technique that allow mass production. All the materials used had been widely used in devices in contact with blood[29, 30, 31, 32, 33]. PPFCs disposable and haemocompatible reduce experiment preparation time and limit false results due residual blood in the chambers.

Computational fluid-dynamic studies were performed on a confined volume to reduce the computation cost. In fact, the three dimensions of the chamber were not comparable (*i.e.,* the height is two orders of magnitude smaller than width), and the creation of fine mesh of all the volume would have requested a too high computational cost. It was chosen therefore the part of the chamber where the arterial samples were placed. This analysis confirmed that the PPFCs could be used to stimulate tissue with a well controlled shear rate, reproducing value observed *in vivo* [18, 19].

Data obtained from the hydraulic characterization show that the chambers behaved as small hydraulic resistances. Value of pressure were negative because of the use of a withdrawal syringe pump, but a configuration with negative pressure favours the hydraulic seal within the chamber. In addition, the small hydraulic resistance offered by the chamber with a flow rate of 1.66 ml/min preserves the sample; in fact, higher pressures could damage or induce the detachment of the arterial slice.

Two different versions of the PPFC were realized, but functional experiments highlighted that the presence of a lid can alter the fluid-dynamics and induce the formation of unspecific thrombi within the chamber. On the other hand, chambers are compatible with microscope imaging and with staining, therefore the collection of the sample is not a strict standard.

As far as we know, the absolute novelty introduced with this device is the use of native tissue. In fact, the PPFCs presented in this work offer the possibility

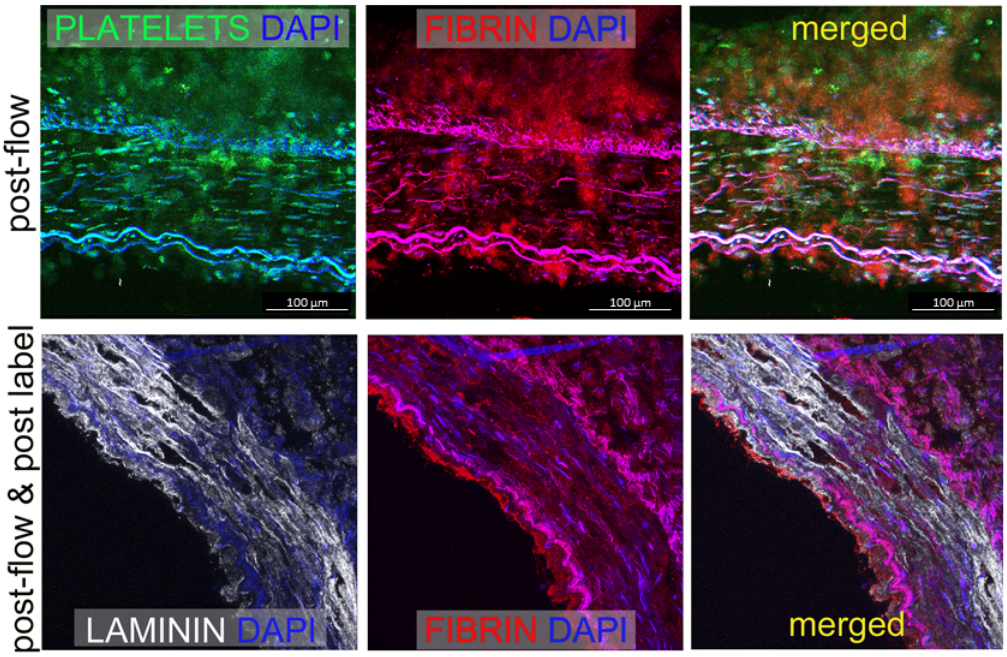

Figure 3.5: Assessment of the functionality of the parallel-plate flow chamber. The confocal analysis of the staining performed within the chambers on human sections of arteries proved that the chambers are compatible with microscopy. In the blood, platelets were labelled with Mepacrine, in green, while anti-fibrin(ogen) was used as a marker of fibrin, in red. In addition, the chambers permit to perform staining within the chamber after the fluid-dynamic conditioning of the sample. Nuclei and laminin were labelled (respectively blue and white) as proof of concept. In the images the structure of the internal and external elastic laminae are clearly visible

to stimulate under a controlled fluid-dynamic environment a complex native arterial structure, while the parallel-plate flow chambers presented in literature are designed for cell monolayers or co-cultures [34, 35, 22].

Once assessed the possibility to perform experiments and staining, the device could be exploited to investigate the nature of vascular cellular and molecular components interacting with blood on human arteries with and without atherosclerosis (*e.g.,* internal mammary artery and carotid plaque). The comparison between the two conditions would help in understanding the pathological processes involved in the acute thrombosis process. The system will be used therefore to screen the effect of different agents either on blood or vessels, in order to clarify mechanism of thrombosis or propose effective therapeutic solutions.

3.6 Conclusion

The parallel-plate flow chamber presented in this chapter represents a valid *ex vivo* model for the investigation of the interactions between vascular cellular compon-

ents and blood under well defined fluid-dynamic conditions. These interactions involve cells, blood and immune system and they are responsible for the development of acute thrombosis. Since the description of the phenomenon could not be restricted to a simple model, the use of an *ex vivo* model represents a valid solution to maintain the complexity of the native tissue but controlling the experimental conditions. From a technical point of view, the system proved to be easy-to-use and compatible with standard laboratory procedures. Functional experiments confirmed that the chambers are not thrombogenic, suitable for performing staining and compatible with microscopy. Further modifications could be implemented to obtain a more realistic model, for example adding a control of the temperature. This model could be exploited to compare blood-cell interactions in pathological versus not pathological tissue to clarify the mechanism of thrombosis and, in perspective, to propose and test therapeutic strategies.

Bibliography

[1] S. P. Jackson. Arterial thrombosis-insidious, unpredictable and deadly. *Nature Medicine*, 17(11):1423–1436, 2011.

[2] F. Otsuka, S. Yasuda, T. Noguchi, and H. Ishibashi-Ueda. Pathology of coronary atherosclerosis and thrombosis. *Cardiovascular diagnosis and therapy*, 6(4):396–408, 2016.

[3] E. Falk. Pathogenesis of Atherosclerosis. *Journal of the American College of Cardiology*, 47(8 Supplement):C7 LP – C12, 2006.

[4] R. Virmani, A. P. Burke, A. Farb, and F. D. Kolodgie. Pathology of the Vulnerable Plaque. *Journal of the American College of Cardiology*, 47(8 Supplement):C13 LP – C18, apr 2006.

[5] B. Furie and B. C. Furie. Mechanisms of Thrombus Formation. *New England Journal of Medicine*, 359(9):938–949, 2008.

[6] H. Q. Yuan, Y. M. Hao, Z. Ren, et al. Tissue factor pathway inhibitor in atherosclerosis. *Clinica Chimica Acta*, 491(September 2018):97–102, 2019.

[7] E. Tremoli, M. Camera, V. Toschi, and S. Colli. Tissue factor in atherosclerosis. *Atherosclerosis*, 144(2):273–283, 1999.

[8] V. Balasubramanian, E. Grabowski, A. Bini, and Y. Nemerson. Platelets, circulating tissue factor, and fibrin colocalize in ex vivo thrombi: Real-time fluorescence images of thrombus formation and propagation under defined flow conditions. *Blood*, 100(8):2787–2792, 2002.

[9] B. Furie and B. C. Furie. Thrombus formation in vivo. *The Journal of clinical investigation*, 115(12):3355–3362, dec 2005.

[10] J. L. Johnson and C. L. Jackson. Atherosclerotic plaque rupture in the apolipoprotein E knockout mouse. *Atherosclerosis*, 154(2):399–406, 2001.

[11] X. F. Leong, C. Y. Ng, and K. Jaarin. Animal Models in Cardiovascular Research: Hypertension and Atherosclerosis. *BioMed Research International*, 2015:11, 2015.

[12] J. A. Frangos, S. G. Eskin, L. McIntire, and C. L. Ives. Flow Effects on Prostacyclin Production by Cultured I Overflow Lowt9a. *Science*, 227(4693):1477–1479, 1985.

[13] M. J. Kuijpers, V. Schulte, W. Bergmeier, et al. Complementary roles of glycoprotein VI and alpha2beta1 integrin in collagen-induced thrombus formation in flowing whole blood ex vivo. *The FASEB journal : official publication of the Federation of American Societies for Experimental Biology*, 17(6):685–687, 2003.

[14] Y. Cadroy, K. S. Sakariassen, J.-p. Charlet, et al. Role of 4 platelet membrane glycoprotein polymorphisms on experimental arterial thrombus formation in men Brief report Role of 4 platelet membrane glycoprotein polymorphisms on experimental arterial thrombus formation in men. *October*, 98(10):3159–3161, 2008.

[15] R. Van Kruchten, J. M. Cosemans, and J. W. Heemskerk. Measurement of whole blood thrombus formation using parallel plate flow chambers a practical guide. *Platelets*, 23(3):229–242, 2012.

[16] K. H. Benam, S. Dauth, B. Hassell, et al. Engineered In Vitro Disease Models. *Annual Review of Pathology: Mechanisms of Disease*, 10(1):195–262, 2015.

[17] P. Marchese, C. Foglieni, A. Gruber, and Z. Ruggeri. Molecular and cellular components of human carotid artery atherosclerotic plaques relevant for thrombus formation: P TU 555. *Journal of Thrombosis and Haemostasis*, 9, 2011.

[18] L. D. C. Casa, D. H. Deaton, and D. N. Ku. Role of high shear rate in thrombosis. *Journal of Vascular Surgery*, 61(4):1068–1080, 2015.

[19] X. Shi, J. Yang, J. Huang, et al. Effects of different shear rates on the attachment and detachment of platelet thrombi. *Molecular Medicine Reports*, 13(3):2447–2456, 2016.

[20] A. M. El-Sabbagh, C. J. Toomasian, J. M. Toomasian, et al. Effect of air exposure and suction on blood cell activation and hemolysis in an in vitro cardiotomy suction model. *ASAIO journal (American Society for Artificial Internal Organs : 1992)*, 59(5):474–479, 2013.

[21] K. S. Sakariassen, L. Orning, and V. T. Turitto. The impact of blood shear rate on arterial thrombus formation. *Future Science OA*, 1(4), 2015.

[22] A. K. Wong, P. LLanos, N. Boroda, S. R. Rosenberg, and S. Y. Rabbany. A Parallel-Plate Flow Chamber for Mechanical Characterization of Endothelial Cells Exposed to Laminar Shear Stress. *Cellular and molecular bioengineering*, 9(1):127–138, mar 2016.

[23] L. S. Han. Hydrodynamic Entrance Lengths N for Incompressible Laminar Flow m Rectangular Ducts. *Journal of Applied Mechanics*, 27(3):403–409, 1960.

[24] E. Beutler and C. West. The Storage of Hard-Packed Red Blood Cells in Citrate Phosphate Dextrose (CPD) and CPD Adenine (CPDA 1). *Blood*, 54(1):280–285, 1979.

[25] L. Dintenfass. Internal Viscosity of the Red Cell and a Blood Viscosity Equation. *Nature*, 219(5157):956–958, 1968.

[26] E. A. Sprague, B. L. Steinbach, R. M. Nerem, and C. J. Schwartz. Influence of a laminar steady-state fluid-imposed wall shear stress on the binding, internalization, and degradation of low-density lipoproteins by cultured arterial endothelium. *Circulation*, 76(3):648–656, 1987.

[27] J. A. McCann, S. D. Peterson, M. W. Plesniak, T. J. Webster, and K. M. Haberstroh. Non-Uniform Flow Behavior in a Parallel Plate Flow Chamber Alters Endothelial Cell Responses. *Annals of Biomedical Engineering*, 33(3):328, 2005.

[28] W. O. Lane, A. E. Jantzen, T. A. Carlon, et al. Parallel-plate Flow Chamber and Continuous Flow Circuit to Evaluate Endothelial Progenitor Cells under Laminar Flow Shear Stress. *JoVE*, (59):e3349, 2012.

[29] A. Colas and J. Curtis. Silicone biomaterials: history and chemistry. In *Silicone biomaterials: history and chemistry and medical applications of silicone*, pages 697–707. 2004.

[30] P. Zemanova, K. Opatrny, L. Vit, and F. Sefrna. Tissue Factor, Its Inhibitor, and the Thrombogenicity of Two New Synthetic Membranes. *Artificial Organs*, 29(8):651–657, 2005.

[31] P. E. Feuser, L. d. S. Bubniak, C. d. N. Bodack, et al. In Vitro Cytotoxicity of Poly(Methyl Methacrylate) Nanoparticles and Nanocapsules Obtained by Miniemulsion Polymerization for Drug Delivery Application, 2016.

[32] P. Wenten, I.G., Aryanti, A. N. Khoiruddin, and N. Himma. Advances in polysulfone-based membranes for hemodialysis. *Journal of Membrane Science and Research*, 2(2):78–89, 2016.

[33] B. Yilmaz, S. Dogan, and S. Celikler Kasimogullari. Hemocompatibility cytotoxicity, and genotoxicity of polymethylmethacrylate nanohydroxyapatite nanocomposites synthesized by melt blending method. *International Journal of Polymeric Materials and Polymeric Biomaterials*, 67(6):351–360, 2018.

[34] M. B. Lawrence, L. V. McIntire, and S. G. Eskin. Effect of flow on polymorphonuclear leukocyte/endothelial cell adhesion. *Blood*, 70(5):1284 LP – 1290, 1987.

[35] G. Rainger, P. Stone, C. M. Morland, and G. B. Nash. A novel system for investigating the ability of smooth muscle cells and fibroblasts to regulate adhesion of flowing leukocytes to endothelial cells. *Journal of Immunological Methods*, 255(1):73–82, 2001.

Chapter 4

Design and characterization of an innovative and versatile culture system for the ex vivo conditioning of arteries

4.1 Introduction

Thrombosis is a pathological process occurring in veins and arteries when blood clots inside the vessels obstruct the physiological blood flow [1]. It is often the result of vascular injuries [2] and it can happen at the late stage of atherosclerosis when acute thrombi are formed within the lumen of the vessel [3]. Thrombosis has been historically studied using animal models, to understand the pathological pathways involved in the onset and development of thrombosis and to test the efficacy and safety of new drugs [4, 5]. Nevertheless, animals typically differ from the human system and this can lead to biased understanding and unreliable predictions of the effects of treatment in humans. Moreover, imaging and characterization of thrombosis *in vivo* are difficult to manage and they cannot achieve high throughput, which is necessary for the screening of treatments [2]. In addition, models lack of a standardization of the protocols used and the protocol differences could affect the results and compromise the comparisons among independent studies [6].

Given this, we developed an *ex vivo* vessel culture system to translate the procedure used *in vivo* to study the thrombosis.

As a proof of concept, we focused on the ferric-chloride ($FeCl_3$) induced thrombosis [7, 8], but the versatility of the system makes it suitable for different studies on *ex vivo* cultures vessels. In $FeCl_3$induced thrombosis, the ferric chloride is applied to the exterior surface of vessels to trigger vascular wall injury and denudation of the endothelium, via the generation of reactive oxygen species. In animal experiment, the exposure of collagen and tissue factor triggers platelet activation coagulation cascade [9].

The system here presented was designed to culture human vessels under controlled fluid-dynamic conditions and to induce vascular injury with $FeCl_3$. Once investigated the pathological mechanism, it is therefore possible to propose therapeutic strategies and to exploit this human *ex vivo* model to assess their efficacy.

The culture system is composed by a culture chamber, which is the bioreactor, and an hydraulic circuit connected to a pump to provide the re-circulation of the culture medium. A stationary fluid-dynamic conditioning reproducing physiological shear stress in the vessel lumen was set in this preliminary study.

The bioreactor was designed to ensure the possibility to induce vessel injury with $FeCl_3$and to be suitable for the following screening of therapeutic and pharmacological treatments.

During this preliminary phase of the work, a functional evaluation of the system was performed. Once assessed that the bioreactor is a reliable tool for culturing *ex vivo* vessels preserving the structure and the cellular distribution, the model will be exploited for further investigations.

The study was performed at the Laboratory of Experimental Micro- and Biofluid-dynamics (μBS Lab) of the Politecnico di Milano and in collaboration with the

Cardiovascular Research Area of IRCSS Ospedale San Raffaele.

4.2 Requirements and specifications

The system needs to fulfil a series of requirements. First of all, it has to guarantee the easy access to the vessel during the experiment, to induce a thrombosis with the methodologies used *in vivo* (*i.e.*, ferric-chloride induced thrombosis) [10].

Another essential requirement, shared with all the culture systems, is the possibility to sterilize the device before each experiment.
The sterility must be kept throughout the experiment, so the design of the bioreactor must provide a barrier to bacteria infiltration. Working with sterile tools and maintaining the sterility, in fact, offer the possibility to perform potentially long-term organ culture studies [11].

The material used for manufacturing the bioreactor has to be biocompatible or, at least, compatible with cell/tissue cultures.

In addition, a multi-chamber device would fulfil the necessity to perform more experiments at the same time.

One important need is the compartmentalization between intra-luminal and extra-adventitial compartments. This characteristic allows to expose the two regions of blood vessels to different biochemical conditions, replicating the *in vivo* environment [12]. Moreover, keeping separated the two compartments is fundamental for inducing differential responses on vessel endothelium and adventitia. It is possible, in particular, to stimulate with cytokines or other inflammatory molecules only the endothelium to induce and study the endothelial dysfunction [13, 14].
As a consequence, small volumes are required for the intra-luminal compartment, to reduce the volume of reagents on equal concentrations.

One major design specification for the device is the versatility. Vessels of different diameters and of different lengths could be mounted within the culture system and properly stimulated.

Finally, a method for mounting and anchoring a-traumatically the vessels in the system needs to be used to avoid vessel damaging, such as endothelial denudation [15].

4.3 Materials and Methods

4.3.1 The preliminary prototype

After outlining the requirements, a first prototype of the bioreactor was designed and manufactured in house in the Laboratory of Experimental Micro- and Biofluid-

dynamics (μBS Lab) of the Dipartimento di Elettronica, Informazione e Bioingegneria of the Politecnico di Milano.

4.3.1.1 Design and manufacturing of the system

The prototype was designed using the three dimensional CAD software PTC Creo Parametric 4.0 (PTC Inc., MA, US) and manufactured with computer numerical control machining (Modela MDX-40, Roland, Japan) from polyoxymethylene blocks (POM, Plasting S.r.l., Italy).

The design of the bioreactor mimics the shape, the dimensions and the functioning of a Petri-dish for cell cultures. The closing of the culture chamber is fulfilled, in fact, with the lid of a standard commercial Petri-dish (100 mm Petri dish, Corning Incorporated, NY, US).

It is composed by two identical and independent culture chambers (Figure 4.1.a). Each chamber consists of a small luminal reservoir, an adventitial reservoir and an overflow reservoir connected to the adventitial one. The luminal reservoir is dedicated to the medium flowing within the lumen of the vessel, while the adventitial reservoir represents the extra-adventitial environment. Inlets and outlets to the culture chamber are provided by threaded female luer lock adapters in polypropylene (PP, Nordson Corporation, OH, US).

The vessel is anchored to barbed polycarbonate (PC, Qosina, NY, US) or PP (Nordson Corporation, OH, US) male luer slip connectors. Connectors of different sizes fit the bioreactor (*i.e.*, 0.8, 1.6, 2.4, 3.2 mm).
The anchoring is performed with small silicone vessel loops (SIM Italia, Italy) using a home made support for mounting the vessels (Figure 4.1.b).

After the mounting procedure, the anchored vessel is moved inside the bioreactor and connected to female luers locks placed within the adventitial reservoir: one PP threaded female luer and a sliding stainless steel female luer needle. The sliding needle allows to adjust the distance, up to 40 mm, between the two female luer connectors (Figure 4.1.c).

Therefore, the vessel is immersed in culture medium in the adventitial reservoir and connected in series to the luminal reservoir through an hydraulic circuit.
The hydraulic circuit is composed by platinum cured silicone tubing (Saint Gobain, France) and a peristaltic pump (323 Du, Watson-Marlow Fluid Technology Group, UK) equipped with a single channel pumping head (314D, Watson-Marlow Fluid Technology Group, UK).

If required, the circulation of medium in the extra-adventitial compartment could be provided by another hydraulic circuit.

A schematic representation of all the configurations that could be obtained with the system is shown in Figure 4.1.d, Figure 4.1.e and Figure 4.1.e

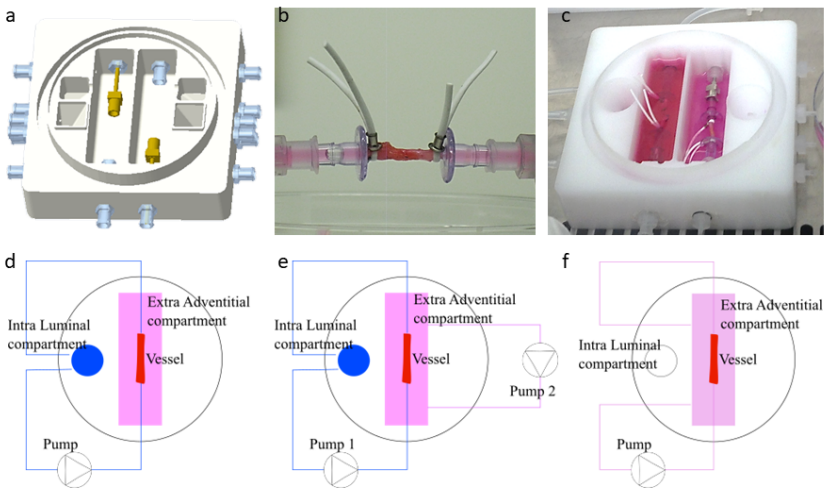

Figure 4.1: The first prototype. (a) 3D CAD drawing of the culture system. Female luer connectors provide inlet and outlet to the system. (b) Vessel holders are used to anchor the vessel to the the male slip barbed luer connectors. After the mounting, the vessel is moved within the bioreactor (c) Picture representing the bioreactor with vessels mounted inside; the first prototype is characterized by the presence of two identical but fluidically independent chambers. Connecting the reservoirs and the vessel in different ways, different configurations are available: (d) There could be re-circulation of the medium only in the intra-luminal compartment, keeping the extra-adventitial compartment static, (e) there could be an independent re-circulation in both the compartments, and, finally, (f) there could be no compartmentation, re-circulating the medium from the lumen of the vessel to the extra-adventitial compartment

4.3.1.2 Functional evaluation of the prototype

A preliminary functional evaluation of the bioreactor was performed with surplus segments of human IMA (n = 4) obtained from patients undergoing coronary artery bypass surgery. This was carried out at the Cardiovascular Research Area of IRCSS Ospedale San Raffaele (Milan, Italy).

After the sterilization, IMA segments were mounted into the system and the luminal circuit was connected as previously described (Chapter 4.3.1.1). The luminal reservoir was filled with 9 ml of DMEM (EuroClone, Italy) additioned with 10% Fetal Bovine Serum (FBS, EuroClone, Italy), 1% Penicillin-Streptomycin (PenStrep, EuroClone, Italy) and fluorescent dextran with two different molecular weight (70000 and 4500).

The adventitial reservoirs was filled with 20 ml of DMEM (EuroClone, Italy) additioned with 10% Fetal Bovine Serum (EuroClone, Italy) and 1% Penicillin-Streptomycin (EuroClone, Italy).

The system was kept in the incubator at 37° C and 5% CO_2 for a culture period of 24 hours. The IMA segments were perfused with a flow rate of 40 ml/min, while the adventitial reservoir was kept in static conditions.
As a control, IMA samples were kept in static conditions into the incubator for

the same time.

After the conditioning period, a central part of each segment was embedded using optimal cutting temperature compound (OCT) and froze down.
Haematoxylin and Eosin (H&E, BioOptica Milano SpA, Italy) histological staining was performed on cryosections. Immunofluorescence staining labelling α-Smooth-Muscle Actin (α-Smooth-Muscle Actin), Smooth muscle protein 22-α (SM22), von Willebrand Factor (vWF) and cluster of differentiation 31 (CD31) was performed and analyzed with confocal microscopy.

4.3.2 An innovative and advanced prototype

Based on the functional experiments and on the general experience with the preliminary prototype, new design specifications were drawn up.

Compared to the initial project, the major modification was implemented to the design of the system, which was drastically changed. In fact, a new design was necessary to limit the handling of the sample after the mounting procedure.
This change had an influence on the material and on the manufacturing technique. In addition, the solution of a multi-chamber device proved to be not ideal for tissue culture. This requirement was deleted to avoid cross-contamination between the chambers.

All the elements of the system, the bioreactor, the actuation system and the hydraulic circuit were reviewed to obtain a reliable *ex vivo* culture system for whole vessels.

Some characteristics of the first prototype have been preserved in the new system.

4.3.2.1 Design of the system

The system was designed using the three dimensional CAD software PTC Creo Parametric 4.0 (PTC Inc., MA, US).
The new bioreactor consists mainly of two parts: (i) an holder for the vessel (Figure 4.2.a), and (ii) a cylindrical chamber where the luminal and the adventitial reservoirs have been obtained (Figure 4.2.b).
The holder is equipped with two female luer locks: a threaded female connector and a sliding stainless steel female luer needle. The needle permits to adjust the distance between the two luer locks.
The female connectors can fit barbed male luer locks of different dimensions (*i.e.*, 0.8, 1.6, 2.4, 3.2 mm).
Once assembled the holder with the proper luer locks, the vessel is anchored on the barbed connectors with a method that will be shown in detail in paragraph 4.3.2.3.
Therefore, the holder, with the vessel firmly anchored, is moved inside the cyl-

indrical chamber

The bioreactor support mimics the shape, the dimensions and the functioning of a Petri-dish for cell cultures. The closing of the culture chamber is fulfilled by the lid of a standard commercial Petri-dish (100 mm Petri dish, Corning Incorporated, NY, US).

Two luminal reservoirs are available in the support: (i) a standard graduated 4-ml reservoir for standard experiments, and (ii) a 600-μl reservoir for applications that require very small amount of reagents.

The hydraulic sealing between the holder and the cylindrical chamber is obtained with custom made silicone gaskets. The gaskets are placed in the gap between the holder and the support and they are properly deformed through screws, as shown in Figure 4.2.c. The silicone gaskets were obtained by addition curing of commercially available silicone rubbers on a custom made mold.

Inlets and outlets to the culture chamber are provided by threaded female luer lock adapters in PP (Nordson Corporation, OH, US).

All the configurations possible for the first prototype (paragraph 4.3.1.1) and shown in Figure 4.1 are possible even with the new system.

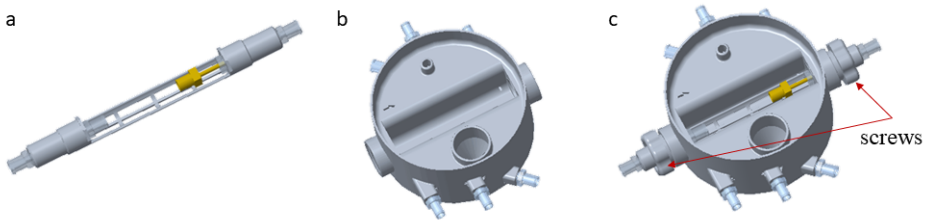

Figure 4.2: Design of the second prototype. The bioreactor is composed by two components: (a) the vessel holder, provided with a sliding female luer needle to adjust the distance between the connectors holding the vessel, and (b) a cylindrical chamber mimicking shape and dimensions of a commercial Petri dish. In the cylindrical chamber two reservoir were realized: (i) a standard 4-ml volume luminal reservoir, and (ii) a 600-μl reservoir. (c) After the matching between the two components, two screws ensure the deformation of two custom made silicone gaskets positioned in the gap between the vessel holder and the cylindrical chamber, guaranteeing the hydraulic sealing.

4.3.2.2 Realization of the new system

The new complex design excludes machining from the list of possible manufacturing technologies. Additive manufacturing was chosen for the realization of the bioreactor.

Manufacturing and material of the new bioreactor Both the holder and the cylindrical chamber were realized in black polyamide 12 (PA12) with the HP MultiJet Fusion technique (Hewlett-Packard Company, CA, US) (Figure 4.3).

The production of the prototypes was outsourced to an external company (Weerg srl, Italy).

Further processing was performed in house to obtain threads for the inlets and outlets to the chamber and to sand the surfaces.

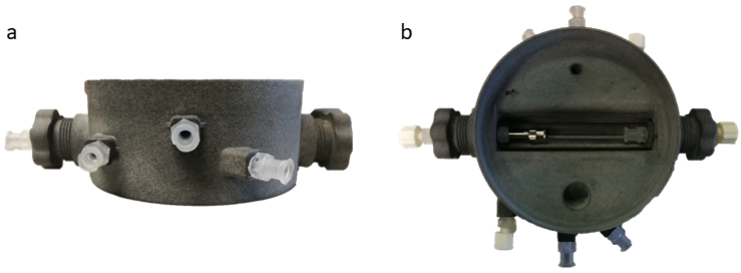

Figure 4.3: Manufacturing of the bioreactor. (a) The lateral view, and (b) the top view of the bioreactor. The bioreactor was realized in black polyamide 12 via additive manufacturing. Post-processing machining was performed to obtain threads for the connectors and to sand the surfaces.

Choice of the actuation system It was chosen to couple the bioreactor with a miniaturized actuation system.

Characteristics and performances of small centrifugal pumps and small peristaltic pumps were compared.

The choice fell on a small commercial roller pump.

As a consequence, a pulsation dampener and a control unit were designed to modulate and control the flow rate values provided within the system.

Realization of a pulsation dampener To filter the noise of the roller pump and to generate a *quasi*-steady flow rate, a pulsation dampener was designed and added to the system.

The dampener is an air chamber that acts as a compliance and it can be coupled with the hydraulic resistance of the system (R) to serve as low-pass RC-hydraulic filter.

To dimension the compliance (C), it was firstly necessary to set the cutoff frequency (f_c) . This value was set two decades lower than the first harmonic of the noise frequency introduced by the pump (f_{noise}), which was derived from the hydraulic characterization of the system (Eq. 4.1) :

$$f_c = 0.01 f_{noise} \tag{4.1}$$

Once determined R from the hydraulic characterization, the compliance was then calculated from the relation between f_c and the time constant (τ) applying the Eq. 4.2:

$$f_c = \frac{1}{2\pi\tau} = \frac{1}{2\pi RC} \tag{4.2}$$

Therefore, a Windkessel model describing the expansion and compression of air within a chamber was used to relate the compliance to the volume of air required for the dampener [16]. In the study, air was approximated to a perfect gas and the calculations were referred to absolute pressure.

The replenishment of the chamber from the initial volume (V_o) and pressure (P_o) up to working volume (V_w) and pressure (P_w) was modelled as an isothermal process (Eq. 4.3):

$$P_0 V_0 = P_w V_w \tag{4.3}$$

The compression and expansion during the working cycle were considered as adiabatic transformations depending on volume (V) and pressure (P) (Eq. 4.4):

$$PV^k = P_w V_w^k \tag{4.4}$$

k is the ratio between the specific heat of the air in a constant pressure process divided by the specific heat of the air in a constant volume process.
Considering the definition of compliance, which is defined as the variation of volume in response to variations of pressure (Eq. 4.5):

$$C = \frac{dV}{dP} \tag{4.5}$$

and combining the Eq. 4.5,4.3, and 4.4, the following equation was found (Eq. 4.6):

$$C = \frac{dV}{dP} = -\frac{P_w}{P^2} V_w^k \frac{1}{k} (\frac{P_w}{P} V_w^k)^{(\frac{1-k}{k})} \tag{4.6}$$

The volume of air could be finally calculated solving the Eq. 4.6 imposing the value of P equal to P_w as shown in Eq.4.7*:*

$$V_0 = -kC\frac{P_w^2}{P_0} \tag{4.7}$$

$P_w$in different working conditions was derived from the hydraulic characterization of the system.

The related air chamber was realized with a 60-ml syringe, fixing the plunger at the desired volume value through an adjustable custom made support.

Development of the control unit A control unit was designed and realized for supplying and controlling the roller pump used in the system.

The control unit employs the micro-controller board Arduino Uno (Arduino, Italy) to control a voltage regulator (MIC29302WT, Microchip, AZ, US) that supplies

the roller pump.
The voltage regulator consists of a non inverting operational amplifier. By adjusting the gain of the amplifier through a potentiometer, different power values can be supplied to the pump. As a consequence, the flow rate provided by the pump can be controlled.

Jack connection was chosen between the pump and the control unit, to guarantee the possibility to connect different kinds of pump.

A dedicated Arduino code was developed to power off/power on the micro-controller (and therefore the pump), to select the maximum power supply suitable for the chosen pump and to switch off the pump in case of excess power.

All the electric components were collected within an electric box, with a custom made and user-friendly interface. An OLED display and a digital voltmeter on the interface permits the user to have a feedback on the power supply and on the state of the pump.

Dimensioning of the fluidic circuit The fluidic circuit was made of platinum cured silicone tubes (Saint Gobain, France) connected through PP luer lock connectors (Nordson Corporation, OH, US). The circuit was dimensioned to guarantee the oxygenation of the culture medium in both the extra-adventitial and the intra-luminal compartments.

Dimensioning of the extra-adventitial compartment The extra-adventitial compartment was considered static, so only diffusion was kept in consideration. This assumption is in favour of safety.
To model the oxygen diffusion in the extra adventitial compartment, it was used the second Fick's law [17].
With the reference system in Figure 4.4.a, the changes of concentration of a solute (C) with respect to time due to diffusion were expressed with the following equation (Eq. 4.8):

$$\frac{\partial C}{\partial t} = D(\frac{\partial^2 C}{\partial x^2} + \frac{\partial^2 C}{\partial y^2} + \frac{\partial^2 C}{\partial z^2}) \tag{4.8}$$

where D is the diffusion coefficient of the solute (in this case oxygen) in the medium, equal to 2.18 10^{-5} cm^2/s.
Under the hypothesis of stationary flow and plane symmetry and adding the value of volumetric consumption of oxygen of the vessel (V_{vessel}), Eq. 4.8was simplified to Eq.4.9:

$$D\frac{\partial}{\partial x}\left(\frac{\partial C}{\partial x}\right) - V_{vessel}(C) = 0 \tag{4.9}$$

The volumetric consumption of oxygen was set equal to 0.18 μmol/ml/s[18]

By integrating the Eq. 4.9, it was possible to obtain the analytical expression of the spatial distribution of oxygen concentration (Eq4.10):

$$C(x) = \frac{1}{2}\left(\frac{V_{vessel}}{D}\right)x^2 - \left(\frac{V_{vessel}h}{D}\right)x + c_{atm} \tag{4.10}$$

where h is the height of the adventitial reservoir (Figure 4.4.a) and c_{atm} is the concentration of oxygen found into the incubator.

The minimum oxygen concentration is reached to the bottom of the adventitial reservoir and it can be calculated imposing the value of x equal to h and obtaining the following equation (Eq.4.11):

$$c_{min} = c_{atm} - \frac{1}{2D}h^2 \tag{4.11}$$

It was chosen a value of h that guaranteed a proper oxygenation of the vessel, compatible with design requirements.

Applying the Henry's low equation (Eq. 4.12) it was possible to obtain the corresponding value of oxygen partial pressure:

$$pO_2 = \frac{c}{\alpha} \tag{4.12}$$

where α is the solubility coefficient of oxygen in the culture medium (equal to the one in water that is 1.35 10^{-9} mol/mmHg/cm^3.

Dimensioning of the intra-luminal compartment To dimension the intra-luminal compartment, the gaseous exchange between the intra-luminal compartment and the incubator environment was modelled using an analytical model adapted from literature[19]. The model is based on the balance between the oxygen replenishment and the oxygen depletion within the system. The exchange occurs via the free surface of the medium in the luminal reservoir, via the oxygen-permeable silicone tubing and via the vessel segment.
To simplify the model and to stay in favour of safety, the reservoir was considered to be not oxygenating, the vessel was considered responsible for oxygen consumption and the replenishment of oxygen was charged only to silicone tubing (Figure 4.4.b).

The global oxygen transfer across the surface and along all the length of the silicone tubing ($VO_{2\ sil}$) was expressed by the equation (Eq. 4.13):

$$VO_{2sil} = \alpha Q\,(pO_{2OUTsil} - pO_{2INsil}) \tag{4.13}$$

where α is the solubility coefficient of oxygen in the culture medium (equal to the one in water that is 1.35 10^{-9} mol/mmHg/cm^3), Q is the flow rate and $pO_{2IN\ sil}$ and $pO_{2OUT\ sil}$ are respectively the oxygen partial pressure at the inlet and at the

outlet of the silicone tube.
The local oxygen transfer across the surface of the silicone tubing ($J\Delta$x) was driven by the different partial pressure between the medium flowing into the tubing at a generic distance x from the inlet ($pO_2\ (x)$) and the constant partial pressure in the incubator environment (pO_{2EXT}), that with an air composed by 5% of $CO_2$was equal to 150 mmHg.
The local oxygen transfer was therefore expressed by the following equation (Eq. 4.14):

$$J\triangle x = UW\triangle x\,(pO_{2EXT} - pO_2(x)) \tag{4.14}$$

In Eq. 4.14 J is the volumetric transport rate of oxygen per unit length, U is the overall mass transfer coefficient of the tubing and W is the logarithmic mean of the inner and outer tubing circumference.
The overall mass transfer coefficient U takes into account the various resistances encountered by the oxygen while diffusing from the medium to the external environment. These resistances are: (i) the medium itself (R_{medium}), (ii) the silicone tube (R_{sil}), and (iii) the outer environment (R_{out}). The Eq. 4.15 expressed the relationship among these resistances and the coefficient U:

$$U = \frac{1}{R_{medium} + R_{sil} + R_{out}} \tag{4.15}$$

Referring to the work of Orr and colleagues [19], the three resistances were modelled considering fluid-dynamic and geometrical parameters.
In particular, R_{medium} was calculated as (Eq. 4.16):

$$R_{medium} = \frac{H}{K_i} \tag{4.16}$$

In the formula 4.16, H is the Henry coefficient (equal to 7.47 10^8 mmHg cm^3/mol) and K_i is the inner tubing film coefficient, which takes into account the Sherwood number in the medium (Sh_i), that depends on Reynolds and Schmidt numbers [20], the diffusion coefficient of oxygen in the medium (D) and the inner diameter of the tubing (d_i). R_{medium} was expressed according with the following equation (Eq. 4.17):

$$k_i = \frac{Sh_i D}{d_i} \tag{4.17}$$

The hindrance to oxygen diffusion exerted by the silicone tubing was calculated as (Eq. 4.18):

$$R_{sil} = \frac{t_m W_i}{\rho_{gas} P_m W} \tag{4.18}$$

where t_m is the tubing thickness, W_i the inner tubing circumference, ρgas the gas density (equal to 4.46 10^{-5} mol/cm^3) and P_m the permeability to oxygen of

silicone (equal to 7.96 10^{-9} $cm^2/s/mmHg$).
Finally, the resistance of the outer environment was calculated using the Eq. 4.19:

$$R_{out} = \frac{RTW_i}{K_o W_e} \tag{4.19}$$

where R is the gas constant (corresponding to 6.24 $10^4 cm^3$ mmHg/ mol K), T the temperature within the incubator (equal to 310 K), W_e the external tubing circumference and K_o the outer tubing film coefficient.
K_o was calculate similarly to K_i, with the Eq.4.20:

$$K_o = \frac{Sh_e D_{air}}{d_e} \tag{4.20}$$

where Sh_e is the outer Sherwood number, calculated considering stagnant gas and corresponding to 0.43, D_e is the diffusion coefficient of oxygen in air (equal to 0.21 cm^2/s) and d_e is the external diameter of the silicone tube.

Once combined the Eq. 4.154.164.174.184.194.20 to obtain the value of U, the global oxygen transfer of the silicone tubing VO_{2sil}can be found integrating the Eq. 4.14 along the length of the tubing (L) (Eq. 4.21):

$$VO_{2sil} = \int_0^L J dx \tag{4.21}$$

Solving Eq. 4.21 for the partial pressure at the outlet of tubing, the following equation was derived (Eq.4.22):

$$pO_{2OUTsil} = pO_{2EXT} - (pO_{2EXT} - pO_{2INsil})\, e^{-\frac{UWL}{\alpha Q}} \tag{4.22}$$

The oxygen consumption along the vessel ($VO_{2vessel}$) was expressed with the following equation (Eq. 4.23) :

$$VO_{2vessel} = \alpha Q\, (pO_{2INvessel} - pO_{2OUTvessel}) \tag{4.23}$$

where $pO_{2INvessel}$ and $pO_{2OUTvessel}$ are respectively the oxygen partial pressure within the medium at the inlet and at the outlet of the vessel. Based on data found in the literature, the $VO_{2vessel}$ was set equal to 3.30 10^{-7}mol/min [18].

Finally, due to the physical continuity between silicone tubing and the vessel, the following equations were written (Eq. 4.244.25):

$$pO_{2OUTsil} = pO_{2INvessel} \tag{4.24}$$

$$pO_{2INsil} = pO_{2OUTvessel} \tag{4.25}$$

Combining the Eq. 4.24 and 4.25 with the Eq. 4.22 and 4.23, it was possible to derive the expression of the length of silicone tubing necessary to guarantee a sufficient replenishment of the oxygen within the system.
This value of length (L) was expressed with the equation (Eq.4.26):

$$L = -\frac{\alpha Q}{UW} \log \frac{pO_{2EXT} - pO_{2OUTsil}}{pO_{2EXT} - pO_{2OUTsil} + \left(\frac{VO_{2vessel}}{\alpha Q}\right)} \tag{4.26}$$

Imposing a target value of oxygen partial pressure at the outlet of the silicone tubing, L was used as parameter for dimensioning the fluidic circuit.

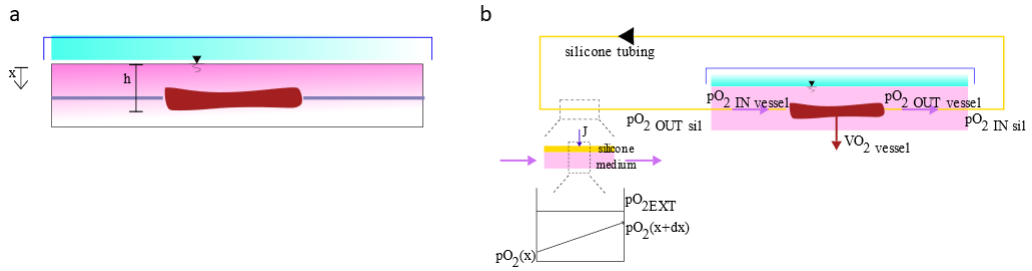

Figure 4.4: Dimensioning of the circuit. (a) The extra-adventitial compartment (pink) was modelled under the hypothesis of stationary flow and plane symmetry. The diffusion of oxygen along the x-direction within the reservoir was modelled according to the second Fick's law. The minimum value of oxygen partial pressure was found at a distance h to the free surface. This distance was calculated keeping into account the encumbrance of the connectors and of the vessel. (b) The oxygen exchange in the intra-luminal compartment was modelled according to Orr et al. [19]. The replenishment of oxygen was attributed to the silicone tubing. The local oxygen transfer (J) across the silicone was driven by the difference between the oxygen partial pressure in the incubator ($pO_{2\ EXT}$) and the oxygen partial pressure within the tube. The consumption of oxygen by the vessel ($VO_{2vessel}$), instead, was responsible for the reduction in the level of oxygen.

4.3.2.3 Development of a new method for anchoring the vessels within the system

An innovative method was developed to guarantee an a-traumatic mounting procedure of the vessels within the bioreactor (Figure 4.5).

The method consisted in the release of rubber bands through a custom made tool, to anchor the vessel to the barbed connectors of the bioreactor.

The bands are silicone bands (KilRoid, WellSpect HealthCare, Sweden) typically used in haemorrhoids treatment.

The release tool was designed using the three dimensional CAD software PTC Creo Parametric 4.0 (PTC Inc., MA, US) and manufactured with computer numerical control machining (Modela MDX-40, Roland, Japan) from a POM block (Plasting S.r.l., Italy).
The tool has an housing for the rubber band and an opportunely dimensioned POM cone was manufactured to help the dilation and the positioning of the rubber

bands around the housing (Figure 4.5.a). A spring mechanism guarantees the fast release of the silicone bands. The tool is characterized by a U-shape to permit its removal once the vessel has been anchored.

Briefly, the mounting procedure with the method here presented is composed by a few steps.
Firstly, male slip connectors of proper size are mounted into the holder described in paragraph 4.3.2.1. The holder is positioned in a home made POM support platform to ease the procedure. One silicone band is mounted on the releasing tool, as previously described. The vessel is partially passed inside the silicone band (and the releasing tool) and then put on the barbed connector. After positioning the vessel, the releasing tool is moved at the base of the connector and the silicone band is released shutting around the vessel on the connector 4.5.b). Finally, the release tool is removed and the procedure is repeated to mount the other end of the vessel to the second connector (Figure 4.5.c).

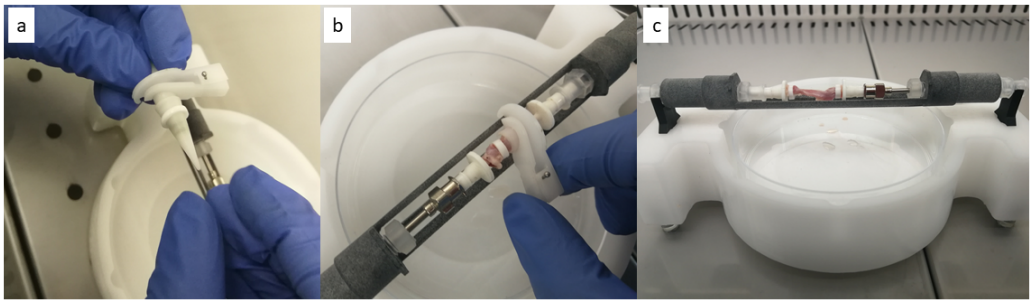

Figure 4.5: The new method for anchoring the vessel within the bioreactor. (a) An elastic band is mounted on the releasing tool with the help of a custom made cone for dilate it. (b) Barbed luer connectors are placed within the vessel holder. The vessel is put on the connector and the elastic band, mounted on the releasing tool, is positioned at the base of the barbed luer connector. Finally, the elastic band is released with the tool. (c) The procedure is repeated twice and the releasing tool is removed from the vessel, that has been anchored to the connectors in the vessel holder.

4.3.2.4 Characterization of the system

Before performing experiments with biological tissue, the system was characterized at the μBS Lab of Politecnico di Milano. The characterization was used both to evaluate the performances of the system but also to dimension some components.

Assessment of the hydraulic seal The performances of the home made silicone gaskets were evaluated through 24/48/72 hours experiments.
During these experiments, gaskets of different materials were compared. In particular, the commercial silicone rubbers used were EcoFlex 00-50 (Smooth-On Inc., PA, US), Dragon Skin (Smooth-On Inc., PA, US), and GLS-Pro 50 (Prochima S.r.l., Italy).

Gaskets of different dimensions (*i.e.*, different internal and external diameter) were tested.

During these experiments, it was also evaluated the deterioration of the gaskets provoked by the use of screws to impose the deformation.

Hydraulic characterization The hydraulic characterization was performed using distilled water as re-circulating medium and using a silicone phantom to mimic the presence of the native blood vessel. The small commercial roller pump chosen for the system was used for the hydraulic characterization.

The system was configured as shown in Figure 4.6. Briefly, the extra-adventitial compartment was kept in static conditions. In the intra-luminal compartment, the medium was re-circulated from the standard luminal reservoir to the vessel through previously dimensioned (paragraph 4.3.2.2) silicone platinum cured tubing connected to the roller pump.

Evaluation of the pressure losses For evaluating the pressure losses within the culture system, two piezoelectric pressure transducers (143PC series, Honeywell Inc, NJ, US) were positioned in derivation upstream and downstream of bioreactor vessel holder (Figure 4.6.a). A transit-time ultrasound flow meter (Transonic System Inc., NY, US) equipped with a ⅛" probe was used for acquiring the flow rate signal. Both pressure and flow rate values were acquired (10 s, sample frequency of 200 Hz) via a customized LabView software (National Instruments Corp., TX, US).

The pressure losses were calculated with two different silicone tubes (*i.e.*, silicone tube with internal diameter of 0.8 mm and thickness 0.8 mm *versus* silicone tube with internal diameter 1.6 mm and thickness 0.8 mm) and, with connectors of different sizes (*i.e.*, 0.8, 1.6, 2.4, 3.2 mm)

For each condition and for each flow rate, three experiments were performed and it was calculated mean and standard deviation values.

Assessment of the performances of the pulse dampener Once calculated the values of compliance using data from the hydraulic characterization, experiments were performed to evaluate the performances of the hydraulic filter.

A setup similar to the one described in the previous paragraph was used, but only one pressure transducer (143PC series, Honeywell Inc, NJ, USA) was positioned in derivation upstream to the vessel (4.6.b). Flow rate was monitored with a transit-time ultrasound flow meter (Transonic System Inc., NY, US) equipped with a ⅛" probe. Both pressure and flow rate values were acquired (10 s, sample frequency of 200 Hz) via a customized LabView software (National Instruments Corp., TX, USA).

The dampener was positioned downstream to the pump and connected through a three-ways-stopcock (Nordson Corporation, OH, US).

For each condition taken into account (*i.e.,* different tubes and different connectors) the value of the corresponding dampener was calculated and its performance tested.

The trend and the oscillation of the flow rate values with or without the dampener were compared.

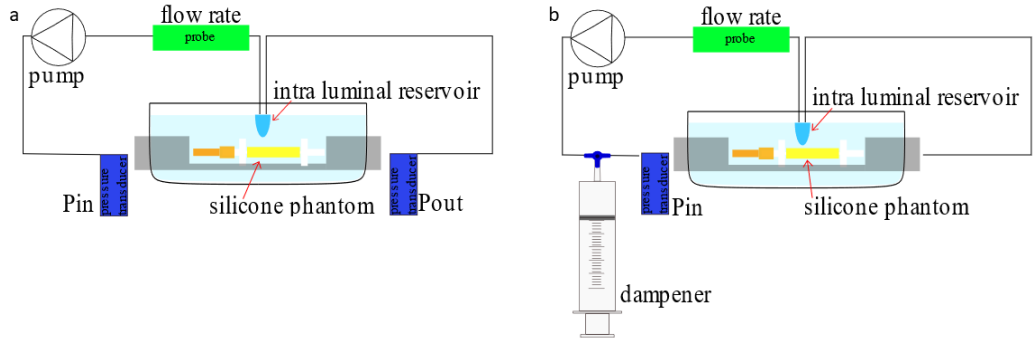

Figure 4.6: Hydraulic characterization of the system. (a) In the setup used for performing the hydraulic characterization, a silicone phantom mimicked the presence of the vessel. The luminal reservoir was connected to the vessel holder through silicone tubing. The medium was re-circulated with a peristaltic pump. The pressure at the inlet and at the outlet of the holder were monitored to evaluate the pressure losses induced by vessel of different size, and therefore different connectors. The flow rate was measured during the characterization using a probe connected to an ultrasound flow meter. (b) For assessing the performances of the pulse dampener, a similar setup was used, but it was monitored only the values of pressure at the inlet of the vessel holder, comparing the oscillations with or without the dampener.

4.3.2.5 Functional evaluation of the system with biological samples

A campaign with biological samples was performed at the μBS Lab of Politecnico di Milano to evaluate the functionality of the system. Animal tissues were chosen as model for the experiments.

Choice, transport and isolation of the animal vessel Porcine right coronary artery (RCA) was chosen as vessel for performing the functional evaluation of the bioreactor.
The tissues used in the experiments came from animals designated for human consumption.

Porcine hearts were withdrawn at a local abattoir immediately after the sacrifice of the animal and put in a preservation medium. The preservation medium consisted of Hank's Balanced Salt Solution (HBSS, EuroClone, Italy) supplemented with 200 U/ml PenStrep (EuroClone, Italy), 200 μg/ml Gentamycin (EuroClone, Italy) and 2.5 μg/ml Amphotericin B (EuroClone, Italia).

The isolation of the vessel was performed under biological hood with sterile tools. Briefly, after identifying the RCA ostium, connective tissue and fat were gently and gradually removed from the area around the coronary artery using surgical tweezers and scissors (Figure 4.7.a).

Images of transversal sections of RCA were acquired using a stereo microscope (Olympus SZX10, Olympus Corporation, Japan) and their diameters were measured using the software ImageJ.

Experiments with porcine coronary arteries All the bioreactor components, included the silicone elastic bands and the releasing tool used for anchoring the vessel, were previously autoclaved.

The experimental flow rate was calculated to guarantee a value of wall shear stress for the RCA samples equal to 20 dynes/cm^2, which corresponds to *in vivo* value [21, 22, 23]. It was found solving the equation of wall shear stress (τ_w) for flow rate, according to the following equation (Eq. 4.27):

$$Q = \frac{\tau_w r^3}{4\pi\mu} \tag{4.27}$$

where Q is the flow rate, r the radium of the vessel and μ the viscosity of the medium (equal to 0.001 Pa$\cdot$s).

Cleaned segments of RCA (n=5) without visible collateral vessels were chosen for the experiments.

In each experiment, the sample was mounted within the bioreactor holder with the method described in paragraph 4.3.2.3(Figure 4.7.b).

After the mounting procedure, the bioreactor was assembled and connected to the hydraulic circuit as shown in Figure 4.7.c. The extra-luminal compartment was kept in static condition and the medium was re-recirculated in the intra-luminal compartment. It was used the standard luminal reservoir. The fluidic circuit was properly dimensioned and equipped with a dampener.

The intra-luminal and the extra-adventitial compartments were filled with respectively 6 ml and 17 ml of DMEM additioned with 10% FBS and 1% PenStrep.

Before moving the system into the incubator, the bioreactor was closed with a sterile lid of a standard Petri-dish, as seen in paragraph 4.3.2.1 (Figure 4.7.d).

Therefore, 24-hours dynamic conditioning of the vessel was performed within the incubator.

As a control, segments of RCA (n=5) were kept in static conditions for 24 hours into the incubator.

One further experiment was conducted to evaluate the capability to maintain the sterility within the bioreactor for 72 hours.

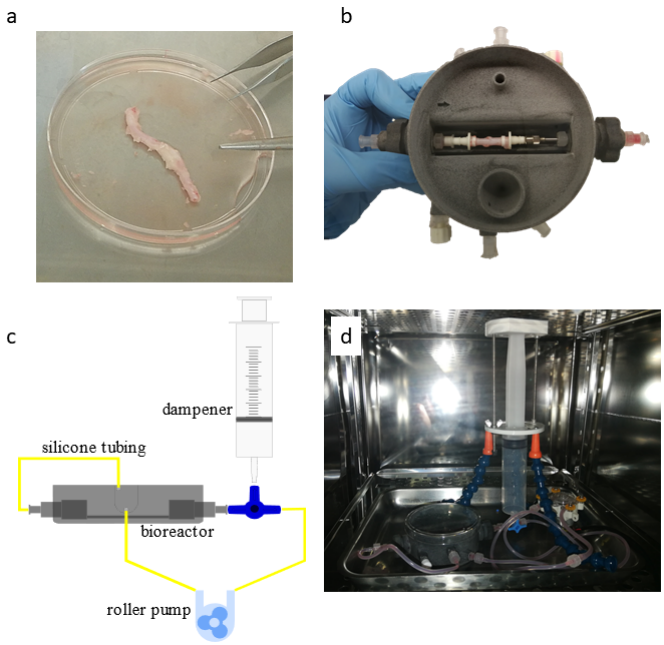

Figure 4.7: Functional evaluation of the system. (a) After the withdrawal of the porcine heart at a local abattoir, the right coronary artery was isolated from the surrounding tissue, and (b) mounted within the bioreactor. (c) The functional evaluation of the system was performed with the setup shown in the scheme. Briefly the extra-adventitial compartment was kept static, while the medium in the intra-luminal compartment was re-circulated into the vessel through a small commercial roller pump. The pulsation of the pump were dampened with the custom made filter. The hydraulic connection was performed via silicone tubing opportunely dimensioned. (d) Picture of the system in the incubator: the fluidic circuit and the roller pump were placed within the incubator during the conditioning period.

Tissue viability evaluation Rings of native and conditioned, both statically and dynamically, RCA samples were stained with methylthiazol tetrazolium (MTT, Sigma-Aldrich, MO, US) [24, 25]. Briefly, MTT powder was dissolved in PBS, obtaining a final concentration of 0.5 mg/ml. The rings were incubated at 37 °C for 1 h in MTT solution. As a negative control, one RCA ring was fixed with 4% formaldehyde overnight and then incubated in MTT solution.

After the incubation, pictures were taken using a stereo microscope (Olympus SZX10, Olympus Corporation, Japan). The rings were then fixed overnight in 4% paraformaldehyde (PFA, Sigma Aldrich, MO, US), embedded in OCT and cut for further qualitative analysis.

Morphological assessment The central part of each sample (*i.e.,* native, dynamically and statically conditioned) was fixed in 4% PFA overnight, OCT-embedded and cut into sections using a cryotome.

H&E staining (BioOptica Milano SpA, Italy) was performed on the sections and images were taken at the microscope to qualitatively evaluate the structure of the

vessel wall.

Immunofluorescence staining for SMCs and ECs were performed. Sections were incubated (4°C, overnight) with goat anti-human SM22 (1:200) for labelling SMCs. The subsequent day they were incubated with secondary antibody Alexa Fluor 488 donkey anti-goat (1:500). Then, ECs were labelled with rabbit anti-human von Willebrand factor (1:200). The incubation was performed for 2 hours at room temperature and followed by 45' of incubation with Alexa Fluor 594 donkey anti-rabbit (1:500). Nuclei were counterstained with DAPI. Digital images were obtained using a fluorescence microscope at a magnification of 20X.

4.4 Results

4.4.1 Evaluation of the performances of the preliminary prototype

The functional evaluation of the first prototype with human IMA samples proved that the system could be compatible with standard laboratory procedures.

The Petri-like design permitted to have easy access to the vessel at any time during the conditioning period.

H&E (Figure 4.8.a) showed that IMA morphology was preserved during the conditioning within the bioreactor.
This result was confirmed by the immunofluorescence staining; in fact the labelling of arterial ECs and SMCs proved the preservation of the morphology, the general preservation of an endothelial layer and the absence of dissecation signs (Figure 4.8.b).
Moreover, the perfusion of fluorescent dextrans in the intra-luminal compartment demonstrated the absence of evident leakages through the arterial wall (Figure 4.8.c).

Nevertheless, some issues were highlighted during this functional validation.

First of all, the experimental campaign showed some technological limits of the material used for manufacturing the chamber. In fact, the threaded connections realized within the POM loosened after a few uses, not ensuring anymore the hydraulic sealing.

In addition, although vessel loops guaranteed a good anchoring of the vessel to the barbed luer connectors, they were not ideal for the tissue. In fact, the closure of the loops required a vigorous procedure that could be harmful for the vessel. Moreover, once anchored to the connectors, the vessel could be damaged when moved into the bioreactor.

The presence in the bioreactor of two chambers, although hydraulically independent, proved to be a potential risk in case of contamination of one of the two

chambers.

Finally, another issue was the oscillation in the flow rate induced by the roller pump, because it provoked an unwanted pulsation of the vessel.

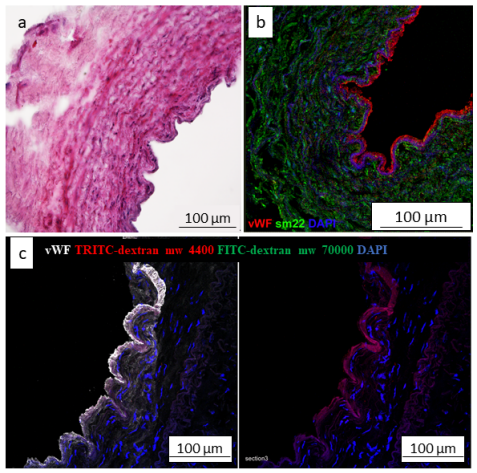

Figure 4.8: Evaluation of the first prototype. (a) Haematoxylin & Eosin histological staining highlighted the presence of the endothelium and a preservation of the structure of the IMA samples conditioned in fluid dynamic conditions within the culture system. (b) Immunofluorescence confirmed the presence of an endothelial lining (endothelial cells were labelled with vonWillebrand factor, red) and a well preserved structure (smooth muscle cells were labelled via sp22, in green). DAPI was used to mark nuclei (in blue). (c) Perfusion of fluorescent dextrans demonstrated the absence of leakage in *ex-vivo* experiments with IMA.

4.4.2 Evaluation of the performances of the advanced prototype

4.4.2.1 Evaluation of the oxygenation

According to the model used to evaluate the oxygen profile within the adventitial reservoir, increasing the height of the reservoir, a lower concentration of oxygen is found. Considering a height of 17 mm, which is compatible with the physical encumbrance of the connectors and of the bioreactor holder, the corresponding minimum oxygen partial pressure is equal to 151.57 mmHg (Figure 4.9.a).

The length of silicone tubing necessary to ensure an intra-luminal compartment oxygenation was evaluated considering two different silicone tube diameters (*i.e.*, 0.8 and 1.6 mm of internal diameter).

Increasing the diameter of silicone tubing, the exchange area increases with a resulting decrease of the length necessary to obtain oxygenation. Moreover, as the flow rate increases the necessary tubing length increases too.

Figure 4.9.b and Figure 4.9.c shows the trend of the length as a function of the flow rate for the two different silicone tubes. In the graph, the length is parameterized for different values of the desired $pO_{2\ OUT\ sil}$.

4.4.2.2 Assessment of the hydraulic seal

Among the different materials used for manufacturing the rubber gaskets used within the bioreactor, only Dragon Skin proved to be suitable for this scope. In fact, with EcoFlex 00-50 and GLS-Pro 50 the hydraulic seal was guaranteed only for a couple of hours.

The chosen silicone gaskets were optimized to permit a good match between vessel holder and bioreactor cylindrical chamber but, at the same time, a good hydraulic sealing.

The tests highlighted that the silicone gaskets were subjected to an important degeneration provoked by the screws used to ensure their deformation. After three experiments, such degeneration affected the capability of the gasket to provide a good sealing. Given this, new gaskets must be used at least every three experiment. The technology used to produce the gaskets proved to be fast and low cost.

4.4.2.3 Hydraulic characterization of the system

Different tubing diameters affect enormously, as expected, the resistivity of the system.
In fact, the values of pressure registered in the circuit with the 0.8-mm-inner-diameter silicone tube (Figure 4.9.d) are much higher than the ones registered in the circuit with the 1.6-mm-inner-diameter silicone tube (Figure 4.9.e).

Comparing the values of pressure upstream and downstream to the bioreactor vessel holder, it was possible to evaluate the pressure loss due to the presence of the connectors and of the vessel. As expected, the 0.8 mm connectors are very resistive. In this case the value of pressure registered upstream to the bioreactor vessel holder were much higher than the ones registered downstream, with both the silicone tubing. With all the other connectors, the pressure loss along the vessel holder was not very high.

Finally, due to the hydraulic resistance of the circuit made with the 0.8-mm-inner-diameter silicone tube, the values of flow rate obtained were much lower than the ones obtained with the same roller pump under the same power supply with the 1.6-mm-inner-diameter silicone tube.

4.4.2.4 Performances of the pulsation dampener

The hydraulic characterization of the system was fundamental for calculating the values of compliance necessary to dampen the oscillation induced by the roller pump into the system.

Comparing the values of pressure in the fluidic circuit equipped with dampener with the values registered in the fluidic circuit not equipped with dampener, a

considerable reduction in the oscillations could be seen.
This behaviour was verified with both the circuits (*i.e.*, 0.8-mm-inner-diameter and 1.6-mm-inner diameter) and with all the connectors, changing each time the value of compliance of the dampener, according to the dimensioning described in paragraph 4.3.2.4.

Figure 4.9.f shows one representative comparison of the pressure oscillation with/without dampener.

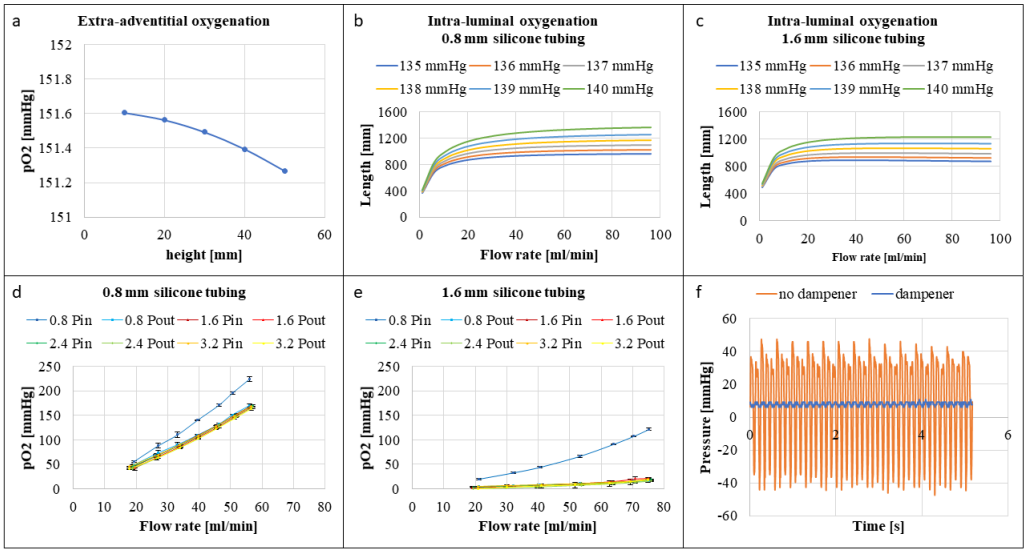

Figure 4.9: Dimensioning and characterization of the system. (a) The graph shows the values of oxygen partial pressure reached into the extra-adventitial compartment at different heights. An height of 17 mm was considered suitable for the system. According to the model, the corresponding value of oxygen partial pressure is 151.57 mmHg. (b) and (c) refer to the modelling of oxygen exchanges in the intra-luminal compartment. The graphs show the length of the tubing necessary to reach the target oxygen partial pressure at the outlet of the silicone tube as a function of the flow rate. At the same flow rate, decreasing the diameter of the tube, longer tubes are necessary to reach the same oxygen partial pressure. The target flow rate values were set in a range going from 135 to 140 mmHg. (d) and (e) show the results of the hydraulic characterization of the system provided with, respectively, 0.8-mm-inner-diameter tube and 1.6-mm-inner-diameter tube. Each experimental curve represents the trend of the pressure at the inlet or at the outlet of the vessel holder as a function of the flow rate using different connectors. For each connector and for each flow rate, three measurements were performed. Mean and standard deviation values are reported in the graph. 0.8-mm-inner-diameter tubing proved to be clearly more resistive then 1.6-mm-inner-diameter tubing. Moreover, 0.8 mm connectors introduce an high minor head loss into the circuit. (f) The values of compliance necessary to dampen the roller pump pulsation were calculated from the hydraulic characterization. For each condition, the performance of the dampener was evaluated. The graph reported is representative for the functioning of the dampener.

4.4.2.5 Experimental campaign with biological samples

Evaluation of the new anchoring method The new method for anchoring the vessels proved to be suitable for mounting biological samples within the bioreactor.

Silicone bands were rapidly mounted on the releasing tool thanks to the cone.

The spring mechanism allowed an easy and fast release of the elastic bands.

With this method, the biological sample underwent a non-damaging manipulation: the possibility to be subjected to damage was really restrained.

Functional evaluation of the system The functional evaluation of the system was performed using porcine right coronary arteries.
From the analysis of the geometrical characteristics of the RCA samples, it was found a mean diameter of 2.71 ± 0.57 mm and a wall of 0.81 ± 0.24 mm.
Therefore, a flow rate of 30 ml/min was chosen to expose the vessel segment to a physiological shear stress.
The fluidic circuit was realized using 1.6-mm-inner-diameter silicone tubing and considering a tubing length of 100 cm.

The experiments with RCA samples proved that the bioreactor was easy to use and compatible with laboratory procedures.

Visual inspection of the culture medium proved that there were no signs of contamination after 24-hours neither 72-hours inside the incubator.

Results of viability tests MTT staining was used to assess tissue viability. Images acquired after 24 hours with the stereo microscope showed that the viability was maintained in samples kept under dynamic conditions (Figure 4.10.a) and under static condition (Figure 4.10.b) similarly to native vessels, used as a positive control (Figure 4.10.c).

Images acquired from sections of the MTT-stained vessels permitted a qualitative evaluation of viability (Figure 4.11). Images showed a de-population of the medial layer of the wall in all the samples, already visible in the native samples (Figure 4.11.a).
The distribution of endothelial cells was in some sections irregular, with some areas lacking of endothelium. It was found more frequently in samples cultured under fluid-dynamic conditions (Figure 4.11.c and Figure 4.11.f).

Histological and immunofluorescence evaluation of vessel structure H&E was used to assess the maintenance of structure of the coronary wall.

Images acquired with the microscope showed a good preservation of the structure, although the a de-population of the medial layer was found in native (Figure 4.12.a), static (Figure 4.12.b) and fluid-dynamic conditioned samples (Figure 4.12.c).

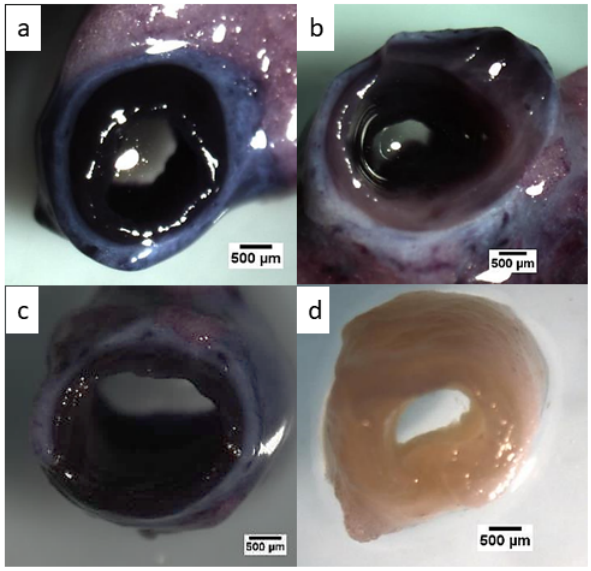

Figure 4.10: Assessment of the viability of the samples. Rings of porcine right coronary artery stained with MTT after 24 hours of culture under (a) dynamic, and (b) static conditions. Native and formaldehyde-fixed tissues were used as positive (c) and negative (d) controls, respectively. The images in the figure are representative of the behaviour observed in all the samples and related control. Images were acquired at the stereo microscope.

Moreover, some samples were characterized by the presence of an atherosclerotic plaque (Figure 4.15).

Immunofluorescence images confirmed a general good preservation of the structure (Fig. 4.13).
The comparison among the native sample (Fig. 4.13.a) and the static (Fig 4.13.b) and the dynamic conditioned ones (Fig. 4.13.c) highlighted a localized loss of continuity of the endothelium mainly in the dynamic sample.

As a proof of concept, immunofluorescence images taken to check the endothelium after 72 hours in dynamic conditions (4.14.a) show that the quality of endothelium is comparable with the endothelium after 24 hours with a luminal perfusion (4.14.b).

4.5 Discussion

In this work, a bioreactor for conditioning *ex vivo* whole vessel was designed, manufactured and characterized. The system could be used to reproduce *ex vivo* mechanisms involved in the progress of atherosclerosis to study the molecular and cellular components involved and, perspectively, to propose and test therapeutic solutions.

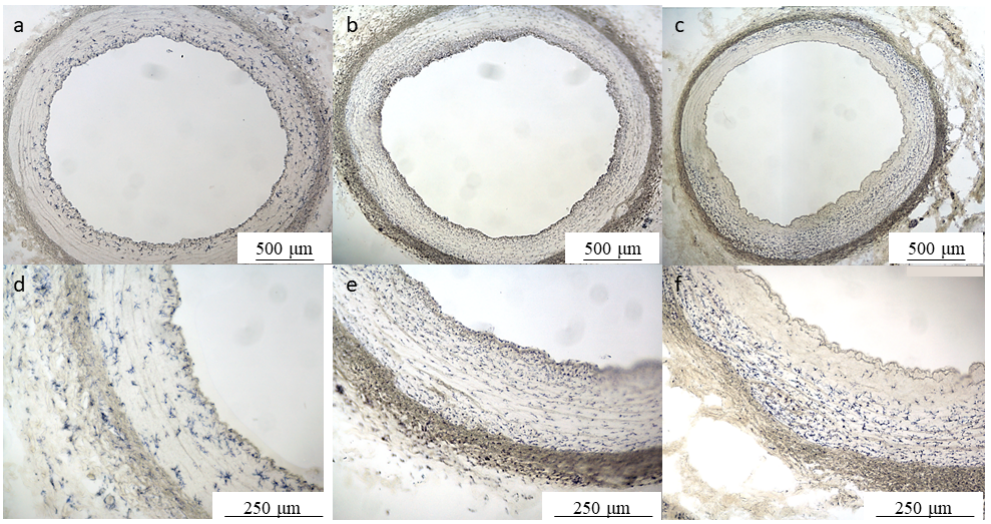

Figure 4.11: Evaluation of MTT staining on sections of vessels. MTT-stained sections of native samples (a) showed a general de-population of the medial layer. (b) Static conditioned samples were characterized by good viability within all the layers. (c) Fluid-dynamic conditioned samples were characterized by a general good viability in the adventitia, but some areas with lacking endothelium were found. (d), (e) and (f) are representative zoomed areas of, respectively, native, static and fluid-dynamic conditioned vessels. The images in the figure are representative of the behaviour observed in all the samples.

One fundamental characteristic of the system is its versatility. In fact, thanks to the design, the vessel holder is suitable for culturing vessels with different diameters and different lengths.

Furthermore, the Petri-like design ensures the possibility to have easy access to the vessel during the conditioning. It is therefore possible to translate into an *ex vivo* model some procedures that, to our knowledge, have been carried out only in animal models. For example, it is possible to reproduce ferric-chloride thrombosis to study *ex vivo* the mechanism of thrombosis and to perform pharmacological tests [26, 27, 28]. Moreover, thanks to its versatility, the design of the vessel holder can be easily modified to obtain an *ex vivo* model of anastomosis. It would allow to study the relationship between anastomosis and thrombosis, which is still a debating topic [29, 30]. All these peculiarities make the bioreactor innovative; in fact, bioreactors found in literature or commercially available cannot be easily opened and therefore the access to the vessel is challenging [31, 32, 33].

In addition, the very low intra-luminal compartment priming volume is an innovative feature for an *ex vivo* culture system. This makes the bioreactor suitable for performing pharmacological tests without increasing the costs.

Furthermore, the separation between the intra-luminal and the extra-adventitial compartments offers the possibility to reproduce more realistic *in vivo* conditions; in fact the two compartments are characterized by different biochemical environment [12].

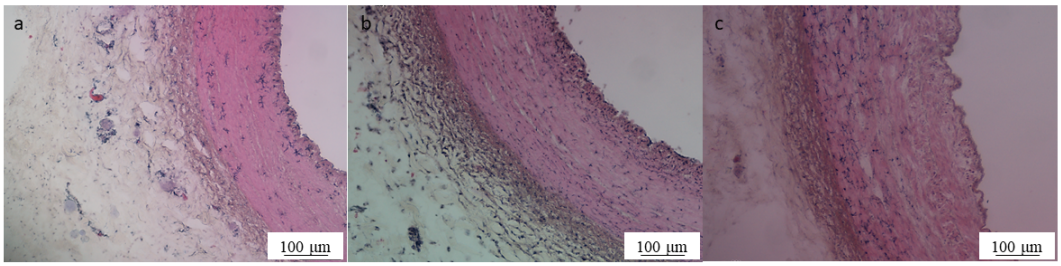

Figure 4.12: Evaluation of the preservation of the wall structure. Haematoxylin and Eosin staining proved that the structure of the wall vessel was preserved in (a) native, (b) static, and (c) fluid-dynamic conditioned vessels. In all the samples, a general de-population of the medial layer could be seen. The images in the figure are representative of the behaviour observed in all the samples.

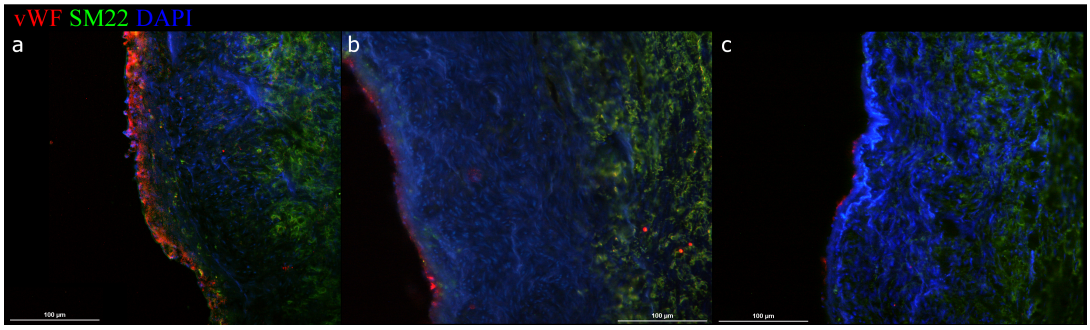

Figure 4.13: Immunofluorescence staining of the slices. (a) The native sample, which is the coronary artery after the isolation of the coronary, is characterized by a good preservation of the structure of the vessel and a continuity of the endothelium. (b) After 24 hours in static conditions, the structure is fine and the endothelium still preserved. (c) In the dynamically conditioned sample, instead, it is visible a discontinuity of the endothelium in some areas. In red von Willebrand Factor labelling the endothelial cells, in green SM22 for smooth muscle cells and in blue the nuclei with DAPI. The images in the figure are representative of the behaviour observed in all the samples.

From a technical point of view, the system proved to be compatible with standard laboratory procedures. The anchoring of the vessel could be performed under biological hood, minimizing the manipulation of the sample. In this way, even fragile vessels could be addressed by this culture system.

Sterility is guaranteed by the use of previously autoclaved components. During the experiment, indeed, the Petri-like design permits a good oxygenation but preventing the bacteria infiltration.

The use of HP MultiJet Fusion additive manufacturing demonstrated to be a good and not expensive solution for realizing a culture system with a complex design. In fact, the material used is biocompatible, autoclavable and suitable for post-processing machining. The post-processing allowed to smooth the surface, to further reduce the probability of bacteria contamination [34].

The matching between the two components of the system, the vessel holder and the cylindrical bioreactor chamber, thought to minimize the manipulation of the

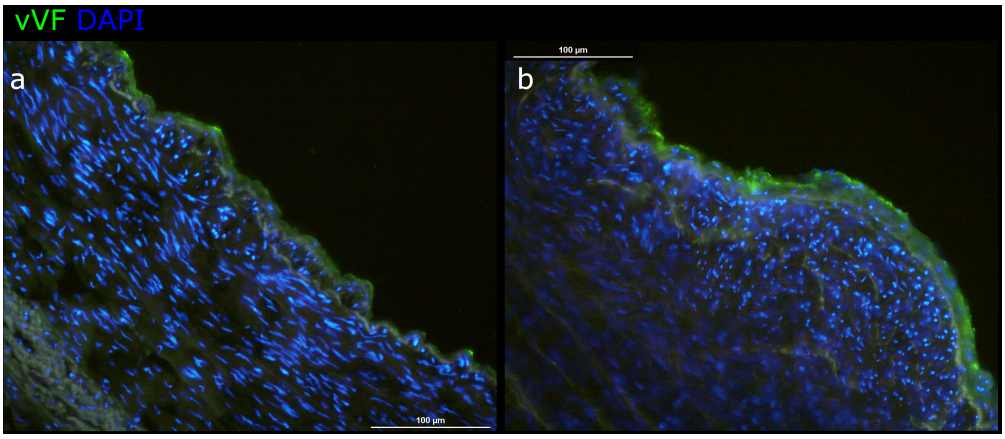

Figure 4.14: Comparison between samples dynamically conditioned for different times. (a) Samples dynamically conditioned for 72 hours show an endothelium preserved but with some areas of disconuity. (b) Pictures taken on samples conditioned for 24 hours are similar to the ones conditioned for 72 hours. In green von Willebrand Factor labelling the endothelial cells, and in blue the nuclei with DAPI. The images in the figure are representative of the behaviour observed in all the samples.

vessels, was made possible by the use of home made silicone gaskets. The silicone material used, Dragon Skin, is biocompatible [35, 36] and the manufacturing technique suitable for mass production. These components can be therefore considered disposable, to avoid the risk of leakages. These components are fundamental; in fact the well functioning of the sealing is also necessary to maintain the sterility during the experiments.

The choice of a small commercial pump was done with the aim of compacting the system and minimizing the priming volumes. These pumps can be placed within the incubator and it represents an innovative characteristic for the bioreactor, compared to the other systems found in literature. In this way, the values of humidity and temperature of the conditioning medium are kept more uniform, limiting evaporation.
Peristaltic pumps were preferred to centrifugal ones, because they are easily sterilized by autoclaving the pump tube. Moreover, peristaltic pumps are not sensible to any changes in the after load and it is an advantage when working with biological samples, to prevent them from drying out in case of sudden increase of the resistance of a component of the fluidic circuit.

To fulfil the control of small commercial roller pumps, a control unit was designed and developed. This component contributed to the compactness of the system, that could be easily transported and used in any laboratory, without having to rely on heavy commercial roller pumps (*e.g.*, the Watson-Marlow used in the first prototype of the system).
The control unit was provided with a micro-controller. In perspective, this could be exploited to implement a feedback control system based on the use of sensors connected to the bioreactor. This would become essential if the fluidic circuit is

implemented to stimulate the samples with a coronary-like flow rate, to obtain a more realistic replication of biomechanical and fluid-dynamic environment [37, 25, 38].

The oxygenation of the medium was a fundamental requirement, necessary to keep the vessel alive during the conditioning period[39]. Analytical models were used to model the oxygen availability within both the intra-luminal and the extra-adventitial compartments. Regarding the intra-luminal compartment, the length of the silicone tubing is a crucial point, because oxygenation must be ensured without increasing excessively the priming volume. According to literature, a value of oxygen in the range 137-140 mmHg was considered to be acceptable for maintaining the viability of the vessel segments [40, 41, 42].

The hydraulic characterization highlighted that 0.8 mm connectors are very resistive components. This had two main consequences. First of all, the value of pressure measured at the inlet of the vessel holder was not representative of the pressure within the vessel. Secondly, the values of pressure within the system were considerably higher if compared with the ones obtained with other connectors. This must be taken into account when dealing with small calibre vessels, to avoid damages due to high pressures.

Animal tissue was chosen for the functional evaluation of the bioreactor. The use of tissue from animals designated for human consumption avoided supply problems. In particular, the elective vessel was the porcine right coronary artery thanks to his easy withdrawal and the presence of a few collateral vessels.

Viability tests and histological staining proved that the structure of the vessel was preserved during the experiments. Nevertheless, in some samples some irregularities were found. In particular, some parts of the endothelium were lacking in cells. This could be explained if the vessels have been already atherosclerotic, as suggested by the presence of atherosclerotic plaques into the lumen.
In the samples exposed to fluid-dynamic stimulus, instead, the partial denudation of the endothelium is more evident. It could be caused by the sudden exposure to a high flow rate. To avoid this problem, the exposure to the target flow rate should be reached gradually, as seen in literature [43].

Moreover, a general qualitative decrease in the number of cells was found in the medial region of all the samples, but it is consistent with other studies found in literature. In fact, the medial layer is characterized by levels of oxygen lower than adventitial and luminal side. The damage occurring in the media during the harvesting could not be restored by the restoration of the oxygen levels at the luminal or at the adventitial sides [12].

Once assessed the viability and the preservation of the structure, vessel wall injury can be induced with ferric-chloride to study the pathological mechanisms involved in the development of thrombosis.

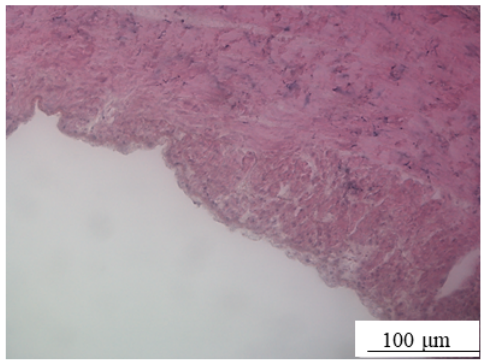

Figure 4.15: Pre-existent atherosclerotic plaque. The presence of atherosclerotic plaques in some samples could be responsible for atherosclerotic damages to the endothelium.

4.6 Conclusions

The design and the manufacturing of an innovative culture system for whole vessel was presented in this chapter.

The main characteristic of this system is its versatility, thanks to an innovative design, obtained with the use of additive manufacturing.

The functional evaluation of the bioreactor proved that it can provide an *ex vivo* model to study cardiovascular diseases.

Nevertheless, long term culture must still be performed with the system to evaluate its reliability.

Moreover, some implementations could be done to obtain a more realistic model. In perspective, for example, a coronary-like flow rate and a biochemical environment more similar to the one found *in vivo* could be reproduced in the bioreactor.

Once assessed that native vessels can be cultured in the system without inducing alteration to the structure, standard *in vivo* procedures can be translated into the *ex vivo* model to induce vessel wall injury.

The *ex vivo* model could be therefore exploited to study the pathological mechanisms and, at a later time, to evaluate the effects of therapeutic treatments.

Bibliography

[1] J. Pudur, C. B. C., G. P. L., and M. Nigel. Animal Models of Thrombosis From Zebrafish to Nonhuman Primates. *Circulation Research*, 118(9):1363–1379, 2016.

[2] Y. S. Zhang, R. Oklu, and H. Albadawi. Bioengineered in vitro models of thrombosis: methods and techniques. *Cardiovascular diagnosis and therapy*, 7(Suppl 3):S329–S335, 2017.

[3] F. Otsuka, S. Yasuda, T. Noguchi, and H. Ishibashi-Ueda. Pathology of coronary atherosclerosis and thrombosis. *Cardiovascular diagnosis and therapy*, 6(4):396–408, 2016.

[4] B. C. Cooley. Murine models of thrombosis. *Thrombosis Research*, 129(2):S62–S64, 2012.

[5] A. C. Weyand and J. A. Shavit. Zebrafish as a model system for the study of hemostasis and thrombosis. *Current opinion in hematology*, 21(5):418–422, 2014.

[6] C. V. Denis, C. Dubois, L. F. Brass, J. W. M. Heemskerk, and P. J. Lenting. Towards standardization of in vivo thrombosis studies in mice. *Journal of Thrombosis and Haemostasis*, 9(8):1641–1644, 2011.

[7] H. C. Whinna. Overview of murine thrombosis models. *Thrombosis Research*, 122(SUPPL.1):64–69, 2008.

[8] W. Li, T. M. McIntyre, and R. L. Silverstein. Ferric chloride-induced murine carotid arterial injury: A model of redox pathology. *Redox Biology*, 1(1):50–55, 2013.

[9] A. P. Owens, Y. Lu, H. C. Whinna, et al. Towards a standardization of the murine ferric chloride-induced carotid arterial thrombosis model. *Journal of Thrombosis and Haemostasis*, 9(9):1862–1863, sep 2011.

[10] B. Furie and B. C. Furie. Thrombus formation in vivo. *The Journal of clinical investigation*, 115(12):3355–3362, dec 2005.

[11] A. Rezvan, C.-W. Ni, N. Alberts-Grill, and H. Jo. Animal, In Vitro , and Ex Vivo Models of Flow-Dependent Atherosclerosis: Role of Oxidative Stress. *Antioxidants & Redox Signaling*, 15(5):1433–1448, 2011.

[12] M. Piola, F. Prandi, G. B. Fiore, et al. Human Saphenous Vein Response to Trans-wall Oxygen Gradients in a Novel Ex Vivo Conditioning Platform. *Annals of Biomedical Engineering*, 44(5):1449–1461, 2016.

[13] L. A. Cox, L. T. Van Eijk, B. P. Ramakers, et al. Inflammatio induced increases in plasma endocan levels are associated with endothelial dysfunction in humans in vivo. *Shock*, 43(4):322–326, 2015.

[14] W. Lee, S.-K. Ku, and J.-S. Bae. Anti inflammatory Effects of Baicalin, Baicalein, and Wogonin In Vitro and In Vivo. *Inflammation*, 38(1):110–125, 2015.

[15] B. Tesfamariam. Endothelial Repair and Regeneration Following Intimal Injury. *Journal of Cardiovascular Translational Research*, 9(2):91–101, 2016.

[16] O. Frank. The basic shape of the arterial pulse. First treatise: mathematical analysis. (English Translation, Original from 1899). *Journal of molecular and cellular cardiology*, 22(3):255–77, 1990.

[17] A. Fick. On liquid diffusion (Reprint). *Journal of Membrane Science*, 100(1):33–38, 1995.

[18] R. J. Paul. Chemical Energetics of Vascular Smooth Muscle. In *Comprehensive Physiology*, Major Reference Works, pages 201–235. 2011.

[19] D. E. Orr and K. J. L. Burg. Design of a modular bioreactor to incorporate both perfusion flow and hydrostatic compression for tissue engineering applications. *Annals of Biomedical Engineering*, 36(7):1228–1241, 2008.

[20] M. S. Isaacson and A. A. Sonin. Sherwood Number and Friction Factor Correlations for Electrodialysis Systems, with Application to Process Optimization. *Industrial and Engineering Chemistry Process Design and Development*, 15(2):313–321, 1976.

[21] R. Mongrain and J. Rodes-Cabau. Role of Shear Stress in Atherosclerosis and Restenosis After Coronary Stent Implantation. *Revista Espanola de Cardiologia*, 59(1):1–4, 2006.

[22] R. Mundargi, D. Venkataraman, S. Kumar, et al. Novel Sensor-Enabled Ex Vivo Bioreactor : A New Approach towards Physiological Parameters and Porcine Artery Viability. *BioMed Research International*, 2015:8, 2015.

[23] M. I. Bogorad, J. DeStefano, A. D. Wong, and P. C. Searson. Tissue engineered 3D microvessel and capillary network models for the study of vascular phenomena. *Microcirculation*, 24(5):e12360, jul 2017.

[24] A. A. Miyakawa, L. A. O. Dallan, S. Lacchini, T. F. Borin, and J. E. Krieger. Human saphenous vein organ culture under controlled hemodynamic conditions. *Clinics*, 63(5):683–688, 2008.

[25] M. Piola, F. Prandi, N. Bono, et al. A compact and automated ex vivo vessel culture system for the pulsatile pressure conditioning of human

saphenous veins. *Journal of Tissue Engineering and Regenerative Medicine*, 10(3):E204E215, 2016.

[26] S. Nouri, M. R. Sharif, and S. Sahba. The effect of ferric chloride on superficial bleeding. *Trauma monthly*, 20(1):e18042–e18042, 2015.

[27] W. Li, M. Nieman, and A. Sen Gupta. Ferric Chloride induced Murine Thrombosis Models. *JoVE*, (115):e54479, 2016.

[28] A. L. Huttinger, D. G. Wheeler, S. Gnyawali, et al. Ferric Chloride-induced Canine Carotid Artery Thrombosis: A Large Animal Model of Vascular Injury. *JoVE*, (139):e57981, 2018.

[29] P. W. Henderson, J. G. Fernandez, Y. Cemal, et al. Successful Salvage of Late Anastomotic Thrombosis after Free Tissue Transfer. *Journal of reconstructive microsurgery*, 32(4):316–324, 2016.

[30] A. Iraj, P. Herle, G. Miller, et al. End to End versus End to Side Microvascular Anastomosis: A Meta-analysis of Free Flap Outcomes. *Journal of Reconstructive Microsurgery*, 33(06):402–411, 2017.

[31] N. Dahan, U. Sarig, T. Bronshtein, et al. Dynamic Autologous Reendothelialization of Small-Caliber Arterial Extracellular Matrix: A Preclinical Large Animal Study. *Tissue engineering. Part A*, 23(1-2):69–79, 2017.

[32] J. Wang, L. Liu, Y. Wu, et al. Ex vivo blood vessel bioreactor for analysis of the biodegradation of magnesium stent models with and without vessel wall integration. *Acta Biomaterialia*, 50:546–555, 2017.

[33] O. Udofot, L. H. Lin, W. H. Thiel, et al. Delivery of Cell-Specific Aptamers to the Arterial Wall with an Occlusion Perfusion Catheter. *Molecular Therapy - Nucleic Acids*, 16(June):360–366, 2019.

[34] G. D. Bayrak, N. Sandalli, S. Selvi-Kuvvetli, N. Topcuoglu, and G. Kulekci. Effect of two different polishing systems on fluoride release, surface roughness and bacterial adhesion of newly developed restorative materials. *Journal of Esthetic and Restorative Dentistry*, 29(6):424–434, 2017.

[35] R. Herbert, J. H. Kim, Y. S. Kim, H. M. Lee, and W. H. Yeo. Soft material enabled, flexible hybrid electronics for medicine, healthcare, and human machine interfaces. *Materials*, 11(2), 2018.

[36] M. Schaffner, J. A. Faber, L. Pianegonda, et al. 3D printing of robotic soft actuators with programmable bioinspired architectures. *Nature Communications*, 9(1), 2018.

[37] F. Prandi, M. Piola, M. Soncini, et al. Adventitial vessel growth and progenitor cells activation in an ex vivo culture system mimicking human saphenous vein wall strain after coronary artery bypass grafting. *PLoS ONE*, 10(2):1–20, 2015.

[38] D. A. Prim, J. D. Potts, and J. F. Eberth. Pulsatile Perfusion Bioreactor for Biomimetic Vascular Impedances. *Journal of Medical Devices*, 12(4):41002–41010, 2018.

[39] J. Kim, K. Kennedy, and G. Vunjak-Novakovic. Bioreactors in Regenerative Medicine. In A. Atala, R. Lanza, A. G. Mikos, and R. B. T. Nerem, editors, *Principles of Regenerative Medicine - Third Edition*, chapter 45, pages 787–803. Academic Press, Boston, 2019.

[40] J.-A. Collins, A. Rudenski, J. Gibson, L. Howard, and R. O'Driscoll. Relating oxygen partial pressure, saturation and content: the haemoglobin-oxygen dissociation curve. *Breathe (Sheffield, England)*, 11(3):194–201, 2015.

[41] J.-O. Dunn, M. G. Mythen, and M. P. Grocott. Physiology of oxygen transport. *BJA Education*, 16(10):341–348, 2016.

[42] E. Ortiz-Prado, J. F. Dunn, J. Vasconez, D. Castillo, and G. Viscor. Partial pressure of oxygen in the human body: a general review. *American journal of blood research*, 9(1):1–14, 2019.

[43] M. H. Kural, G. Dai, L. E. Niklason, and L. Gui. An Ex Vivo Vessel Injury Model to Study Remodeling. *Cell Transplantation*, 27(9):1375–1389, 2018.

Chapter 5

Design and characterization of a tubular synthetic graft used as model to study vascular diseases

5.1 Introduction

Neo-vascularization in atherosclerotic lesion greatly contributes to plaque instability [1]. In atherosclerotic lesions, the angiogenic mechanism occurs from pre-existing *vasa vasorum*. In fact, in atherosclerotic plaques, the oxygen availability could be insufficient due to intimal thickening and resulting decreased diffusion. Therefore hypoxia and inflammatory conditions induces the release of angiogenic factors that stimulate the neo-vascularization sprouting from pre-existing *vasa vasorum*. This neo-vascularization could be initially protective, but it also intensifies inflammation within the plaque, with consequent progression of the atherosclerotic lesion [2].

In mammalian tissues, hypoxia is one of the most important angiogenic stimuli and the hypoxia-inducible factor (HIF) is the major oxygen regulator, responsible for the most transcriptional responses to low oxygen availability [3]. Up-regulation of HIF, for example, induces the expression of vascular endothelial growth factor (VEGF) [4, 5] and angiopoietin [3], which are well known to be inducers of angiogenesis [6, 7].

These neo-vascularization mechanisms can be addressed as target for therapeutic strategy for reducing plaque instability. But, still, players involved in the regulation of endothelial cells functions related to the disease still need to be completely unveiled [8].

Tissue-engineered models could be exploited for this scope. In fact, they permit to isolate specific stimuli and to select specific cellular populations to study aspects related to vascular pathologies. In addition, if compared to standard *in vitro* cultures, they offer the possibility to mimic more realistic structures, allowing cells to grow and interact in a three-dimensional environment, but guaranteeing at the same time a good reproducibility of experiments [9].

As a proof of concept, we developed a tissue-engineered model for studying the angiogenic profile of adventitial progenitor cells (APCs) cultured on tubular scaffolds and exposed to hypoxic conditions.

Previous studies, in fact, highlighted that APCs are involved in angiogenic processes [10] and, in particular, we focused on the hypoxia-mediated up-regulation of trophoblast glycoprotein (TPBG), which is responsible for migratory and angiogenic activity of adventitial progenitor cells [11].
The tissue engineered model was designed to investigate this mechanisms under fluid-dynamic and three-dimensional conditions, assessing whereas the hypoxia-mediated effects are enhanced.

The study was entirely performed at the School of Translational Health Science of the University of Bristol, during a six-months period sponsored by the Erasmus Plus Traineeship.

5.2 Materials and Methods

5.2.1 Manufacturing of the scaffolds

Tubular scaffolds were fabricated using the ND-ES laboratory electrospinning unit (Nadetech Innovations, Spain) (Figure 5.1.a). The electrospinning machine is an independent and automatized unit consisting in: (i) a controllable high voltage source, that can provide a voltage up to 30 kV, (ii) a grounded rotating collector, made of a steel rod connected to a stepper motor, and (iii) a syringe pump (Figure 5.1.b). The device is equipped with its own control software, which permits a fine control of voltage, collector speed and flow rate.

As the polymer jet leaves the needle connected to the high voltage source, it wraps around the rotating collector and create a cylindrical sheet. The mandrel has a diameter of 6 mm and a length of 200 mm (Figure 5.1.c).

Since the deposition of the fibres is not uniform along the length of the mandrel, the pump was customized to allow the placement of multiple syringes though a PLA 3D printed multi-syringes support (Figure 5.1.d). The distance between adjacent syringes was calculated to obtain a uniform structure along the mandrel.

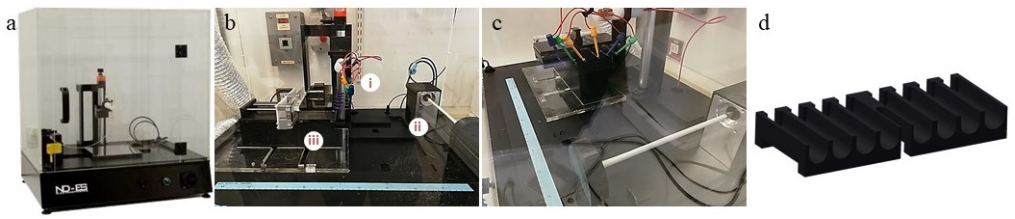

Figure 5.1: The electrospinning setup. (a) The ND-ES electrospinning unit is a stand-alone machine equipped with its own control software. (b) It consists of (i) a controllable high voltage source, (ii) a grounded collector, and (iii) a syringe pump. (c) The collector is a rotating mandrel where nanofibres wrap around, creating the tubular scaffold. (d) The syringe pump was customized with a support for multiple syringe to obtain a uniform structure.

5.2.1.1 Electrospinning of gelatin fibres

The polymer solution used to electrospun fibres of GL was composed of 15% v/w GL (Type A gelatin from porcine skin, Sigma Aldrich) dissolved in a liquid solution of $^{60}/_{40}$ v/v acetic acid/deionized water by stirring and heated at 50°C. γ-glycidoxypropyltrimethoxy silane (GPTMS) was used as crosslinker for GL. Before electrospinning, 200 µl of GPTMS were added for each gram of GL. The final liquid solution was stirred for one hour. Then, three 5-ml syringes were loaded with the solution, mounted on the syringe pump and connected to high voltage source.

A tuning of the main parameters of electrospinning was performed to achieve the optimal manufacturing of the fibres in terms of fiber diameter, porosity and pore diameter.

In particular, the morphological characteristics of the fibres were evaluated after 10 minutes of electrospinning, with a rotation speed of the collector of 1000 rpm and varying the following parameters one by one:

- voltage: 20, 25 30 kV;
- distance between emitter and collector: 15, 20, 25 mm;
- flow rate: 0.1, 0.2, 0.3 ml/h.

After the electrospinning process, the scaffolds specimens were dried in a vented oven for 48 hours at 37° C.

Therefore, Scanning Electron Microscopy (SEM, Quanta FEG model 200, FEI, US) was used to acquire images of the fibres for further morphological analysis. Before the acquisition with SEM, the samples were sputtered with a gold-palladium alloy and finally placed in a specimen stand. Pictures were acquired at different magnifications.

The analysis of the morphology of the fibres and of the porosity was carried out using the software ImageJ.

Briefly, on each snap, the average diameter was evaluated on each picture measuring with the software the diameter of 10 random fibres and calculating the mean and the standard deviation.
After the binarization of the image, the porosity was calculated as the ratio between the areas of the image not occupied by fibres pixel, corresponding to pores, and black pixel, corresponding to the areas of the image occupied by fibres. Finally, the dimension of the pores was evaluated selecting 10 random pores, measuring the area of each pore and deriving the value of the diameter, approximating each pore to a circle.

5.2.1.2 Electrospinning of polycaprolactone fibres

The polymer solution used to electrospun PCL fibres was composed by PCL (mean Mn 80000, Sigma Aldrich) dissolved in chloroform. Once dissolved the PCL, three 5-ml syringes were loaded with the solution, mounted on the syringe pump and connected to high voltage source.

A tuning of the main parameters of electrospinning was performed to achieve the optimal manufacturing of the fibres.

In particular, the morphological characteristics of the fibres were evaluated after 15 minutes of electrospinning, with a rotation speed of the collector of 1000 rpm and varying the following parameters one by one:

- concentration of PCL solution: 7.5% (w/v), 10% (v/w) and 15% (v/w);

- voltage: 20, 25 30 kV:
- distance between emitter and collector: 15, 20, 25 mm;
- flow rate: 0.1, 0.2, 0.3 ml/h.

Scanning Electron Microscopy (SEM, Quanta FEG model 200, FEI, US) was used to acquire images of the fibres for further analysis. Before the acquisition with SEM, the samples were sputtered with a gold-palladium alloy and finally placed in a specimen stand. Pictures were acquired at different magnifications.

The general morphology of the fibres was evaluated.

Fibres diameter, porosity and pore size were calculated on PCL fibres obtained with the working parameters using the software ImageJ as previously explained (paragraph 5.2.1.1).

5.2.1.3 Final structure of the scaffolds

The tubular scaffold used for functionalization and further experiments was designed as a double-layer scaffold.

In particular, it consisted of an inner layer of gelatin, an intermediate layer of gelatin and PCL and an outer layer of PCL.

Two fundamental requirements were kept into consideration for the structure of the scaffolds: (i) the layers must not peel off, and (ii) the scaffold must have good mechanical properties.

Realization of the scaffolds The analysis of images obtained from SEM was used to define a range of parameters to electrospin both GL and PCL nanofibres with optimal features for cells adhesion.

The electrospinning protocol for the manufacturing of the double-layers scaffolds consisted of three phases: (i) electrospinning of GL fibres alone, (ii) electrospinning of fibres of GL and PCL simultaneously, and (iii) electrospinning of PCL fibres alone.
During the first phase three 5-ml syringes are filled with 15% (w/v) GL solution and the fibres are electrospun for 45 minutes. After this phase, three 5-ml syringes filled with PCL 15% (w/v) are added and and GL and PCL are extruded at the same time for 45 minutes. Finally, the third phase is carried out with six 5-ml syringes loaded with PCL 15% (w/v) and PCL is electrospun from the six syringes for one hour.

After the electrospinning process, scaffolds were dried out in oven for 48 hours at 37°C.

Mechanical characterization of the scaffolds Mechanical properties of the double-layer (GL/PCL) scaffolds were measured and compared to gelatin scaffolds to assess its proper composition.

Mechanical properties were measured using Instron 3343 (© Illinois Tool Works Inc., US) (Figure 5.2.a) equipped with BioPlus Bath to perform the tests in wet conditions at 37°C.

The experiment was set up following ISO 7198:2016 specifications. GL and GL/PCL tubular samples were cut and longitudinal stripes of 10 x 20 mm with 0.5±0.1 mm of thickness were prepared. The comparison of mechanical properties was carried out on longitudinal scaffold axes, setting a steady strain speed of ± 50 $mm \cdot min^{-1}$(Figure 5.2.b).

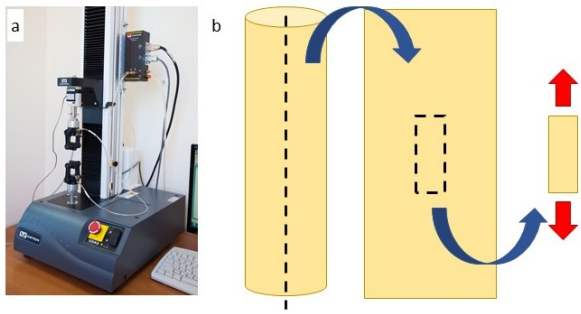

Figure 5.2: Mechanical characterization of the scaffolds. (a) The characterization was performed using the Instron 3343 (© Illinois Tool Works Inc., US). (b) Scaffolds were cut longitudinally and stripes of 10 x 20 mm were used for testing the mechanical properties along the longitudinal axes.

5.2.2 Biological functionalization of the scaffolds

Tubular cellular constructs were obtained by the functionalization of the scaffolds. Two different cellular types were taken into consideration during this study: (i) adventitial progenitor cells (APCs), and (ii) coronary artery endothelial cells (CAECs).

5.2.2.1 Cells source

Adventitial progenitor cells In the laboratory of the University of Bristol (Bristol Heart Institute, level 7, School of Translational Health), where this study was performed, it was identified a source of vascular progenitor cells (*i.e.,* the adventitial progenitor cells), which express typical pericyte (NG2, PDGFRβ), mesenchymal (CD44, CD90, CD105) and stemness (c-kit, GATA-4) markers [12]. These cells are isolated from leftovers of saphenous vein from coronary artery bypass surgery using a standard protocol explained elsewhere [12].

APCs were cultured at 37 °C, 20 % Oxygen, 5 % carbon dioxide in complete

Endothelial Growth Medium-2 (EGM-2) (PromoCell) supplemented with 2% FBS.

The expansion of the cells were performed with the following protocol.
APCs were plated on gelatin/fibronectin (10μg/mL) coated plates in presence of EGM-2. Once cells reached 60/70% of confluence, adherent colonies were passaged to new culture dishes. For splitting the cells, they were detached from the culture dish by washing with PBS and incubating at 37°C, 20% oxygen, 5% carbon dioxide for 5 minutes in a solution of 0.05% (w/v) trypsin. Then trypsin activity was neutralize with a solution of 10% FBS added in a volume double with respect to the volume of trypsin used. The suspension was centrifuged at 400 g for 10 minutes and the supernatant discarded. APCs pellet was re-suspended in 1 ml of EGM-2, cells counted with a Neubauer chamber and seeded in a new culturing plate at the density of 10000 cell·cm^{-2}.

All *in vitro* experiments were set up with cells at passage 7.

Human coronary artery endothelial cells Coronary artery endothelial cells (CAECs, from PromoCell, Germany) were cultured at 37 °C, 20% Oxygen, 5% carbon dioxide in Endothelial Cell Growth Medium MV (PromoCell, Germany) supplemented with 0.05 ml/ml Fetal Calf Serum (FCS), 0.004 ml/ml endothelial cell growth supplement, 10 ng/ml epidermal growth factor, 90 μg/ml heparin and 1 μg/ml hydrocortisone.

The expansion processes was performed splitting the cells once 70% confluence was reached.
Briefly, cells were washed with PBS and incubated with a solution of 0.05% (w/v) trypsin at RT for a few minutes to detach them from the culture plate. Detachment was monitored with a microscope. Trypsin activity was then neutralized with a solution of 10% FBS added in a volume double with respect to the volume of trypsin used. The suspension was then centrifuged at 300 g for 3 minutes, the supernatant discarded and cells re-suspended in 1 ml of medium. Cells were counted with a Neubauer chamber and seeded in new culturing plate at the density of 8000 cell·cm^{-2}.

5.2.2.2 Functional evaluation of double-layer scaffolds

Functional assays were performed to assess the behaviour of the cells in terms of viability on different three dimensional support. In particular, GL/PCL and PCL scaffolds were compared.

Scaffolds were cut into square pieces of 1 cm^2 and sterilized. The sterilization of the scaffolds was performed as follow. Scaffolds were decontaminated with ethanol 70%, washed with phosphate buffer solution (PBS) to remove any trace of ethanol and dried out exposing each side to the UV light for 15 minutes. After the exposure to UV, scaffolds were incubated in a solution of 1% v/v PenStrep

(ThermoFisher, MA, US) and 1 µg/ml amphotericin B (ThermoFisher, MA, US) for 2 hours. Then, scaffolds were washed three times with PBS and incubated overnight at 37°C, 20% Oxygen, 5% carbon dioxide with EGM-2.

For the functional experiment, scaffolds pieces were placed in a 24-multiwell plate and APCs were seeded with a density of 7500 cell.cm^{-2}on both GL/PCL scaffolds and on PCL scaffolds. As a positive control, APCs were seeded with the same density in 48-multiwell plates.

As a cellular comparison, CAECs were seeded with a density of 6000 cell.cm^{-2}on GL/PCL scaffolds, PCL scaffolds and culture plates.

For each condition, three replicates were realized.

Cell viability was assessed at day 1, 3 and 7, using the Biotium viability/cytotoxicity assay (Biotium, CA, US).

Briefly, at the moment of the assessment, the culturing medium contained in the multiwell plate was removed and samples were washed with PBS. The samples were then maintained for 30 min in the incubator with a solution of Calcein [1:2000], EthD-III [1:500] and Hoechst [1:100] in serum free medium. After incubation at 37°C, 5% carbon dioxide for 30 min, the scaffolds were analysed by fluorescence microscopy using the microscope Zeiss Axio observer Z1 (Carl Zeiss, Germany). For each condition, five snaps were acquired and cell viability was calculated as (Eq. 5.1):

$$V\% = \frac{calcein^{+}cells}{total\_cellnumber} * 100 \tag{5.1}$$

where calcein positive cells are the viable cells.

5.2.2.3 Cell seeding into the tubular scaffolds

The seeding of APCs into the tubular scaffolds was performed using a rotating bioreactor previously developed and characterized in the laboratory.

The seeding procedure consists of four steps: (i) mounting of the scaffolds on luer connectors, (ii) sterilization of the scaffolds, (iii) manual injection of the cells within the scaffolds, and (iv) rotating seeding.

Mounting of the scaffolds First, the scaffolds are cut into 5-cm-long tubular pieces and placed into distilled water in one Petri dish. A POM assembling tool is used to anchor the scaffolds on ⅛" barbed male slip luer connectors (Figure 5.3.a). The tool has an elliptic hole where the luer connector is placed, and an external support for two rubber bands. Once the scaffold fits the luer, the rubber bands are pushed on the scaffolds through a pair of tweezers. The scaffold is then firmly

anchored on the connector (Figure 5.3.b). The same procedure is repeated for the other end of the scaffold.

After the mounting procedure, the scaffold anchored to the luer connectors was moved in a POM holder. The holder was designed to keep the scaffolds straight and in the proper position during the manual injection and the rotating seeding (Figure 5.3.c).
The holders fitted perfectly a 15-ml falcon tube (*i.e.,* 65 mm long and 13.6 mm diameter) and were provided with two connection trails for the luer connectors. A 3-mm-hole was obtained to their upper part of the holders, to allow the use of tweezers to handle them without damaging the scaffolds.

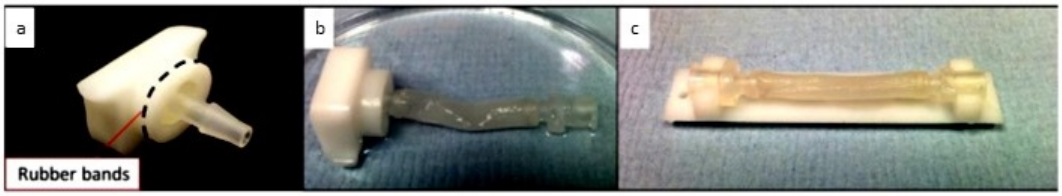

Figure 5.3: Mounting procedure for the scaffolds. (a) The POM assembling tool is used for helping in the anchoring of the scaffolds on the 1/8" barbed male slip luer connectors though rubber bands. (b) Once the scaffold fits the connector, the rubber bands are released on it. (c) When both the ends of the scaffold are anchored to the connectors, it is moved in a POM holder.

Scaffold sterilization For sterilizing the scaffolds a precise protocol was set. First, scaffolds are washed in PBS with three washes of 10 minutes each. Then, scaffolds are dipped in ethanol 70% for 10 minutes and again washed in sterile PBS for 10 minutes. The rotating bioreactor and the scaffolds are exposed to UV light for 15 minutes each side. One PDMS custom made lid is then inserted within the bottom end of the scaffold.
Finally, two subsequent washes of 30 minutes each are performed with a solution of 1% v/v PenStrep (ThermoFisher, MA, US) and 1 µg/ml Amphotericin B (ThermoFisher, MA, US) in PBS. The scaffolds are then soaked overnight in a fresh solution of 1% v/v PenStrep and 1 µg/ml Amphotericin B in PBS. Before the seeding, the scaffolds are submerged in PBS for 2 hours in the incubator at 37°C.

Cells manual injection APCs are detached from the culture plate as explained in paragraph 5.2.2.1. Then, using a 1-ml syringe and a stainless steel needle (18 G), a volume of PBS equal to 300 µl is removed from the luminal volume of the scaffold and a suspension of 450000 cells is injected through the upper male luer connector, as previously optimized in this laboratory.
Finally, the upper connector is sealed with a second silicone lid and the POM holder is moved into a 15-ml Falcon tube.

Rotating seeding Falcon tubes containing the POM holder with cellular construct are placed in the rotating bioreactor and the rotating seeding is performed at 37°C, 20% oxygen and 5% carbon dioxide. The bioreactor was designed, developed and characterized at the laboratories of Bristol Heart Institute in a previous work. Briefly, it consists of: (i) a waterproof control case with a switch button, a USB interface, and a power input, (ii) a motor to perform the rotation necessary for the dynamic seeding, (iii) electric components (*i.e.*, a micro-controller Arduino and a motor driver), and (iv) a tube carrier for 15-ml falcon tubes fitting up to six falcon tubes (Figure 5.4.a).

The rotating seeding protocol was optimized in a previous work. The rotation is performed for 6 hours alternating 20 seconds clockwise to 30 seconds anticlockwise, followed by 5 minutes of rest. The rotational speed was set equal to 13.4 rpm and followed an initial step of one minute of rotation at 20 rpm.

After the rotating seeding, cellular constructs are kept at 37°C, 20% oxygen and 5% carbon dioxide over night.

To assess the rotating seeding efficacy, phalloidin (Conjugated Alexa Fluor 555 Phalloidin A34055, Life Technologies, CA, US) was used to stain the cytoskeleton of the cells. The day following the seeding, the cellular constructs were extracted from the holders, washed in PBS and the cells were fixed in 4% PFA. 0.1% Triton (Sigma-Aldrich, MO, US) for 5 minutes was used for permeabilizing the membranes, then constructs were washed twice with PBS. Then, the tubular constructs were cut along the longitudinal axis and incubated for 20 minutes in 25 µL/ml phalloidin solution in PBS at room temperature. Incubation with the secondary antibody (Alexa Fluor 568, Life technologies, CA, US) followed a wash in PBS and was performed for one hour at room temperature. Finally, the constructs were incubate for 5 minutes in DAPI solution, washed with PBS and placed in a 6-multiwell plate with glycerol 80%. Images were acquired with the fluorescence microscope Zeiss Axio observer Z1 (Carl Zeiss, Germany).

5.2.3 Angiogenic effects of hypoxia on APCs

The rationale of the study was to assess the angiogenic effects induced by hypoxia on cells cultured in three-dimensional matrix, and on cells cultured on a three dimensional matrix and exposed to dynamic conditions. Given this, tubular constructs were cultured both in static and in dynamic conditions in normoxic and hypoxic environments. Culture of APCs on standard plates was used a control.

5.2.3.1 Design of the experiments

After the rotating seeding, the tubular constructs were removed from the POM holders.

Custom made PMMA supports were designed for the static conditioning with the three dimensional CAD software PTC Creo Parametric 4.0 (PTC Inc., MA, US) and realized by laser cutting. The aim of the supports was to hold the constructs submersed in the medium inside the Petri-dishes, to avoid them to expose to air and to dry out.
Before the experiments, the PMMA supports were autoclaved with an anti-fungi and an anti-bacterial solution.
Therefore, for the static conditioning, the constructs (n=2) were placed in two different Petri-dish equipped with the PMMA support and filled with 50 ml of EGM-2 supplemented with 1% v/v PenStrep but without FCS and VEGF (Figure 5.4.b).
For the normoxic conditioning, the Petri-dish was placed in incubator and cultured at 37°C, 20% oxygen, 5% carbon dioxide for 24 hours. The hypoxic environment was obtained with an hypoxic incubator (*i.e.*, 37°C and 2% oxygen). Hypoxic conditioning was performed for 24 hours.

For the dynamic conditioning of the constructs (n=4), the commercially available 3DCulturePro™ Bioreactor (TA Instruments, UK) and a custom made bioreactor developed by our group during my Ph. D. project were used for, respectively, the normoxic fluid-dynamic stimulation (n=2 constructs) and the hypoxic fluid-dynamic stimulation (n=2 constructs). All the components were previously autoclaved.

The 3DCulturePro™ Bioreactor consists of a peristaltic pump (Masterflex L/S digital 07528-20, Germany), silicone tubing (3.175 mm inner diameter and 6.35 mm outer diameter) connecting all the components of the bioreactor, a pump tube (PharMed BPT tubing, 2.79 mm inner diameter), a multi-chamber stand, and the 3DCulturePro bioreactor chamber. The 3DCulturePro chamber is composed by two separated chambers: one chamber serves as reservoir and one chamber hosts tubular constructs. This chamber is equipped with female luer locks that fit the male luer connectors to which the scaffolds had been anchored (Figure 5.4.c).
Once assembled the 3DCulturePro™ Bioreactor, the cellular construct was placed within 3DCulturePro chamber, the bioreactor was filled with 140 ml of EGM-2 supplemented with 1% v/v PenStrep but without FCS and VEGF and placed within the incubator at 37°C, 20% oxygen, 5% carbon dioxide for 24 hours. The target flow rate was set equal to 20 ml/min and reached gradually (Figure 5.4.d).

The description of the custom made bioreactor used for the hypoxic conditioning can be found elsewhere in this thesis (paragraph 4.3.1). The chamber was partially modified to permit the housing of the scaffolds. In particular, the sliding needle was removed and replaced with a threaded female luer connector, so that 5-cm long tubular constructs can be fitted within the chamber. Silicone tubing (3.175 mm inner diameter and 6.35 mm outer diameter) and a peristaltic pump (Watson-Marlow 323 Du, Watson-Marlow Fluid Technology Group, UK) equipped with a single channel pumping head (314D, Watson-Marlow Fluid Technology Group,

UK) were connected to the Petri-like bioreactor (Figure 5.4.e).
The bioreactor was filled with 40 ml of EGM-2 supplemented with 1% v/v Pen-Strep but without FCS and VEGF and placed within the hypoxic incubator at 37°C, 2% oxygen, 5% carbon dioxide for 24 hours. The target flow rate was set equal to 20 ml/min and reached gradually (Figure 5.4.f).

As a control, APCs were seeded in 24-multiwell with a density of 5000 cell$\cdot$cm^{-2}.

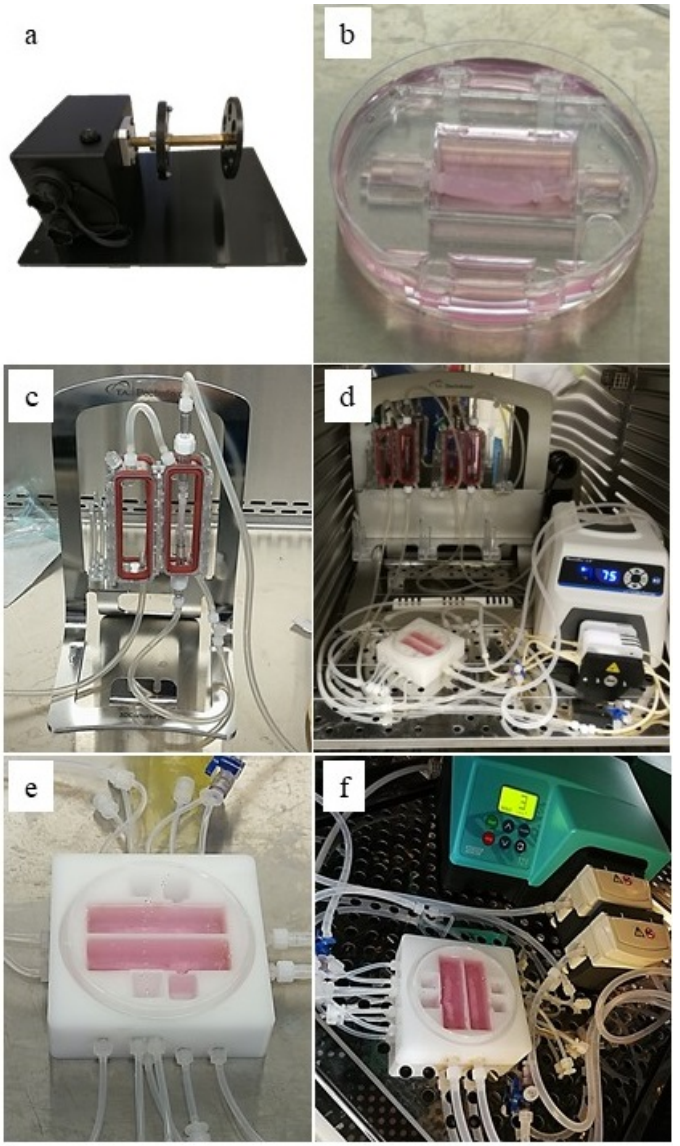

Figure 5.4: Evaluation of the angiogenic profile of adventitial progenitors cultured on tubular scaffolds. (a) The adventitial progenitor cells (APCs) were seeded into the luminal side of the scaffolds using a rotating bioreactor. (b) Cellular constructs were exposed to hypoxic and normoxic environment but in static conditions using Petri-dishes equipped with custom made supports to hold the scaffolds in the medium. (c) The 3DCulturePro™ Bioreactor was used for culturing the cellular constructs under dynamic conditions in normoxic environment. (d) Culture medium was flowed inside the lumen of the scaffold with a flow rate of 20 ml/min using a peristaltic pump. (e) A bioreactor developed at the Laboratory of Micro- and Bio-fluid Dynamics of the Politecnico di Milano was used to expose the cellular constructs to hypoxia. (f) The bioreactor was placed in a hypoxic incubator (2% of Oxygen) and connected to a peristaltic pump to culture the APCs with a medium flow rate of 20 ml/min.

5.2.3.2 Analysis of the samples

After the conditioning, the constructs were removed from the luer connectors and cut into pieces for performing biological analysis: (i) viability assay, (ii) immunofluorescence staining, (iii) quantitative Polymerase Chain Reaction (q-PCR), and (iv) ELISA analysis.

The protocol used are explained below.

The viability test was performed on a piece extracted from the cellular construct following the protocol shown in paragraph 5.2.2.2.

Immunofluorescence staining was used for labelling TBPG. Briefly, the piece of cell construct is placed in a 24-multi-well, washed with PBS and fixed with 4% PFA for 15 minutes at room temperature. Then, two PBS washes are performed and cells are permeabilized using 0.1% v/v Triton in PBS for 10 minutes at 4°C. The construct is washed again with PBS twice, then blocked for 30 minutes at room temperature. The TPBG-blocking solution used is composed by 5% v/v FBS in a solution of PBS and 0.05% v/v Tween 20. Therefore, incubation with primary rabbit monoclonal anti-TPBG antibody (ab134162, Abcam, UK) is performed over night at 4°C in TPBG-blocking solution [1:200]. The following day, after washing with PBS, sample is incubated with secondary antibody at 1:200 dilution in TPBG-blocking solution for one hour at 4°C. Finally, the construct is washed in PBS twice, incubated with DAPI for 5 minutes at room temperature, washed with PBS and distilled water and mounted using Fluoromont G.
Images were acquired using the microscope Zeiss Axio observer Z1 (Carl Zeiss, Germany).

One part of the cellular construct was used for isolating RNA using a standardized phenol-chloroform protocol to perform q-PCR. Briefly, the samples were lyzed into RNAase hydrogen/DNA free tube containing 1.4 ml of Qiazol and put at -80°C. Therefore, the miRNeasy Micro Kit (Cat Nbr #217084, QIAGEN) was used for the RNA extraction. RNA quality was evaluated with a Nanodrop considering the ratio of absorbance 260/280. Total RNA (100 ng) was reverse-transcribed into single-stranded complementary DNA (c-DNA) using a High Capacity RNA-to-cDNA Kit (Life Technologies, UK). The RT-PCR was performed using first-strand cDNA with TaqMan Fast Universal PCR Master Mix (Life Technologies, UK).

The target transcript considered for this study were:

- UBC (Hs00824723_m1): housekeeping (*i.e.*, constitutive genes that are required for the maintenance of basic cellular function and are used as a reference point for the analysis of expression levels of other genes).
- BAX (Hs00180269_m1): pro-apoptotic gene
- BCL2 (Hs04986394_s1): regulator of apoptosis

- CSPG4/NG2 (Hs00361541_g1): chondroitin sulfate proteoglycan, it is a pericyte marker
- PDGFRb (Hs01019589_m1): platelet-derived growth factor receptor beta, it is a pericyte marker
- GATA4 (Hs00171403_m1): transcription factor GATA4, stemness marker
- NANOG (Hs04399610_g1): stemness marker
- SOX2 (Hs01053049_s1): stemness marker
- ANGPT1 (Hs00375822_m1, angiopoietin-1): pro-angiogenic marker
- VEGF-A (Hs00900055_m1, vascular endothelial growth factor-A): pro-angiogenic marker
- BACH1 (Hs00230917_m1): Transcription regulator protein
- TPBG (Hs00272649_s1): responsible for angiogenic activities of APCs
- CXCL12 (Hs03676656_mH): responsible for angiogenic activities of APCs

All reactions were performed in a 5µL volume with a concentration of cDNA of 5 ng/µl.

Quantitative PCR was performed on a QuantaStudio Real-Time PCR system (Applied Biosystems, UK).

Finally, cell conditioned media (CCM) was collected from controls and from static and dynamic experiments to perform ELISA to quantify the release of angiogenic factors, such as ANPT1 and VEGF in the medium (secretome profile). First, medium from bioreactors, both 3DCulturePro™ Bioreactor and Petri-like, had to be concentrated. Two subsequent ultra-filtration were performed using filters (Amicon-ultra, UFC200324 and UFC201024) to collect proteins in the range 3-10 kDa.
Quantities of secreted VEGF and Angpt1 (DY293B and DY923, respectively, R&D Systems, UK) were determined following the manufacturer's instructions.

All the analysis performed on cell constructs were performed even on APCs cultured in the multiwell plates.

5.2.3.3 Critical issues

During the procedure explained in the paragraphs 5.2.3.1 and 5.2.3.2 some critical issues were highlighted. These problems affected the results obtained during this study, as explained below.

Mould contamination During the experiments with the tubular constructs we encountered a series of problems due to mould contamination, even though a sterilization with anti-fungi and exposure to UV light were performed.
Evaluating one by one all the components used for static and dynamic stimulation, we attributed to scaffolds the origin of contamination.

Therefore, we set a protocol (5.2.2.3), increasing the number of washes and the exposure time to anti-fungi solution.

Assessment of angiogenic profile All PCR results regarding tubular constructs were negative, included the amplification of housekeeping genes.

We tried therefore to analyse the problem to find the reason of this result.

First, we tried to perform a mechanical homogenization of the samples before performing the RNA extraction and we carried out a q-PCR. The results were still all negative, so we decided to run a gel to check the integrity of RNA and cDNA.
We run a gel for comparing mRNA and cDNA from cell constructs homogenized before RNA extraction, cell constructs not homogenized before RNA extraction and APCs cultured on standard cultured plate, as a control (*i.e.*, cDNAs were amplified by q-PCR in this case).

Secondly, we run a q-PCR with only the housekeeping gene at different concentration (from 10 ng/µl to 0.07 ng/µl) using cDNAs from cell constructs homogenized before RNA extraction, and APCs cultured on standard cultured plate, as a control.

5.3 Results

5.3.1 Morphological characterization

The analysis of SEM images of the GL electrospun fibres highlighted that they were randomly distributed and in general they did not show any defects or beads (Figure 5.6.a).
The diameter of the fibres was in the range 80-100 nm. The size of the fibres increased as the supply voltage increased (Figure 5.5.a), while it decreased increasing distance between emitter and collector (Figure 5.5.d) and flow rate (Figure 5.5.g). The porosity was in a range between 20 and 50 % with pores presenting a diameter between 0.30 and 0.45 µm. An increase in the porosity corresponded to an increase in the pore diameter (Figure 5.5.b, 5.5.c, 5.5.e, 5.5.f, 5.5.h 5.5.i)
The changes in porosity and pore size are not linear with voltage, distance between emitter and collector and flow rate (Figure 5.5.b, 5.5.c, 5.5.e, 5.5.f, 5.5.h 5.5.i).

After the tuning, voltage was set equal to 25 kV, distance from the emitter and

the collector equal to 20 cm, flow rate 0.2 ml/hour, and 1000 rpm as collector rotation speed. With these parameters, electrospun fibres of GL with a diameter of 90 ± 1 nm , a porosity of 23.50 ± 0.43 % and a pore mean diameter of 280 ± 7 nm were obtained (results expressed in mean±standard deviation).

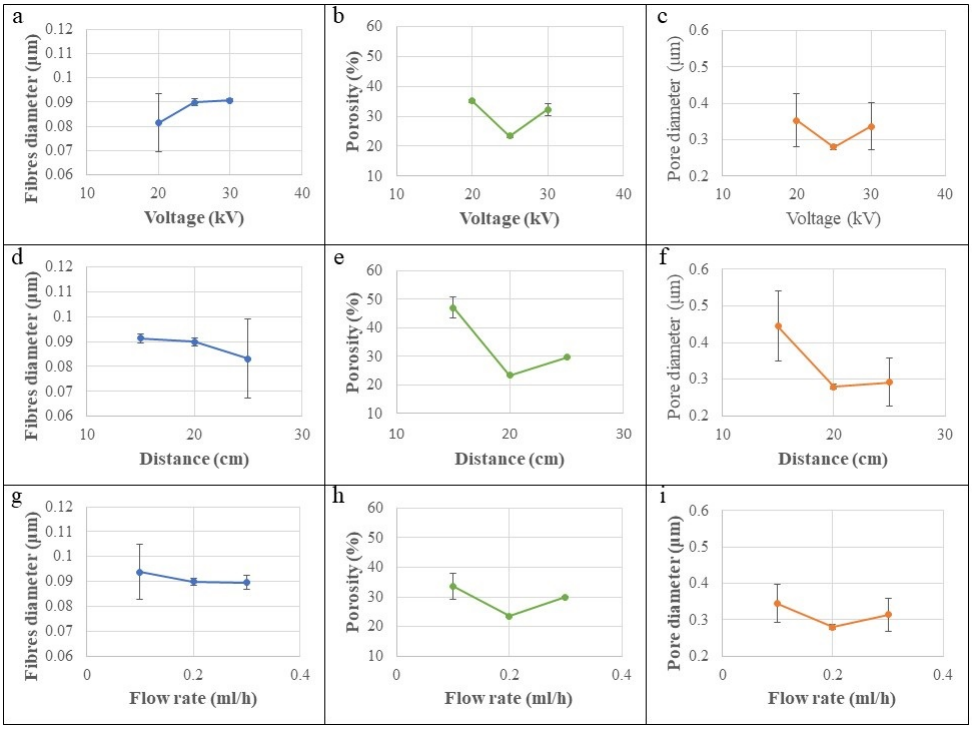

Figure 5.5: Tuning of the electrospinning parameters for gelatin nanofibres. (a) The diameters of the nanofibres increased as increasing the voltage supply, while (b) the values of porosity and (c) the diameters of the pores are not linear with increasing voltage. (d) As distance from emitter and collector increases, instead, fibres diameter decreases, while again the same non-linear relationship between distance and (e) porosity and (f) pore dimensions was found. Finally, (g) the fibres diameter decreases with the increasing of flow rate. Again (h) porosity, and (i) pore diameter are not linear with flow rate. Varying the parameters, a correlation between increasing/decreasing in porosity and increasing/decreasing of pore diameter could be seen. The graphs show the mean values ± standard deviation.

SEM images from PCL fibres, instead, highlighted that a tuning of the concentration of the PCL solution was required; in fact, with lower concentrations (*i.e.*, 7.5% w/v and 10% v/w) nanofibres were characterized by the presence of many defects and beads, while the highly concentrated 15% w/v PCL solution avoided the presence of beads.
In general, the diameter of PCL electrospun fibres was bigger if compared to GL fibres (Figure 5.6.b). The smallest fibres were obtained with 25 kV voltage, 20 cm distance between the needle and the collector, and 0.2 ml/hour flow rate. This setup configuration corresponded with the parameters used for GL fibres, so it was chosen as target configuration.
PCL fibres with a mean diameter of 1.13 ± 0.15 µm, porosity of 36.08 ± 8.49 %

and pore size of 3.64 ± 0.44 μm (results expressed in mean±standard deviation) were obtained.

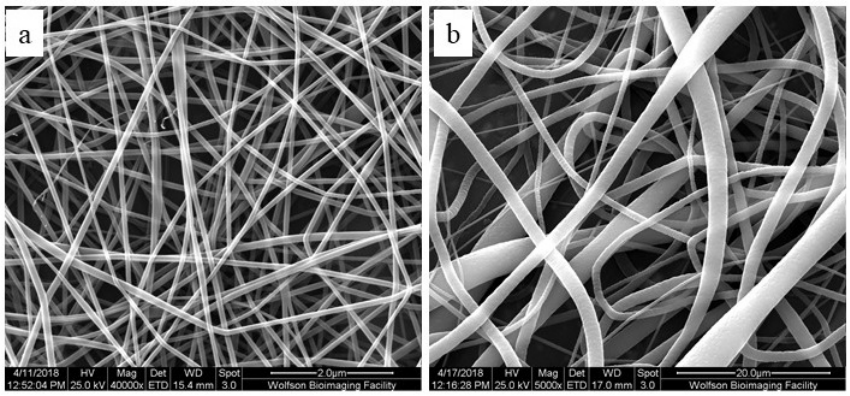

Figure 5.6: Morphological aspect of electrospun nanofibres. (a) Gelatin electrospun fibres were in general randomly distributed and without beads (b) Polycaprolactone (PCL) fibres were much bigger than gelatin ones. Moreover, it was necessary to find a proper concentration of the PCL solution to avoid the presence of beads.
Representative images are reported. Snaps were acquired with scanning electron microscopy, the bar scale is representative for the magnification.

5.3.2 Structure of the scaffolds

The final structure of the double-layer scaffolds was obtained electrospinning in subsequent phases GL alone, GL and PCL together to constitute an intermediate layer, and PCL alone. The combination of timing for the three phases permitted to avoid de-lamination of the layers, with the intermediate hybrid layer creating a mesh of PCL and GL and serving as conjunction element between the inner and the outer layer.

5.3.2.1 Mechanical characterization

GL/PCL and GL scaffolds were compared to determine differences in mechanical strength of the double-layer approach (5.7.a). The results of the tensile test carried out following the ISO specification showed that the Young Modulus of GL/PCL scaffold was 1.70 ± 0.66 MPa while GL scaffold Young Modulus was 0.38 ± 0.14 MPa (results expressed in mean ± standard deviation) (Figure 5.7.b). The difference between the two types of scaffold was significant, but more important was that the raised mechanical strength of the double-layer scaffold reduced the gap with the native coronary artery (1.48 ± 0.24 MPa) (5.7.a).

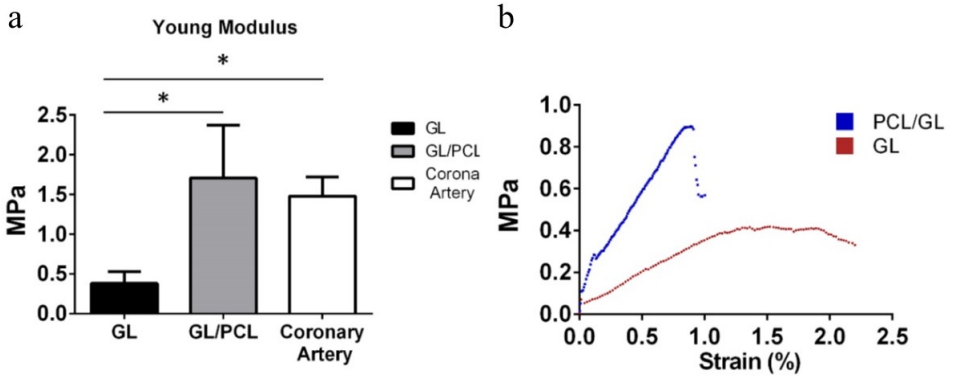

Figure 5.7: Mechanical characterization of the double-layer scaffolds. (a) From the graph bar of the Elastic Modulus of GL, Gl/PCL, and coronary artery it was found that GL/PCL scaffolds not only have an higher Young Modulus if compared to GL scaffolds, but their mechanical characteristics are more similar to native coronary artery. (b) In the graph, stress-strain curves of GL (in red) and GL/PCL (in blue) scaffolds are compared.
In the graphs, mean values ± standard deviation are reported (n=3).

5.3.3 Functional evaluation of the scaffolds

5.3.3.1 Assessment of cell viability on GL/PCL scaffolds

Cell viability on double-layer scaffolds was evaluated to assess the capability of the three-dimensional structure to promote cells adhesion and proliferation. Results of the viability tests highlighted that GL/PCL scaffolds guaranteed a good viability of APCs. In particular, the viability the first day after seeding was equal to 71.87 ±18.06 % and after seven days the viability increased up to 90.21 ± 5.26 %. As a control, APCs were seeded on standard culture plates and on PCL scaffolds. As expected, APCs on culture plates maintained an high viability during time (98.25 ± 0.73 % at day 1 and 96.71 ± 3.17 % at day 7). APCs cultured on PCL scaffolds were subjected to a big decrease in viability after 3 days (from the initial viability of 86.86 ± 3.61 % to a value of viability of 60.55 ± 15.78 %), but at day 7 an higher viability was found (84.31 ± 2.22 %) (Figure 5.8.a).

Endothelial cells (*i.e.*, CAECs) used as cellular control, showed a behaviour similar to APCs. In fact, on GL/PCL scaffolds there was a monotone increase of viability from day 1 (71.25 ± 6.47 %) to day 7 (89.33 ± 2.85 %). The viability on multi-well plates used a positive control was kept almost constant from the day subsequent the seeding (98.37 ± 0.43 %) to the seventh day (98.10± 0.35 %). Finally, analysing the cell viability of CAECs on PCL scaffolds, a strong decrease was found from day 1 (74.73 ± 12.75 %) to day 3 (32.87± 15.24 %), followed by an increasing at day 7 (cell viability at day 7 was found equal to 83.11 ± 1.35 %) (Figure 5.8.b).

All the results are expressed in mean ± standard deviation.

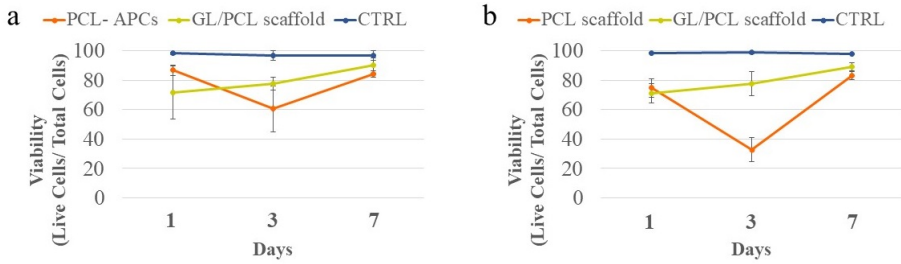

Figure 5.8: Assessment of cell viability on the scaffolds. (a) The trend of viability for APCs seeded on PCL scaffolds (orange), GL/PCL scaffolds (yellow) and culture plates as control (blue) at day 1, 3, and 7 is reported. (b) A similar trend was seen for CAECs seeded on PCL scaffolds (orange), GL/PCL scaffolds (yellow) and culture plates used as positive control (blue).
Mean values ± standard deviation are reported.

5.3.3.2 Assessment of the rotating seeding protocol

The use of the extended sterilization protocol, consisting in many subsequent washes and a long period of soaking within PenStrep and amphotericin B solution, proved to be effective and no mould contaminations were encountered.

A qualitative analysis of phalloidin staining on APCs seeded on scaffolds via rotating seeding confirmed a good distribution and good morphology of the cells on the three-dimensional structure (Figure 5.9).

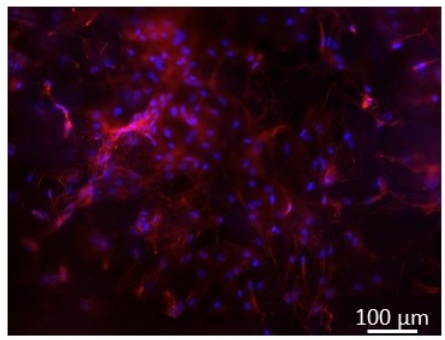

Figure 5.9: Phalloidin staining. The qualitative analysis of phalloidin staining on APCs after the rotating seeding highlighted the presence of spreading and well distributed cells on the scaffolds. A representative image was reported.

5.3.4 Assessment of the angiogenic profile

The viability assays performed on the cellular constructs showed a good viability after both dynamic and static conditioning in normoxic and hypoxic environment. Some signs of mortality could be found in correspondence with areas were the construct was cut with scalpel (Figure 5.10).

The qualitative analysis of immunofluorescence staining showed that, in general,

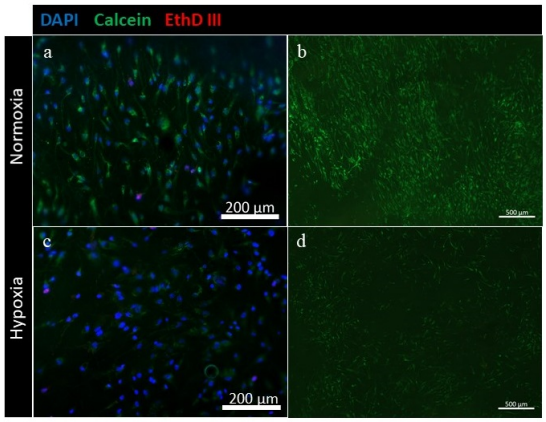

Figure 5.10: Analysis of viability on scaffolds after perfusion into the bioreactors. (a) The qualitative analysis of cell viability on scaffolds cultured under dynamic conditions in the normoxic environment highlighted a good viability. (b) Lower magnification. (c) A good viability was found even on cellular constructs cultured within a bioreactor in hypoxic environment. (d) Lower magnification.
Representative images were reported.
Similar results were found on scaffolds cultured statically.
Viable cells were labelled with calcein (green), dead cells with EthD-III III (red), and the nuclei with DAPI (blue) after fixation.

TBPG was not expressed by APCs cultured in any conditions A.3. Only a few positive TPBG-cells were stained in constructs cultured under dynamic conditions in hypoxic environments (Figure 5.11.d, 5.11..e, 5.11..f).

As explained in paragraph 5.2.3.3, q-PCR highlighted no amplification of any cDNA coming from cell constructs.
Technical mistakes were excluded because cDNAs from APCs cultured on multi-well plates were amplified. Our efforts were then sought at understanding the reasons of this unexpected outcome.
The running of a gel with mRNA and cDNA from both cell constructs and multi-well plate confirmed that both nucleic acids were preserved after RNA extraction and retro-transcriptase reaction, but with a low ratio of absorbance at 260 and 280 nm. Homogenization proved to provide a better mRNA, and therefore cDNA, quality.
Therefore, q-PCR with different concentrations of cDNA coming from cell constructs showed that decreasing the concentration of cDNA used for the reaction, there is a beginning of amplification, but the concentrations are too low for obtaining a proper amplification.

ELISA assays was not positive for all the CCM coming from cellular constructs, both from bioreactors and static cultures. A further ultra-centrifugation process would have been required.

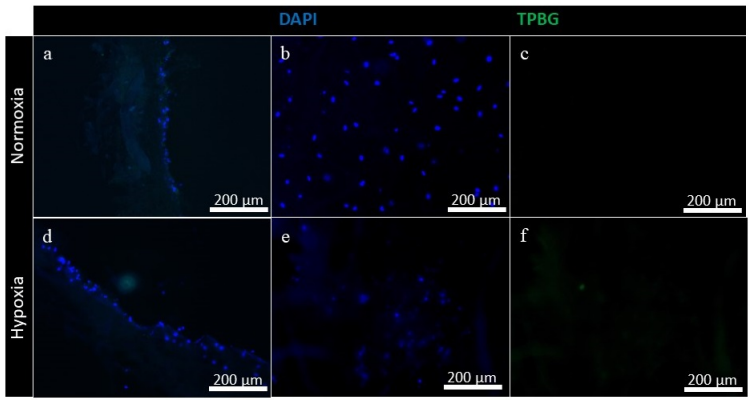

Figure 5.11: Labelling of TPBG. (a) Immunofluorence analysis of TPBG expression (green) by APC cultured under fluid-dynamic conditions proved (b) a good distribution of cells, (c) but without expression of TPBG. (d) Cellular constructs exposed to hypoxia under fluid-dynamic conditions were characterized as well by (e) a good distribution of cells, and (f) some positive TPBG staining.
Nuclei are labelled with DAPI (blue).
Representative images were reported.

5.4 Discussion

The aim of this study was to propose a tissue-engineered vascular model exploiting a tubular synthetic structure seeded with vascular cells. In particular, as a proof of concept, adventitial progenitor cells were seeded on electrospun fibres and exposed under dynamic conditions to hypoxic environment to investigate the angiogenic effects induced on this particular cell type.

APCs can be easily isolated from the tissue and they are easily expanded and cultured *in vitro*. Many evidences highlighted that they play an important role in angiogenesis and in vascular stabilization [13, 10, 14]. Given this, it was interesting to investigate their angiogenic profile in a more-realistic environment (*i.e.*, three-dimensional structure and fluid-dynamic conditions).

From a technical point of view, electrospinning was chosen as scaffold manufacturing technique because of the possibility to tune morphological characteristics of GL and PCL fibres by modifying some electrospinning parameters. Among the possible materials, the choice of GL was due to its biocompatibility, biodegradability and the capability to drive cell attachment [15]. To evaluate the electrospinning parameters, the morphological characteristics of GL fibres obtained were compared to previous studies. The non-linear correlation between the electrospinning parameters (*i.e.*, voltage, flow rate, distance) and the porosity and the pore dimension suggested that the variation of these parameters occurred around a minimum point [16]. Diameter of the nanofibres and characteristics of porosity guaranteed good biocompatibility characteristics and good cell proliferation [17, 18, 19, 20]. Nevertheless, lack of durability of GL and low mechanical properties led to the ap-

plication of a second layer of synthetic material. For this second layer it was chosen PCL, because it has excellent biocompatibility, biodegradability, workability, and both mechanical and chemical properties [21, 22]. For all these reasons, PCL has been approved by Food and Drug Administration. Regarding the morphology of PCL nanofibres, the concentration of the solution was found to be fundamental for obtaining fibres without beads. Fibres diameter and porosity characteristics were found to be bigger if compared to GL ones, but this values of porosity, even if bigger that GL's one, does not allow an unwanted penetration of the cells within the structure [23].

The double-layer structure ensured good cell adhesion and proliferation, but at the same time good durability and proper mechanical characteristic, making the scaffold a good model of artery. In fact, scaffolds with improved mechanical characteristics were more similar to native arteries, which is a major requirement for vascular substitute since the mismatch between commercial grafts and native blood vessels is one of the main reasons for grafts failure [24]. The compactness of the structure was then guaranteed by the introduction of the intermediate layer. In fact, this intermediate meshed layer prevented the scaffolds from de-lamination, avoiding inner layers peeling off.

The results of the biological functionalization confirmed that GL/PCL scaffolds ensured a good cell viability. A different behaviour was found for cells cultured on PCL scaffolds, where a strong decrease in cell viability was followed by an increase of the viability index. Since the same results were found for both cellular population (*i.e.,* APCs and SVPs), this result must be attributed to the material properties. To better understand viability data, any changes in cell density must be evaluated. The qualitative comparison between the cell density at different time points suggested, in fact, that the increase of viability at day 7 on PCL scaffolds could be due to a corresponding decrease in the cell density (Figure A.1.a, Figure A.1.b, Figure A.2.a, and Figure A.2.b).

The rotating seeding proved to be an efficient procedure, compatible with standard laboratory practise and not harmful for the scaffolds, thanks to the use of custom made POM holders. The main issue came from the sterilization of the scaffolds. In fact, they were identified as responsible for massive mould contaminations occurring in the three-dimensional cultures. This could be due to the manufacturing of the scaffolds, which was not performed under sterile condition, and to the configuration and the porosity of the structure, which could hold spores that in a humid environment spread into moulds. Subsequent washes to dilute the contaminants and an extended exposure to anti-fungi solution were performed to effectively sterilize the scaffolds.

The culturing of scaffolds under dynamic conditions in hypoxic environment was performed with the custom made bioreactor shown in paragraph 4.3.1 because lower priming volume guaranteed a complete de-oxygenation of the medium in less time. In addition, the configuration of the bioreactor mimicking the func-

tioning of a Petri-dish permitted an higher exchange area and a more effective de-oxygenation of the medium.
Qualitative analysis of immunofluorescence suggested that fluid-dynamic conditioning of the APCs enhanced the angiogenic potential of hypoxia; in fact, TPBG expression was found after 24 hours, while previous studies found an increased expression of TPBG only after 3 days under static culture in plates [11]. But these qualitative results must be considered only as a preliminary data; in fact, it was not possible to obtain any results from q-PCR neither from ELISA.
We highlighted two possible reasons for this unexpected outcome. First of all, the quality of the RNA suggested that cells could be dying at the moment of RNA harvesting. A faster process without manipulation of the samples would be required to increase RNA, and therefore cDNA, quality. Moreover, decreasing the amount of cDNA to amplify with q-PCR it was obtained a better amplification. An interference was then hypothesized as cause of the absence of amplification.
A protocol for further filtration of the medium must be assessed, instead, for obtaining reliable results from ELISA assay.

All these technical issues have to be solved for obtaining quantitative results about the angiogenic profile induced by hypoxia on APCs in the tissue engineered model.

5.5 Conclusions

This study aimed at proposing a tissue-engineered model for study vascular diseases.
As a proof of concept we seeded adventitial progenitor cells on tubular scaffolds. Cellular constructs were then cultured under fluid-dynamic conditions to assess any angiogenic effects induced by hypoxia on cells cultured on a structure more realistic than standard *in vitro* models. Hypoxia, in fact, is a well-established angiogenic stimulus and it plays an important role in the progression of atherosclerotic lesion. For this reason, it could be addressed as therapeutic target.

The possibility to tune the properties of the materials and to select one or more specific cellular populations is a big advantage in comparison to *ex vivo* models with native arteries. These models are therefore very promising tools for the studying of vascular pathologies.

Nevertheless, the use of tissue-engineered models is still far from being used as reliable model of vascular diseases, due to biological and technical issues. In fact, we are far from obtaining grafts reproducing *in toto* the biology and the cellular behaviour of native vessels.
Moreover, technical issues due to the matching of traditional culture techniques and assays with innovative tissue-engineering approaches must be faced, as well explained in this work.

To conclude, preliminary results are promising, but some efforts still need to

be made to establish reliable tissue-engineering derived models to study vascular pathophysiology.

Bibliography

[1] A. Patel. Does the Role of Angiogenesis Play a Role in Atherosclerosis and Plaque Instability? *Anatomy & Physiology*, 04(03), 2013.

[2] C. Camaré, M. Pucelle, A. Nègre-Salvayre, and R. Salvayre. Angiogenesis in the atherosclerotic plaque. *Redox Biology*, 12(2017):18–34, 2017.

[3] B. L. Krock, N. Skuli, and M. C. Simon. Hypoxia-induced angiogenesis: good and evil. *Genes & cancer*, 2(12):1117–1133, 2011.

[4] C. Lin, R. McGough, B. Aswad, J. A. Block, and R. Terek. Hypoxia induces HIF 1 alpha and VEGF expression in chondrosarcoma cells and chondrocytes. *Journal of Orthopaedic Research*, 22(6):1175–1181, 2004.

[5] T. Kurihara, P. D. Westenskow, and M. Friedlander. Hypoxia-inducible factor (HIF)/vascular endothelial growth factor (VEGF) signaling in the retina. *Advances in Experimental Medicine and Biology*, 801(2014):275–281, 2014.

[6] A. Hoeben, B. Landuyt, M. S. Highley, et al. Vascular Endothelial Growth Factor and Angiogenesis. *Pharmacological Reviews*, 56(4):549 LP – 580, 2004.

[7] E. Fagiani and G. Christofori. Angiopoietins in angiogenesis. *Cancer Letters*, 328(1):18–26, 2013.

[8] D. G. Sedding, E. C. Boyle, J. A. Demandt, et al. Vasa vasorum angiogenesis: Key player in the initiation and progression of atherosclerosis and potential target for the treatment of cardiovascular disease. *Frontiers in Immunology*, 9:9–14, 2018.

[9] S. Caddeo, M. Boffito, and S. Sartori. Tissue Engineering Approaches in the Design of Healthy and Pathological In Vitro Tissue Models. *Frontiers in Bioengineering and Biotechnology*, 5(2017):40, 2017.

[10] R. G. Katare and P. Madeddu. Pericytes from human veins for treatment of myocardial ischemia. *Trends in Cardiovascular Medicine*, 23(3):66–70, 2013.

[11] H. L. Spencer, E. Jover, W. Cathery, et al. Role of TPBG (Trophoblast Glycoprotein) Antigen in Human Pericyte Migratory and Angiogenic Activity. *Arteriosclerosis, thrombosis, and vascular biology*, 39(6):1113–1124, 2019.

[12] P. Campagnolo, D. Cesselli, A. Al Haj Zen, et al. Human Adult Vena Saphena Contains Perivascular Progenitor Cells Endowed With Clonogenic and Proangiogenic Potential. *Circulation*, 121(15):1735–1745, 2010.

[13] R. Katare, F. Riu, K. Mitchell, et al. Transplantation of Human Pericyte Progenitor Cells Improves the Repair of Infarcted Heart Through Activation of an Angiogenic Program Involving Micro-RNA-132. *Circulation Research*, 109(8):894–906, 2011.

[14] E. Avolio and P. Madeddu. Discovering cardiac pericyte biology: From physiopathological mechanisms to potential therapeutic applications in ischemic heart disease. *Vascular Pharmacology*, 86(2016):53–63, 2016.

[15] M. C. Echave, L. S. Burgo, J. L. Pedraz, and G. Orive. Gelatin as Biomaterial for Tissue Engineering. *Current Pharmaceutical Design*, 23(24):3567–3584, 2017.

[16] K. A. G. Katsogiannis, G. T. Vladisavljević, and S. Georgiadou. Porous electrospun polycaprolactone fibers: Effect of process parameters. *Journal of Polymer Science, Part B: Polymer Physics*, 54(18):1878–1888, 2016.

[17] M. Chen, P. K. Patra, S. B. Warner, and S. Bhowmick. Role of Fiber Diameter in Adhesion and Proliferation of NIH 3T3 Fibroblast on Electrospun Polycaprolactone Scaffolds. *Tissue Engineering*, 13(3):579–587, 2007.

[18] H. M. Powell and S. T. Boyce. Fiber density of electrospun gelatin scaffolds regulates morphogenesis of dermal epidermal skin substitutes. *Journal of Biomedical Materials Research Part A*, 84A(4):1078–1086, 2008.

[19] C. A. Bashur, R. D. Shaffer, L. A. Dahlgren, S. A. Guelcher, and A. S. Goldstein. Effect of Fiber Diameter and Alignment of Electrospun Polyurethane Meshes on Mesenchymal Progenitor Cells. *Tissue Engineering Part A*, 15(9):2435–2445, 2009.

[20] V. Milleret, T. Hefti, H. Hall, V. Vogel, and D. Eberli. Influence of the fiber diameter and surface roughness of electrospun vascular grafts on blood activation. *Acta Biomaterialia*, 8(12):4349–4356, 2012.

[21] D. W. Hutmacher, T. Schantz, I. Zein, et al. Mechanical properties and cell cultural response of polycaprolactone scaffolds designed and fabricated via fused deposition modeling. *Journal of Biomedical Materials Research*, 55(2):203–216, 2001.

[22] A. Cipitria, A. Skelton, T. R. Dargaville, P. D. Dalton, and D. W. Hutmacher. Design, fabrication and characterization of PCL electrospun scaffolds - A review. *Journal of Materials Chemistry*, 21(26):9419–9453, 2011.

[23] D. G. Han, C. B. Ahn, J. H. Lee, et al. Optimization of electrospun poly(caprolactone) fiber diameter for vascular scaffolds to maximize smooth muscle cell infiltration and phenotype modulation. *Polymers*, 11(4):643, 2019.

[24] S. E. Greenwald and C. L. Berry. Improving vascular grafts: the importance of mechanical and haemodynamic properties. *The Journal of Pathology*, 190(3):292–299, 2000.

Chapter 6

General conclusions

In the scientific community the need of studying atherosclerosis is still of primary importance. In fact, although many efforts have been dedicated to the study of this pathology, many mechanisms still remain unveiled. Atherosclerosis is a complex multi-factorial disease [1] that develops in different stages during decades in the whole life of a patient [2]. From the onset of the disease to the acute manifestation with the thrombosis, each stage is characterized by specific mechanisms with peculiar molecular and cellular pathways [3]. Given this, studies must be addressed to investigate each of these stages, with the aim of deeply examine the causes to identify molecular targets that have to be addressed with pharmacological or clinical treatments.

The complexity of this disease can be ascribed to the coexistence of mutually dependent risk factors and to the interplay of several inflammatory cues [4, 5]. Atherosclerosis, in fact, is mainly caused by systemic and local inflammatory events. These events mediate all the steps of plaque development, progression, and rupture: immune cells play a key role in early atherosclerotic lesions, their effector molecules induce the progression of the plaques, and activation of inflammation can elicit acute coronary syndromes [3].

This complexity could not be reproduced with the standard *in vitro* approaches, even though they provide a first essential simplification that is necessary to identify the effects of specific cues on cell populations involved in the disease.

At the same time, animal models are unavoidable for reproducing *in toto* the atherosclerotic process, and therefore they are unavoidable for testing new drugs or new devices. Nevertheless, technical, ethical, and economic issues affect this model.

The necessity of new approaches for studying atherosclerosis arises from all these evidences. Then, the goal of this doctoral thesis was to design and develop innovative *ex vivo* models aiming at investigating different aspects related to the atherosclerotic process. These approaches do not claim to substitute *in vitro* and *in vivo* models. But, instead, they yearn for supporting traditional approaches. *Ex vivo* models, in fact, have been described as the bridge between *in vitro* and *in vivo* models because they permit to isolate and investigate specific stimuli, but without loosing the complexity of the tissue. They are useful for examine cues involved in vascular pathology and they can serve as a preliminary screening for drugs and devices before using animal models.

To fulfil this aim, a multi-disciplinary effort is needed; the collaboration among clinicians, biologists, biotechnologists and engineers is required to obtain reliable and useful models.
In fact, in comparison to *in vitro* and *in vivo* standard approaches, *ex vivo* models have not been already established. For this reason, they have to be designed from specific needs and tailor-made for biologists and clinicians, who have to be involved in their development. Only then *ex vivo* models can become standard laboratory methods.

The projects of the bioreactors presented in this thesis were born from the necessity to analyse some complex aspects related to atherosclerosis.

In the chapter 3 it was presented a model for studying the cellular and molecular mechanisms involved in the spreading of thrombosis. The culture chamber consists of a parallel-plate chamber were slices of arteries are exposed to a well-controlled shear rate (and therefore shear stress). The device was thought to be very easy to use and compliant with standard laboratory techniques and microscopy. The novelty introduced by this model is the use of arterial arteries, while this kind of studies are usually performed on single cell population or co-culture. Maintaining all the components of the artery, it is therefore possible to mimic a more realistic condition. The system was characterized and preliminary tests assessed the potentiality of this platform. By culturing atherosclerotic plaques under well-controlled environmental and fluid-dynamic stimuli, the model can be exploited for discovering all the players involved in thrombus formation. Pharmacological treatments can be therefore designed and, potentially, the parallel-plate device could be used as a screening platform.

The platform shown in the chapter 4 aimed at translating in *ex vivo* models procedures that have been employed to study thrombosis *in vivo*. This approach allows not only to reduce the costs and the ethical implications of the use of animal models, but it permits also to obtain more reproducible and well controlled models, since in *ex vivo* models isolated and controlled stimuli are reproduced. In particular, we focused on the ferric-chloride induced thrombosis, that, as far as we know, has been studied only within animal models. The bioreactor was then designed for this scope. It allowed to culture whole vessels with different diameter and length under fluid-dynamic conditions. Once assessed the capability to maintain the viability of the tissue within the culture system, it could be exploited to induce vessel damage and to study the pathways involved. A big advantage is represented by the possibility to add stimuli, both biochemical and biomechanical, to obtain an environment mimicking more and more *in vivo* conditions, but still controlled.

In the chapter 5 the potential of tissue-engineered models for studying atherosclerosis was investigated. In fact, besides traditional *ex vivo* models with explanted tissue, tissue-engineered inspired models have been used thanks to the possibility to maintain the complexity of *in vivo* structures, but controlling cellular composition. As a proof of concept, we cultivated adventitial progenitor cells on tubular electrospun scaffolds under fluid-dynamic conditions to assess angiogenic effects of hypoxia. The relationship between angiogenesis and atherosclerosis have been widely accepted as one of the mayor causes of plaque vulnerability and the cellular components involved in this mechanism could be addressed as therapeutic target. The model proved to be suitable for this kind of consideration, but, before exploiting its potentiality, technical problems must be solved. In fact, one main drawback is related to the necessity to adapt traditional analysis protocols to these

innovative approaches.

In summary, the multi-disciplinary approach of the present doctoral thesis has highlighted how new technical solutions could be applied to enhance the relevance of *in vitro* and *in vivo* methods for the study of the onset and of the progression of atherosclerosis. In addition, preliminary results achieved suggest the effective potentiality of the platforms here developed as tools for successfully supporting biological and pharmacological researches.

Bibliography

[1] R. B. Singh, S. A. Mengi, Y.-J. Xu, A. S. Arneja, and N. S. Dhalla. Pathogenesis of atherosclerosis: A multifactorial process. *Experimental and clinical cardiology*, 7(1):40–53, 2002.

[2] F. Otsuka, M. C. A. Kramer, P. Woudstra, et al. Natural progression of atherosclerosis from pathologic intimal thickening to late fibroatheroma in human coronary arteries: A pathology study. *Atherosclerosis*, 241(2):772–782, 2015.

[3] G. K. Hansson. Inflammation, Atherosclerosis, and Coronary Artery Disease. *The New England Journal of Medicine*, 325(16):1685–1695, 2005.

[4] S. A. Ramsey, E. S. Gold, and A. Aderem. A systems biology approach to understanding atherosclerosis. *EMBO Molecular Medicine*, 2(3):79–89, 2010.

[5] I. Gregersen and B. Halvorsen. Inflammatory Mechanisms in Atherosclerosis. In B. H. E. L. Gianturco, editor, *Atherosclerosis Yesterday, Today and Tomorrowh*, page Ch. 3. IntechOpen, Rijeka, 2018.

Appendix A

Supplementary materials

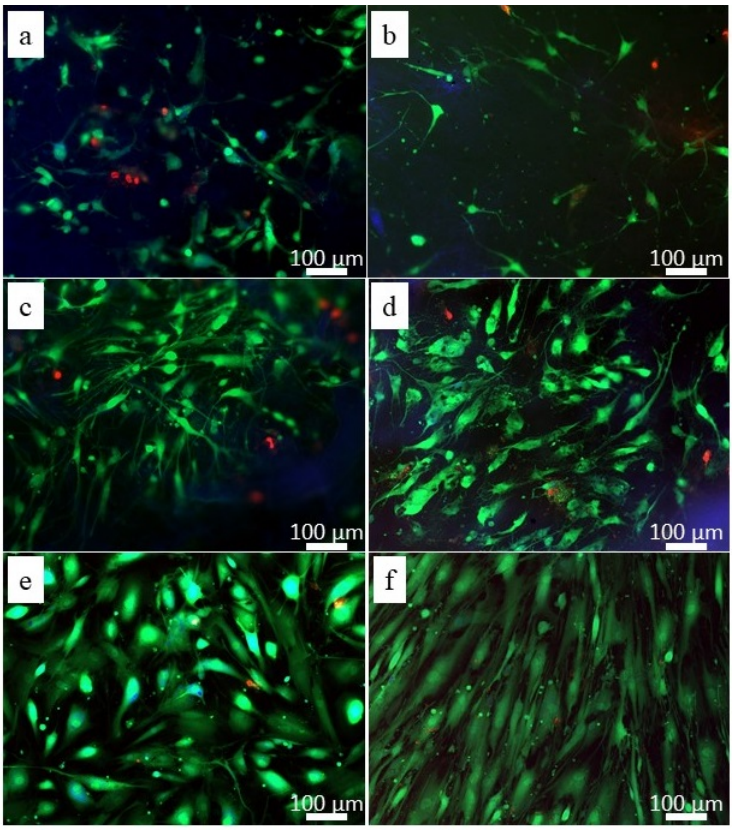

Figure A.1: Adventitial progenitor cells viability on different substrates at different time points. (a) Viability of the adventitial progenitor cells (APCs) cultured on polycaprolactone (PCL) scaffolds at day 1, and (b) at dat 7. A worst morphology and a reduced density could be noticed. (c) APCs cultured on double-layer scaffolds at day 1, and (d) at day 7. In this case the morphology is still good after 7 days. (e) As a positive control, APCs were cultured on multi-well plate and the results at day 1, and (f) at day 7 could be seen in the figure. Representative images were reported.

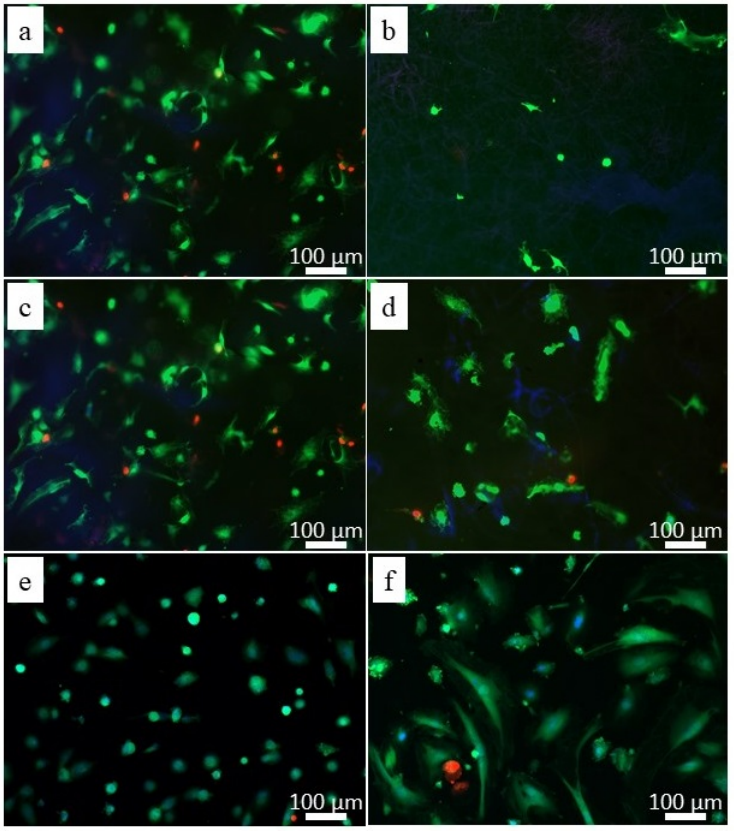

Figure A.2: Endothelial cells viability on different substrates at different time points. (a) Viability of the coronary artery endothelial cells (CAECs) cultured on polycaprolactone (PCL) scaffolds at day 1, and (b) at dat 7. A strong reduction in the number of cells can be seen. (c) CAECs cultured on double-layer scaffolds at day 1, and (d) at day 7. In this case the reduction in cell density is less evident. (e) As a positive control, CAECs were cultured on multi-well plate and the results at day 1, and (f) at day 7 could be seen in the figure. Representative images were reported

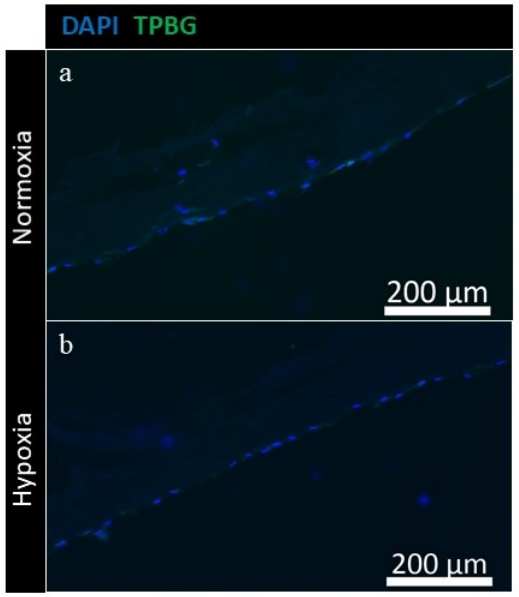

Figure A.3: Labelling of TPBG. (a) Immunofluorescence from scaffolds cultured in static conditions showed a good distribution of cell on the lumen of the scaffolds both in normoxic, and (b) in hypoxic environment. In both cases, no positive TPBG staining (green) were optained.
Nuclei are labelled with DAPI (blue)
Representative images were reported.